NANYANG TECHNOLOGICAL UNIVERSITY
SINGAPORE

Development and validation of a soft robotic exosuit for assistance of the upper limbs

Michele Xiloyannis

Interdisciplinary Graduate School

NTU Institute for Health Technologies

Development and validation of a soft robotic exosuit for assistance of the upper limbs

Michele Xiloyannis

Interdisciplinary Graduate School

NTU Institute for Health Technologies

Supervisors:

Assoc. Prof. Lorenzo Masia

Assoc. Prof. Dino Accoto

Co-supervisor:

Prof Chen Shen-Hsing Annabel

A thesis submitted to the Nanyang Technological University in partial fulfillment of the requirements for the degree of Doctor of Philosophy

2019

Statement of Originality

I hereby certify that the intellectual content of this thesis is the product of my original research work and has not been submitted for a higher degree to any other University or Institution.

02/05/2019
.....
Date


.....
Michele Xiloyannis

Supervisor Declaration Statement

I have reviewed the content and presentation style of this thesis and declare it is free of plagiarism and of sufficient grammatical clarity to be examined. To the best of my knowledge, the research and writing are those of the candidate except as acknowledged in the Author Attribution Statement. I confirm that the investigations were conducted in accord with the ethics policies and integrity standards of Nanyang Technological University and that the research data are presented honestly and without prejudice.

02/05/2019
Date


Assoc. Prof. Lorenzo Masia

02/05/2019
Date


Assoc. Prof. Dino Accoto

Authorship Attribution Statement

This thesis contains material from 10 manuscripts, including book chapters and conference proceedings, published in the following peer-reviewed journal(s), book(s) or proceeding(s) where I was the first and/or corresponding author. The work outlined in this thesis was performed the the Robotics Research Center, School of Mechanical & Aerospace Engineering, Nanyang Technological University, and Center for Advanced Rehabilitation Therapeutic (CART) at Tan Tock Seng Hospital.

Chapter 2 is based on the following book chapter:

- M. Xiloyannis, K. D. Binh, L. Cappello, C. W. Antuvan and L. Masia, "Chapter 10. A Soft Wearable Elbow Exosuit: Design Considerations". In *Wearable Technology for Medicine and Healthcare, 1^{st} edition*, Elsevier, 2018.
  Authors' contribution: MX, LC and LM designed the exosuit. DBK, MX and LM developed the controller. DBK, MX and LM designed the experiment. DBK and MX performed the experiment. DBK, MX, LC and LM analysed and interpreted the data. MX and LM prepared the manuscript. All authors provided critical feedback on the manuscript. All authors read and approved the final manuscript.

Sections 3.2 and 3.3 are based on the following manuscript:

- M. Xiloyannis, L. Cappello, K. D. Binh, C. W. Antuvan and L. Masia, "Preliminary design and control of a soft exosuit for assisting elbow movements and hand grasping in activities of daily living", in *Rehabilitation and Assistive Technology Engineering (RATE)*, vol. 4, 2017.
  Authors' contribution: MX, LC and LM designed the exosuit. DBK, MX and LM developed the controller. DBK, MX and LM designed the experiment. DBK and MX performed the experiment. DBK, MX, LC and LM analysed and interpreted the data. MX and LM prepared the manuscript. All authors provided critical feedback on the manuscript. All authors read and approved the final manuscript.

Section 3.4.1,3.4.2 and 3.4.3 are based on the following manuscripts:

- M. Xiloyannis, D. Chiaradia, A. Frisoli, L. Masia, "Characterisation of a Soft Exosuit for Assitstance of the Elbow Joint", in *International Symposium on Wearable Robotics (WeRob)*, Houston, 2017, pp. 1-1.
  Authors' contribution: MX, DC and LM designed the exosuit. MX, DC and LM designed the experiment. MX and DC performed the experiment. MX, DC, AF and LM analysed and interpreted the data. MX, DC, AF and LM prepared the manuscript. All authors provided critical feedback on the manuscript. All authors read and approved the final manuscript.

– M. Xiloyannis, D. Chiaradia, A. Frisoli and L. Masia, "Characterisation of pressure distribution at the interface of a soft exosuit: towards a more comfortable wear", in *International Symposium on Wearable Robotics (WeRob)*, Pisa, Italy, 2018, pp. 35-38.
Authors' contribution: MX, DC and LM designed the exosuit. MX, DC and LM designed the experiment. MX performed the experiment. MX, DC, AF and LM analysed and interpreted the data. MX, DC, AF and LM prepared the manuscript. All authors provided critical feedback on the manuscript. All authors read and approved the final manuscript.

Section 4.1 is based on the following book chapter:

– L. Masia, M. Xiloyannis, K. D. Binh, C. W. Antuvan, S. Contu and Y. Kim,"Chapter 4. Actuation for Robot-Aided-Rehabilitation: Design and Control Strategies", in *Rehabilitation Robotics, 1st edition*, Elsevier, 2018, pp. 47-61.
Authors' contribution: MX, DBK, CWA, YK and LM prepared the manuscript. All authors provided critical feedback on the manuscript. All authors read and approved the final manuscript.

Section 4.2-4.4 are based on the following manuscript:

– D. Chiaradia, M. Xiloyannis, C. W. Antuvan, A. Frisoli, L. Masia, "Design and Embedded Control of a Soft Elbow Exosuit", in *IEEE International Conference on Soft Robotics (RoboSoft)*, Livorno, Italy, 2018, pp. 565-571.
Authors' contribution: MX, DC and LM designed the exosuit. MX, DC and LM developed the controller. MX, DC, AF and LM designed the experiment. DC and CWA performed the experiment. MX, DC, AF and LM analysed and interpreted the data. MX, DC, AF and LM prepared the manuscript. All authors provided critical feedback on the manuscript. All authors read and approved the final manuscript.

Chapter 5 is based on the following manuscript:

– M. Xiloyannis, D. Chiaradia, A. Frisoli and L. Masia, "Physiological and Kinematic Effects of a Soft Exosuit on Arm Movements", in *Journal of NeuroEngineering and Rehabilitation (JNER). In press.*
Authors' contribution: MX, DC and LM designed the exosuit. MX, DC and LM developed the controller. MX, DC, AF and LM designed the experiment. MX and DC performed the experiment. MX, DC and LM analysed and interpreted the data. MX, DC and LM prepared the manuscript. All authors provided critical feedback on the manuscript. All authors read and approved the final manuscript.

Chapter 6 is based on the following manuscripts:

- M. Xiloyannis, E. Annese, M. Canesi, A. Kodian, A. Bicchi, S. Micera, A. Ajoudani and L. Masia, "Modular One-to-many Clutchable Actuator for a Soft Elbow Exosuit", in *Frontiers in Neurorobotics*, *Under Review.*
  Authors' contribution: LM conceived the mechanism. MC, MX, EA and LM designed the OTM module. AK, EA, MX and LM developed the controller. EA, MX, AK, MC and LM designed the experiments. EA, MX, MC, AK and LM performed the experiments. All authors analyzed and interpreted the data. All authors prepared the manuscript. All authors provided critical feedback on the manuscript. All authors read and approved the final manuscript.

- M. Canesi, M. Xiloyannis, A. Ajoudani, A Bicchi and L. Masia, "Modular One-to-many Clutchable Actuator for a Soft Elbow Exosuit", in *IEEE International Conference on Rehabilitation Robotics, London (ICORR)*, London, 2017, pp. 1679-1685.
  Authors' contribution: LM conceived the mechanism. MC, MX and LM designed the OTM module. MC, MX and LM developed the controller. MX, MC and LM designed the experiments. MC and MX performed the experiment. MC, MX and LM analyzed and interpreted the data. All authors prepared the manuscript. All authors provided critical feedback on the manuscript. All authors read and approved the final manuscript.

Appendix A is based on the following manuscript:

- D. Chiaradia, M. Xiloyannis, M. Sollazzi , L. Masia and A. Frisoli, "Comparison of a Soft Exosuit and a Rigid Exoskeleton in an Assistive Task", *International Symposium on Wearable Robotics (WeRob)*, Pisa, Italy, 2018.
  Authors' contribution: MX, DC and LM designed the exosuit. DC, MS and AF designed the exoskeleton. MX, DC and LM developed the controller for the exosuit. DC, MS and AF developed the controller for the exoskeleton. DC, MX and MS designed the experiment. DC and MX performed the experiment. DC, MX and MS analysed and interpreted the data. MX and DC prepared the manuscript. All authors provided critical feedback on the manuscript. All authors read and approved the final manuscript.

02/05/2019
Date


Michele Xiloyannis

Acknowledgements

Doing a PhD is harder than I thought and more rewarding than I could have ever imagined. I have had this essay from Martin A. Schwartz hanging on my desk for the past four years, it's called "The importance of stupidity in scientific research". My favourite line goes *"What makes it difficult is that research is immersion in the unknown. We just dont know what were doing."* It can be a daunting feeling. One that teaches, even an introvert like me, to appreciate all the support he can get from those around him.

My greatest thanks undoubtedly go to Lorenzo, that I do not here call "my supervisor" only because he has been much more than that over the last four years. I thank him for his scientific advice, for making me passionate about research, for believing in my skills and for all the inspiring talks we had about my project. Most of all, however, I owe him my deepest gratitude for being a mentor in life.

Leonardo Cappello made me feel at home when I first arrived in Singapore, nearly 10 000 km from home. He guided me through the first steps in the world of research when I was a naïve first year PhD student, and thaught me all he could, especially about CAD design, with immense patience. I would here like to express my thanks and admiration.

Francesca Marini inspired me to always be curious, to never stop learning and to embrace new challenges. Her friendship enriched me and continues to do so, in spite of the distance. A great thank you to one of the most talented people I know.

I owe a debt of gratitude to Domenico Chiaradia, for flying all the way to Singapore for six months, renouncing Italy's good food and weather, to help me with the electronics and the design of the admittance controller. I have learnt a lot from him.

I would like to thank Chris, Khanh, Angelo, Asif, Carlo, Sara, Fabio, Didier, Helena, Simone, Kieran and Adele for inspiring discussions and the dynamic and

friendly environment over the past years. Special thanks go to Dinh Binh Khanh for his help with the development of the controller for the exosuit, I think we developed an unspoken friendship that will last well beyond this project.

I would like to acknowledge the support from Dino Accoto over the last months of my PhD. I'm thankful for his inputs, interest and ideas as well as the scientific discussions which were of great help.

I would like to thank Agnes, Mr Lim and Mr You for making things possible in the Robotics Research Centre. Your efforts, expertise and generosity in helping a small army of PhD students every day are greatly appreciated.

I want to express my appreciation to all the undergraduate and master students whom I supervised during the course of my PhD and who contributed to the successful completion of the project:
Fook Choon Wee (Elfred) for his help in the design of the first actuator; Liu Dongqing (Cathy), for her contribution to the design of the distal anchor point of the suit and for the first tests to quantify comfort; Marco Canesi, for the first design of the OTM module, and for his entertaining skills; Anil Kodian, for the development of the PI-modulated PWM controller for the OTM module; Eugenio Annese, for the characterization and human testing on the OTM module; Luca Tiseni, for the mechanical design and testing of a portable exoskeleton for the shoulder, and for teaching me to properly make my own pasta sauce.

Patrick Steinbrenner made coffee (which he rarely does) for me today, 19^{th}, January 2019, in exchange for his name to be included in the acknowledgements. He would have been here anyway, together with Jess and Andrea: very few things are as valuable as coming home from work and sharing a meal or watching a movie with such perfect flatmates and great friends. Thank you.

I would like to thank my family, for their unconditional and ever-present support.

Finally, I would particularly like to thank my girlfriend Meiqi, for all the love, support and happiness she brought to my life.

Singapore, Michele Xiloyannis *May 1, 2019*

"Entia non sunt multiplicanda praeter necessitatem". [1]

–William of Ockham (1287-1347 A.D.)

To Mamma, Babbo, Giacomo and Giulio.

[1] Law of parsimony: *More things should not be used than are necessary.*

Abstract

Robots have been used in physical rehabilitation to increase the intensity of practice and relieve therapists from the demanding task of manually assisting the patient. Robot-assisted therapy has shown encouraging results, comparable to the ones achieved with traditional therapy, while allowing greater patient compliance and a quantitative, more accurate monitoring of the subject's performance. Unfortunately, currently available robotic platforms are not logistically capable of following the patient after discharge from physical therapy. Patients go back home, training stops and their conditions plateau or even deteriorate.

The fairly recent introduction of soft materials to design robotic devices has had a significant impact on assistive technologies. Wearable robots made of fabric and elastomers, also known as exosuit, are a promising way of delivering power to the human body, with potential applications in the medical field. Being lightweight, ergonomic and low power-demanding, exosuits are an attractive tool to provide assistance, not only in clinical settings but also in daily life. Understanding how these devices affect the physiology and mechanics of human movements is fundamental for quantifying their benefits and drawbacks, assessing their suitability for medical use and guiding a continuous design refinement.

In this thesis we hypothesize that a soft exosuit can comfortably deliver assistive forces to the joints of the upper limbs, working in parallel with the human muscles to delay the onset of fatigue, without altering kinematic characteristics of human movements such as smoothness and accuracy.

To address these question, we present the development and evaluation of a wearable exosuit for assistance of the elbow joint and introduce a controller that compensates for gravitational forces acting on the limb while allowing the suit to cooperatively move with its wearer. We examine the feasibility of using the device to assist human movement by testing its effect on the kinetics and kinematics of healthy subjects. Subjects wore the exosuit and performed elbow movements in two conditions: with assistance from the device (powered) and without assistance (unpowered). The test

included a dynamic task, to evaluate the impact of the assistance on the kinematics and dynamics of human movement, and an isometric task, to assess its influence on the onset of muscular fatigue.

Powered movements showed a low but significant degradation in accuracy and smoothness when compared to the unpowered ones. The degradation in kinematics was accompanied by an average reduction of $59.20 \pm 5.58\%$ (mean $\pm$ standard error) of the biological torque and $64.8 \pm 7.66\%$ drop in muscular effort when the exosuit assisted its wearer. An analysis of the electromyographic signals of the biceps brachii during the isometric task revealed that the exosuit delays the onset of muscular fatigue.

The thesis then proposes an actuation paradigm to reduce the size and power consumption of soft wearable devices by independently controlling many degrees of freedom using a single electric motor (One-To-Many). In Chapter 6, we detail the design and functioning principle of this mechanism and test its performance on the soft exosuit for the elbow joint, comparing it with the performance obtained using a traditional DC motor. The exosuit powered by the One-To-Many actuator reduces the biological torque required to move the forearm by an average of 46.2%, compared to the unpowered condition, but negatively affects movement smoothness and accuracy. When compared to the DC motor case, it slightly deteriorates performance. Despite the technical limitations of the current design, the One-To-Many paradigm is a promising scheme to design lighter, more portable wearable robots.

The results of this thesis demonstrate a high potential of soft exosuits as tools for assistance of upper limb movements and propose an innovative method for enhancing their portability. Furthermore, the design process, control, and assessment methodology presented in the thesis can serve as a basis for the future development of exosuit and exoskeleton platforms.

Contents

List of Figures

List of Tables

Notations

Acronyms

QoL	Quality of life
DALYs	Disability-adjusted life years
ADLs	Activities of daily living
WPs	Work packages
EHPA	Exoskeletons for human performance augmentation
SPI	Spinal Cord Injury
DoF	Degree of freedom
MAS	Modified Ashworth scale
RoM	Range of motion
HRI	Human-robot interaction
MJT	Minimum jerk trajectory
BBBW	Beaglebone black wireless
SEA	Series elastic actuators
PTFE	Polytetrafluoroethylene
PE	Polyethilene
PID	Proportional integral derivative
RMSE	Root mean square error
MJT	Minimum-jerk trajectory
EMG	Electromyography
MVC	Maximum voluntary contraction
SPARC	Spectral arc length
RMS	Root mean square
MNF	Median frequency
ARV	Average rectified value
SEM	Standard error of the mean

nRMSE	Normalised root mean square error
OTM	One-To-Many
SMD	Single motor-driven
IVT	Infinite variable transmissions
DASA	Distributed Active-Semi Active
EM	Electro-magnetic
MR	Magneto-rheological
PWM	Pulse-width modulation

Constants and variables

m	Mass of the forearm and hand
g	Gravitational acceleration = $9.81\,\mathrm{m/s^2}$
l	Length of the forearm
l_c	Distance of the forearm's centre of mass from the elbow' axis of rotation
R	Radius of the elbow
θ	Elbow joint angle on the sagittal plane
$h_f(\theta)$,$h_e(\theta)$	Extension functions
$P(\theta)$	Tendons' position-dependent moment arm
f	Tension on the suit's tendons
M	Mass matrix
$C(\theta)$	Centrifugal and Coriolis matrix
$N(\theta)$	Gravity-related forces matrix
$Y(s)$	Admittance
ω_d	Desired rotational velocity of the motor
τ_g	Torque on the elbow due to gravity
τ_{exo}	Assistive torque on the elbow exerted by the exosuit
τ_{bio}	Biological torque on the elbow
$PWM(e(t_k))$	PWM operator
T_{PWM}	Period of the PWM signal
$e(t_k)$	Position/velocity error at time t_k
ω_{in}	Velocity of the prime mover
$u(t)$	Control signal
$\tau(e(t_k))$	Duty ratio function

Chapter 1

Introduction

1.1 The humble sea squirt

We move to reach, grasp, gesture, feel, touch, feed, discover, play, dance, communicate and speak. Movement is the only way we have of affecting the world around us, points out the distinguished neuroscientist Daniel Wolpert. In his beautiful TED talk in 2011, he addresses a simple and fundamental question: Why do we have a brain?
"If you think about this problem for any length of time, it is blindingly obvious why we have a brain. We have a brain for one and one reason only, and that is to produce adaptable and complex movements." [1].

Wolpert invites us to reflect that all living beings that move voluntarily have a brain, and all living beings that do not move, e.g. plants, do not have a brain. The clinging evidence, however, is a rudimentary creature: the sea squirt. It has a nervous system and swims in the ocean in its juvenile life until it finds a rock on which it settles and never leaves; upon doing so, it digests its own nervous system for food. Once it does not need to move, it does not have the luxury of having a brain.

The complexity of movement somewhat reflects the complexity of our brain. Both still raise more questions that we can not answer. Our limited understanding of how the central nervous system deals with movement is clear when comparing the dexterity of humans with that of state of the art robotic platforms (a humorous

demonstration can be found here). This gap has fundamental implications for helping those that have, to some degree, lost the ability to move independently.

1.2 Broken movement

Damage to the central nervous system can significantly affect one's ability to move, with drastic consequences for one's Quality of Life (QoL). Disorders of the nervous system account for approximately 28% of all years of life lived with disability worldwide [2]. These include, among others, disorders related to age, spinal cord injury, multiple sclerosis, traumatic brain injury and cerebral palsy, and stroke outweighs all others combined in terms of disability-adjusted life years (DALYs) [3]. Although epidemiological studies report controversial results, 30% to 60% of stroke survivors experience chronic movement dysfunction in the upper limbs 6 months after the stroke [4]. The distal parts of the limbs are known to be the most affected by persistent deficits, with weakness of voluntary contraction and hypertonus of the flexor muscles strongly reducing the ability to extend the joints [5]. Losing the remarkable and unmatched dexterity of our arms in manipulating and communicating severely hampers one's ability to accomplish simple, yet fundamental, activities of daily living (ADLs) such as eating, drinking and getting dressed.

The incidence of stroke increases significantly with age [6] and, as the lifetime expectancy rises, its prevalence and impact on society are expected to grow. Various strategies have been explored to improve motor recovery after stroke, and, so far, repetitively performing isolated [7] and functional [8, 9] movements in the acute phase of recovery has produced the best outcomes. These findings support the hypothesis that practice is the main leading factor in promoting synaptogenesis and brain plasticity [10].

Robots have been used to increase the intensity of practice and relieve therapists from the demanding task of manually assisting the patient. Robot-assisted therapy has shown encouraging results, comparable to the ones achieved with traditional therapy [11], while allowing greater patient compliance and a quantitative, more accurate monitoring of the subject's performance.

Unfortunately, currently available robotic platforms are not logistically capable of following the patient after discharge from physical therapy. Patients go back home, training stops and their conditions plateau or even deteriorate.

1.3 Out of sight, out of mind?

Only 5% to 20% of patients fully recover their lost motor function [12] before being discharged from physical therapy, and the great majority do not regain enough dexterity to be independent. Even those who do are at high risk of deterioration.

In a critical comment on the practices of physical therapy after stroke, MacLeod and Turner point out that by the 12^{th} month after the incident, one in six people loses the gains achieved in the first three months of training [13]. Among other factors, the lack of continuous monitoring and the abrupt interruption of training play a key role in the deterioration process.

In a thoughtful essay on the theoretical perspectives of neurorehabilitation, James Gordon states: *"It is easy enough to facilitate a certain pattern of movement. What is difficult is to get patients to use that pattern when they are carrying out some functional activity. This is the fundamental challenge facing rehabilitation therapists"*[14].

Despite this compelling evidence for the need of movement assistance after discharge from physiotherapy, the current contribution of robotic devices is limited to the clinical environment. Very little effort has been committed to design and evaluate a wearable robot that is simple and portable enough to be used both in a clinical setting and at home, in common daily activities. Most of the robots designed so far are made of a heavy and bulky frame. Their structural complexity makes them ideal to perform accurate movements and apply high forces on their wearers joints, but these same features cause them to be very poor candidates for daily use, outside of specialized clinics or research laboratories.

The use of soft materials could be a solution to this problem. Clothing-like exoskeletons, known as exosuits, for transmitting forces to the human body represents an appealing solution for human motion assistance. Their intrinsic compliance, low

profile and quasi-negligible inertia make them likely candidates for use on a daily-basis. The absence of a rigid structure, moreover, avoids the joint misalignment problem and makes the device completely transparent to human kinematics, resulting in a svelte, ergonomic and low power-demanding device.

Extensive work has been carried out to demonstrate the effectiveness of this technology for aiding locomotion, while very little research exists for the upper limbs, whose function in daily life is equally, if not more, important.

In this thesis, we present the design, control and validation of a soft exosuit for the elbow, with the aim of filling this research gap.

1.4 Motivation and aim of the thesis

1.4.1 Problem statement and hypotheses

Neuromuscular disorders such as stroke can significantly affect's one's ability to move, reducing independence in daily tasks, integration in social activities and affecting one's physical and psychological well-being. Robotic platforms have been shown to be effective tools in physical therapy, but their use is limited to the clinical environment. There is compelling evidence to suggest that patients might benefit from a robotic platform able to assist a patient not only in the clinical setting but also in a domestic environment, in activities of daily living.

This sets a number of strict design requirements on the weight, size, power consumption, ease of use, comfort and aesthetic impact of the assistive apparatus, that are unlikely achievable with a traditional rigid robot. While soft devices have been engineered for assisting locomotion, little effort has been devoted to design something similar for the upper limbs.

We believe that soft, lightweight clothing-like robots can be likely candidates to satisfy these requirements while effectively assisting the upper limbs. We aim at testing this paradigm on a simple but fundamental joint, i.e. the elbow, confident that the same principles can generalize to more complex joints like the wrist and shoulder.

- **H1**: We hypothesize that an exosuit working in parallel with the human muscles can reduce the effort that its wearer needs to exert to perform the movement and hold a position.
- **H2**: We hypothesize that an exosuit working in parallel with the human muscles can delay the onset of fatigue.
- **H3**: We speculate that the low inertia and intrinsic compliance of the suit will allow its wearer to move without significantly affecting his/her natural kinematics.

Addressing the engineering challenges to verify H1-H3 will bring us one step closer to verify the feasibility of exosuits as both tools for clinical therapy and for assistance in ADLs.

1.4.2 Aim of the thesis

The broad aim of this thesis is to design, build and validate a soft exosuit for supporting the arm, addressing hypothesis H1-H3, where the device needs to be lightweight, cosmetically acceptable, low-power consuming, comfortable and intuitive to use.

This objective involves the following work packages (WP), constituting the three building blocks of the thesis:

- **WP1: Design of the exosuit** – Design and realization of a soft, lightweight and comfortable robotic garment, able to support and assist arm movements.
- **WP2: Control of the exosuit** – Implementation of a control paradigm that allows the suit to move in concert with its wearer, while providing, in whole or in part, the power needed to perform the task.
- **WP3: Validation of the exosuit** – Design of an experimental protocol and performance indexes to evaluate the bio-mechanical and physiological response of the suit's wearer. This work package directly addresses H1-H3.

Reaching WP3 involves addressing a moderate degree of engineering challenges. This, as the reader might expect, was achieved more through a trial-and-error process rather than a strict scientific hypothesis-driven approach (Appendix A shows the "history" of the exosuit's design). In addressing the challenge of making the exosuit as light and low power-consuming as possible, we embarked in experimenting the feasibility of a novel actuation method; this is the topic of Chapter 6.

Common to all the objectives addressed in this thesis is the idea of evaluating the performance of the exosuit using, as a performance index, the bio-mechanical and physiological response of its wearer. We believe that keeping the human being in the loop is fundamental for an objective, data-driven and effective design of wearable devices.

1.4.3 Challenges

The specific technical challenge in designing an active exosuit for assistance of arm movements resides in designing the optimal robotic hardware and human-suit interface to effectively and comfortably transmit forces to the human body. The difficulty is imposed by the scarcity of studies addressing the same issue and by the unconventional fabrication techniques.

The control and validation work packages involved more methodological challenges. The controller needs to move in concert with its wearer while providing assistance, allowing for a comfortable, cooperative and sensitive interaction. These requirements are made more challenging by the non-linearities arising from the soft nature of the device and the inefficiency of the transmission.

1.5 Outline of the thesis

Chapter 2 presents an historical digression on the development of wearable robots. This section puts emphasis on the limitations of rigid exoskeleton and on the recent introduction of soft robotics in the field of wearable assistive devices. The aim of this chapter is to highlight the research gap that this thesis attempts to bridge.

The rest of the thesis is structured around the three building blocks mentioned in Section 1.4.2, with an additional chapter presenting an engineering solution to reduce the weight and power consumption of the actuation stage.

Chapter 3 presents the design process of the suit. This starts with an analysis of the requirements of the device, based on practical considerations, anthropometric data an an inverse dynamic model of the human arm. The results are used to dimension the actuation stage and the transmission. The design is further refined through a data-driven approach to reduce friction and backlash, maximize the stiffness of the suit and improve comfort.

Chapter 4 presents the design of the controller. The chapter introduces an overview of the methods used for force control of compliant robots, with emphasis on the constrains imposed by the non-backdrivability of the actuation stage. We evaluate the tracking performance, bandwidth and report on the efficiency of the suit.

Chapter 5 evaluates the physiological and bio-mechanic effects of the assistance of the exosuit on human movements. The testing is performed on a cohort of healthy subjects, using the suit with the controller described in Chapter 4 to execute static and dynamic tasks.

Chapter 6 present a method to reduce the weight, power consumption and volume of the actuation stage of a soft exosuit. This involves the design and control of a mechanism to independently move multiple degrees of freedom using a single electric motor. This new paradigm is compared to the design proposed in Chapter 3 using the methodology outlined in Chapter 5.

The last Chapter draws general conclusions on the work, highlights our major contributions and elaborates on the open questions and paths for future work.

Chapter 2

A brief history of wearable robots

This chapter aims at examining the literature of active wearable robots, with the aim of highlighting the research gap that will be addressed in this thesis. This is done through an historical excursus of the development of wearable robots, starting from the visionary designs of the late 1960s, to the commercialized products available today. We here focused on exoskeleton technology, purposefully overlooking end-effector designs, less likely to be used as portable assistive devices.

2.1 Early days

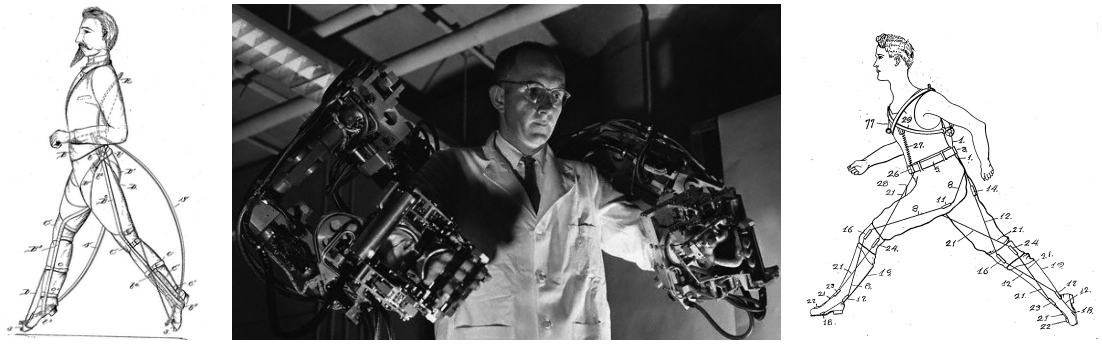

(a) (b) (c)

FIGURE 2.1: **First exoskeletons.** Among the first known designs of exoskeletal robotic devices are Yagn's spring-like structure, working in parallel with the human legs [15], shown in (a), Mosher's Hardiman [16], (b), and a tendon-driven exosuit's patent from 1919 [17]. From left to right, images from [15],[16] and [17], respectively.

In the never-ending quest to push the boundaries of their motor performance, humans have designed a wealth of wearable robotic devices. In one of the earliest recorded attempts to do so, in 1967, Mosher aspired to create a symbiotic unit that would have the "*...alacrity of man's information and control system coupled with the machine's power and ruggedness* "[16]. His design of the *Hardiman*, although visionary, ran into fundamental technological limitations.

Designing a robot that can successfully and effectively interface with the human body is indeed not a trivial task. As a matter of fact, most of the known early designs, dating back since 1890, never left the drawing board. The first design sketch of an augmenting exoskeleton was proposed by Yagn in the last decade of the nineteenth century [15], the system (shown in Figure 2.1.a) was a passive, bow-like structure operating in parallel to the user's legs, featuring a locking mechanism that was engaged in the stance phase of walking but allowed the users' leg to be free in the swing phase.
In 1963 Zarodney, from the U.S. Army Exterior Ballistics Laboratory, proposed a concept of possibly the very first powered exoskeleton conceived [18]. Although being only a concept paper, the work by Zarodney addressed some of the major issues involved in the design of a powered exoskeleton, namely the necessity of a portable power supply, the difficulty in interfacing with the human body, the effect on human motion kinematics and the fine sensing and control required.
The first powered prototype (shown in Figure 2.1.b) was brought from paper to hardware in the late 1960s by General Electric Research. The device was designed to drastically increase the wearer's strength (by a factor of 25) but weighted over 600 kg [16]. Most of the issues with the first prototype were never solved.
In the 1980s Jeffrey Moore proposed the design of a wearable robot to augment the capabilities of ground soldiers. This was most probably the work that planted the seed that then grew into the DARPA Exoskeletons for Human Performance Augmentation (EHPA) program.
Most of the state-of-the-art technology in exoskeletons was brought to us by the EHPA program. Even though 2 of the 3 major contributors to the program focused on lower limb exoskeletons, they highlighted some of the major limitations of rigid exoskeletons.
The Berkley Bleex, the Sarcos and the MIT Exoskeletons, all designed to assist the lower limbs, are the three most significant outcomes of the program launched in 2001. A key feature of the first two designs was to introduce energetic autonomy.

Moreover, they were successfully tested in ground-level walking, with the BLEEX having a power requirement of over 1300 W [19, 20] (compared to the 165 W of a 75 kg human adult).
The Sarcos was proven to be able to replicate complex actions such as kneeling, squatting, and carrying over 80 kg at a walking speed of 1.6 m/s [21, 22]. The high power requirements still clearly are a big limitation, even though their capabilities and performance have massively been improved.
The approach used in designing the MIT exoskeleton was inherently different: knowledge on the kinematics and bio-mechanics of human walking was used to significantly reduce the power requirements of the assistive device. The exoskeleton described in [23] only uses passive elements, i.e. springs and variable dampers, to assist walking, with a total weight of 11kg and an overall power consumption of 2 W. Nevertheless, wearing the exoskeleton resulted in a 10% increase in walking metabolic cost [24].
A key point here is that the increase in metabolic cost was identified to be mostly caused by the kinematic constrains imposed by the rigid linkage structure of the robot on the human joints. These were interfering with the natural and efficient dynamic of human walking, altering the metabolic cost of walking more than the added mass was.

2.2 Recent exoskeletons

In the last decade, advances in materials science, electronics and energy storage have enabled an exponential growth of the field, with state-of-the-art exoskeletons arguably accomplishing Mosher's vision [21]. Wearable robotic technology has been successful in reducing the metabolic cost of human walking [25, 26], restoring ambulatory capabilities to paraplegic patients [27], assisting in rehabilitating stroke patients [28, 29], harvesting energy from human movements [30] and helping to study fundamental principles underlying human motor control [31, 32].

The devices used to achieve these feats, some examples of which are shown in Figure 2.2, were all made of rigid links of metal and capable of accurately and precisely delivering high forces to their wearer. While this is undeniably an advantage, it comes at a cost: 1) a significant inertia, which affects both the kinematics of human movement and the power requirements of the device; 2) the need for the joints of

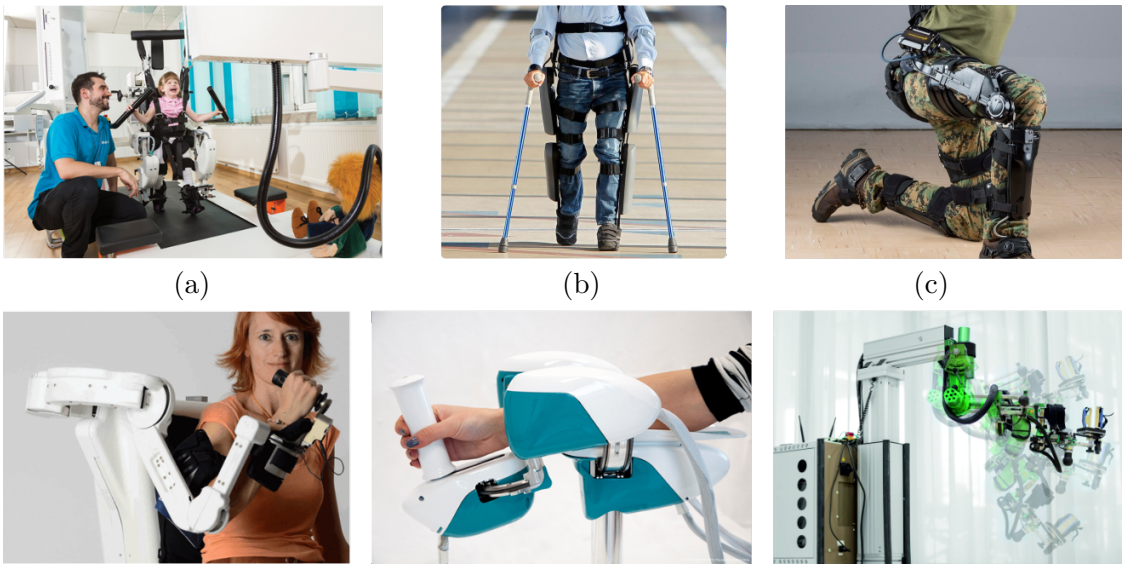

(a) (b) (c)

(d) (e) (f)

FIGURE 2.2: **Rigid exoskeletons.** Recently designed active exoskeletons are far lighter and effective and have been use in a plethora of applications such as rehabilitation, military augmentation and as tools to further our understanding of human movement. (a) LokomatPro, pediatric stationary exoskeleton for rehabilitation. Picture: Hocoma, Switzerland. (b) ReWalk personal 6.0 is a portable exoskeleton for walking assistance. Picture: ReWalk Robotics, Israel. (c) Lockeed-Martin ONYX helps soldiers carry heavier loads. Picture: Lockheed-Martin, US. (d) ALEX, a lightweight, tendon-driven exoskeleton for haptics and rehabilitation. Picture: PERCRO Lab, Scuola Superiore Sant'Anna, Italy. (e) The Wristbot is a 3DoF stationary robot for rehabilitation and study of proprioception. Picture from www.lorenzomasia.com. (f) ARMin is a stationary exoskeleton used for neurorehbilitation. Picture: SMS Lab, ETH Zurich, Switzerland.

the robot to be aligned with the biological joints [33], resulting in increased mechanical complexity and size [34]; 3) a strong cosmetic impact, shown to be linked with psychological health and well-being [35].

Despite the unquestionable progress of the last years, exoskeleton technology still struggles to become ubiquitous part of our daily lives. These devices are confined in research laboratories, expensive clinics and selected hospitals. The grates limitation probably lies in their complexity, responsible for increasing cost, weight and size. Part of this complexity comes from the need of a rigid exoskeleton to accurately accommodate the intricate motions of the human limbs and joints.

2.3 Attaching a robot to the human body

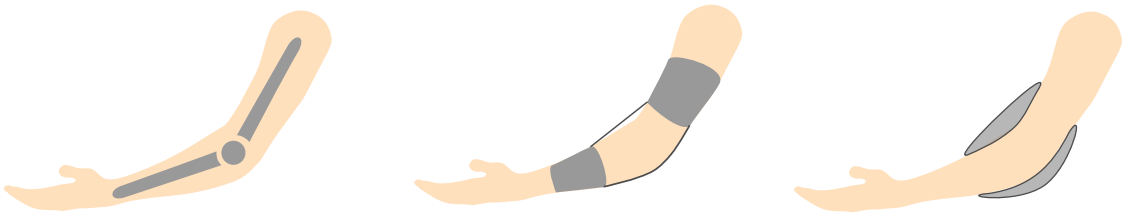

(a) (b) (c)

FIGURE 2.3: **Means of transmitting forces and torques to the elbow.** (a) The typical approach consists of using a rigid link, possibly aligned with the human joints. (b) One can apply a torque to the joint by tensioning a flexing or extending cable, attached on both sided of the joint using a clothing-like anchor point. This paradigm allows to locate the actuation stage away from the limb. (c) Pneumatic or hydraulic inflatable chambers, attached to the joint, can be pressurized to flex or extend the elbow.

"The exoskeleton is an external structural mechanism with joints and links corresponding to those of the human body."[36]. One of the first definitions of exoskeleton, dating 2007, assumes that a wearable anthropomorphic robot can be perfectly aligned with the joints and limbs of the human body (a schematic representation of this idea for the elbow joint is shown in Figure 2.3.a). This soon turned out to be a troublesome task.

Morphology of the human limbs and joints drastically varies between subjects and, for a given subject, the joint kinematics are very complex and cannot be imitated by conventional robot joints. Perfect alignment between the robot and the body is not achievable. This kinematic incompatibility leads to the generation of unwanted forces and torques at the Human-Robot Interface (HRI) that significantly affect the device's performance [37].

These parasitic forces can be reduced by trying to make the kinematics of the robot adaptable in the directions where one does not want to apply forces. The most common solution consists in adding passive degrees of freedom [34]. This comes at the cost of increased mechanical complexity and movement inertia.

For this reason, when designing a rigid exoskeleton, one needs to face the daunting trade-off between avoiding misalignment and making the device simple and portable enough to be used in daily scenarios.

2.4 Stronger, smarter, softer

(a) (b)

FIGURE 2.4: **Fluid-driven soft exosuits.**(a) Soft exosuit for the shoulder, driven by soft textile pneumatic actuators and (b) similar concept applied to assist Spinal Cord Injury (SPI) patients in grasping. Pictures: Wyss Institute, Harvard, US.

The recent introduction of soft materials to transmit forces and torques to the human body [38] has allowed to design wearable robotic devices on the other side of the spectrum: lightweight, low-profile and compliant machines that sacrifice accuracy and magnitude of assistance for the sake of portability and svelteness.

Soft exoskeletons, or exosuits, are clothing-like devices made of fabric or elastomers that wrap around a person's limb and work in parallel with his/her muscles [39, 40]. Characteristic of exosuits is that they rely on the structural integrity of the human body to transfer reaction forces between body segments, rather than having their own frame, thus acting more like external muscles than an external skeleton. Their intrinsic compliance removes the need for alignment with the joints and their low-profile allows to wear them underneath everyday clothing.

Exosuits actively transmit power to the human body either using cables, moved by electric motors (Figure 2.3.b), or soft pneumatic actuators (Figure 2.3.c), embedded in the garment. The latter paradigm was probably among the first to be proposed [41] and has been explored to assist stroke patients during walking [42], to increase shoulder mobility in subjects with neuromuscular conditions [43], to help elbow movements [44] and for rehabilitation purposes to train and aid grasping [45–47]. The devices detailed in [43] and [47] are shown in Figure 2.4.

(a) (b) (c) (d) (e)

FIGURE 2.5: **Tendon-driven soft exosuits.** (a) The Polyglove is a silicone-based wearable robot that uses a Bowden cables and a flexible structure to assist SPI patients in grasping. (b) The same group developed a fabric-based glove to achive the same goal. (c)-(d)-(e) The Superflex from SRI, the exosuit from the Wyss Institute at Harvard and the Myosuit from Myoswiss, shown from left to right, all use electric motors, driving tendons routed in the fabric, to assist locomotion.

Cable-driven exosuits (Figure 2.5), instead, include a DC motor that transmits power to the suit using Bowden cables. This flexible transmission allows to locate the actuation stage where its additional weight has the least metabolic impact on its wearer. Using this paradigm to provide assistance to the lower limbs has resulted in unprecedented levels of walking economy in healthy subjects [48] and improved symmetry and efficiency of mobility in stroke patients [49]. Similar principles were used to provide active support to hip and knee extension, reducing activation of the gluteus maximus in sit-to-stand and stand-to-sit transitions [50].

Cable-driven exosuits seem to work particularly well for lower-limbs movements, where small bursts of well-timed assistance can have a big impact on the dynamics and metabolic cost of locomotion [51]. Yet, Park *et al.* have shown that they have the potential for assisting the upper-limbs in quasi-static movements too: using a

tendon-driving mechanism, a textile interface and an elastic component they found a significant reduction in the activity of the deltoid muscle when supporting the weight of the arm [52].

2.5 Research gaps

Considerable work has been done by the Harvard Biodesign Lab to engineer soft exosuits for the lower limbs [53]. Walsh and colleagues have has defined a set of principles to be used to successfully design a wearable, textile based robot for the lower limbs. Similar work for the upper limbs has not yet been done, and is the topic of Chapter 3.

The current soft robotics landscape lacks of methods for controlling these upper limb exosuits. The device proposed by O'Neill *et al.* [43] and Park and colleagues [52], for example, are tested in static configurations, with a fixed force delivered by the suit's actuators. In contrast to the abundance of algorithms to detect the phase of walking and deliver assistive forces accordingly, the literature lacks of ways to detect the user's intention and move the device in a suitable way. This is understandable if one considers the rhythmic nature of walking, that allows to anticipate, with a good degree of accuracy, torques and joint trajectories. Addressing this issue is the objective of Chapter 4.

Similarly, while there is extensive work on the analysis of the effects of wearing a soft exosuit on the kinematics, energetics and muscular activation during walking [54], the authors are unaware of comparable studies on movements of the upper limbs, whose variety of volitional motions is fundamentally different from the rhythmic nature of walking. This is the aim of Chapter 5.

Chapter 3

Design principles

This chapter presents the design of the suit. An overview of the complexity of the elbow and the kinematic and dynamic requirements of the joint serve as basis for the subsequent sections. These present, in detail, the design of the suit, transmission and actuation stage of the device. The suit is then characterized and its materials are chosen to achieve high efficiency, control performance and comfort.

3.1 Anatomy of the elbow joint

The elbow is a synovial joint between the humerus, in the upper arm, and the radio and ulna in the forearm, that allows the forearm to be moved towards and away from the body. The joint is made up of three junctures, namely the humeroulnar joint, the humeroradial joint and the proximal radioulnar joint. To a first approximation, these are modelled as a simple hinge joint. Fairly recent studies, however, have shown that the joint also includes laxity [55], that causes it to behave like a loose hinge joint.

Over its range of motion, the elbow axis is not fixed but moves along the surface of a double conic frustum (shown in Figure 3.1.b). The frustum's vertex angles on the frontal and horizontal plane, indicated in Figure 3.1.b by β_u and β_h, respectively, vary among subjects and depend on the flexion mode, i.e. if the elbow is being moved actively or passively, on the forearm position and any varus or valgus torque on the joint. The frustum vertex angles β_u and β_h can assume values up to 10 deg.

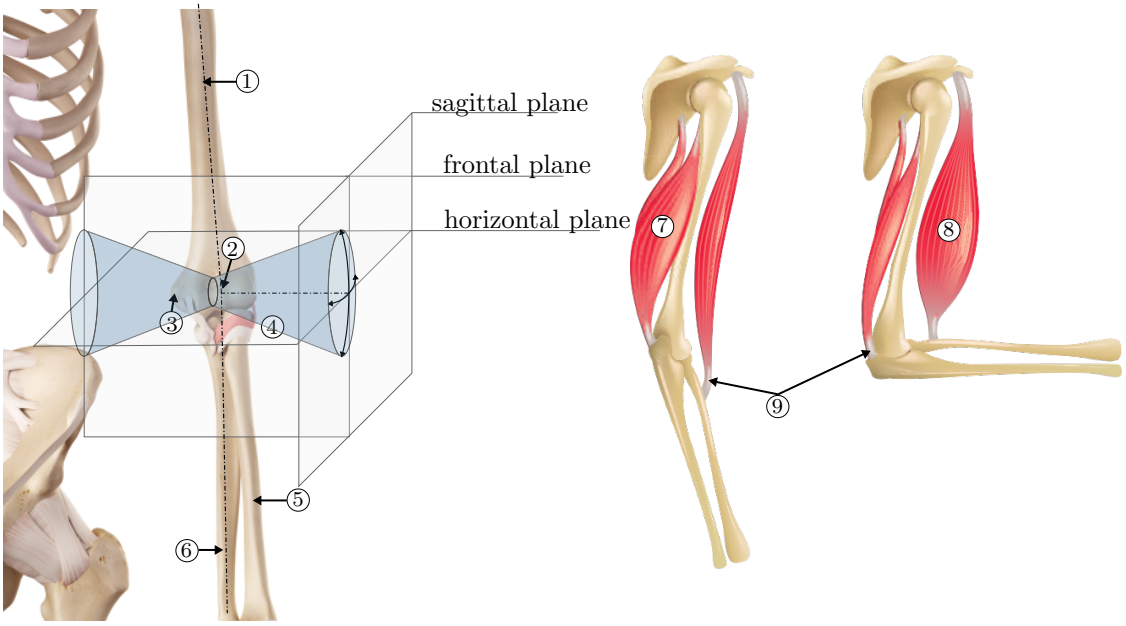

FIGURE 3.1: **Anatomy of the elbow joint.** Double conic frustum, spanning the surface that the joint's axis moves along during elbow flexion/extension.

In addition, the axis of rotation of the joint forms an angle of 80-92 deg with the axis of the humerus A_h on the frontal plane and a varying angle of ± 5 deg with the medial-lateral anatomic axis A_{ml} on the horizontal plane [55].

This complexity is usually overlooked when designing an exoskeleton robot that assists the elbow, with the valid argument that pragmatism should be prioritized over complexity. The work by Vitiello *et al.*, however, uses a different approach and accounts for the elbow's laxity to avoid misalignment. This resulted in an exoskeleton with 13 passive Degrees of Freedom (DoF) and 1 active one, to assist elbow flexion/extension. Despite being an extreme case, this highlights the challenges of comfortably fitting a rigid robot to the human body, even for a simple joint like the elbow.

When designing a soft wearable robot, on the other hand, one needs not worry about these issues: by definition, the device does not have its own kinematic chain and will rely on the skeletal structure of its wearer to transmit forces or torques to the limbs and joints.

It is interesting to observe how the two main muscles moving the elbow joint, namely the biceps and triceps brachii, transmit power to the skeletal structure. The biceps originates proximally from the coracoid process and supraglenoid tubercle of

the scapula. These two heads converge in a single tendon and attach to the radial tuberosity distally. The triceps brachii originates in the the infraglenoid tubercle of the scapula and the back of the humerus and converge to a single tendon to insert onto the olecranon process of the ulna.

It is said of the 16^{th} century polymath Leonardo Da Vinci, that *"when he dissected a limb and drew its muscles and sinews, it led him to also sketch ropes and levers"*[56]. Indeed, skeletal muscles in our body work like an actuator-tendon couple.

3.1.1 On the choice of a tendon-driven design

This observation above was among the factors that led us to choose to design a tendon-driven exosuit rather than a fluid-driven one (this distinction is shown in Figure 2.3): tendon-driven transmissions seem to have survived the pitiless selection of nature.

Unlike direct-drive setups, cables allow to locate the actuator away from the joint. This has the advantage of reducing the added mass on the limb, without sacrificing power. This is obvious, for example, if looking at the muscles that move our hands: nearly all of them are placed in the forearm and transmit power to the fingers through an intricate network of tendons. In a portable device and with the use of Bowden cables, this further allows to choose the location of the actuation stage, possibly where it least impacts on the metabolic cost of moving.

The third reason is that electric motors are more easily controllable than hydraulic or pneumatic soft actuators. With off-the-shelves electronics and with now ubiquitous and high-power-density Lithium polymer batteries, one can supply and control high power motors in a contained volume and weight. A fluid-driven system requires a source of pressure for the fluid, making it hard to satisfy the portability requirements of a mobile platform.

3.2 Design requirements

Defining the requirements of soft wearable devices for clinical use is still an open question. So far, exosuits have been proven to be effective increasing the efficiency

FIGURE 3.2: **Design requirements.**

of movement in unimpaired subjects [48] and have shown to yield improvements in key gait metrics in stroke patients [57, 58], but complications such as severe spasticity and/or disuse osteoporosis–a localised bone loss condition due to reduction in mechanical stress, common in stroke patients– might cause such devices to perform rather poorly.

In this study we thus assume that our elbow exosuit will be used for assisting people suffering from muscle weakness but having no major spasticity or contractures (Modified Ashworth Scale (MAS) 0-2). Figure 3.2 gives an overview of the requirements that a soft assistive device for assistance in ADLs needs to fulfill. Our design objective are based on the average dynamic and kinematic requirements necessary to perform ADLs (range of motion, torque, speed) alongside reasonable practical considerations on the weight, size, adaptability and safety of the system.

3.2.1 Dimensions and force and motion characteristics

Range of motion

It is, first of all, fundamental for the device to span the whole range of motion (RoM) of the human joints. Magermans *et al.* [59] analysed the range of motion of the elbow and shoulder in non-impaired subjects, finding a mean of 146 deg (0 deg corresponding to the fully extended configuration) for the elbow.

Kinetics and kinematics

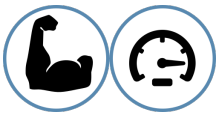

Similarly, a wealth of studies have evaluated torques and average speeds of human joints in ADLs. Elbow flexion can require up to 4.45 N m, with a mean of 1 N m [60] for male adult. Average peak velocities of movement are 126 deg/s [61], neglecting fast ballistic movements. Assuming a sinusoidal motion with a peak to peak movement equal to the RoM, these correspond to a frequency of movement of 1.2 Hz.

Assistance level

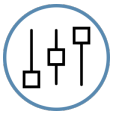

The suit was designed with the aim of supporting the aim of the forearm in ADLs. To do this, the controller applies a position-dependent torque equal and opposite to gravity. The mass of the forearm and hand of each subject was, again, estimated from anthropometric data, from the wearer's weight (more details in Chapter 4). A knob was used to allow the user to adjust the percentage of assistance received.

Weight

Being portability one of our main goals, we require the total weight mounted distally to be negligible when compared to the limb's weight (on average,1.52 kg for females and 2.56 kg for males [62]); an acceptable value would be 0.3 kg. This can be easily achieved if the motors, controller and

battery are located proximally (i.e. in a backpack or on a belt at the waist) and transmit forces to the joint via Bowden cables. A reasonable upper-limit for the proximally-located part of the system, comprising the motor, controllers and power supply, is 2.5 kg.

Safety

Because of the intrinsic compliance of its transmission, the suit benefits from the features of traditional series elastic actuators: its elasticity decouples the actuator's rotor inertia from the limb, should an impact occur, and the low impedance is preserved even in case of failure. The low mass of the device, moreover, practically eliminates inadvertent damage to the environment. A second layer of safety should, nevertheless, be added in the controller, to prevent the motor from exerting extremely high forces on the tendons or moving the elbow at a high speed. This requires at least a force sensor, preferably located distally (e.g. on the joint) and a position sensor to estimate the velocity of movement of the limb.

Size

The size of the initial design was based on the 50^{th} percentile of anthropometric data of healthy adult males. The suit, however, was designed to be adaptable, and should be replicated in at least threes sizes. Table 3.2 reports the anthropometric data used for the first design. Values were extracted from [63], for combined sexes of healthy subjects above 18 years of age.

Table 3.1: Anthropometric data

Body segment [mm]	Percentile	
	50^{th}	95^{th}
Upper arm length	318	344
Upper arm circumference	275	315
Forearm length	251	280
Forearm circumference	248	280

Comfort

Schiele and colleagues found a correlation between the pressure of the cuffs of an exoskeleton at the interface with the skin and a qualitative measure of comfort [64]. Exoskeleton users preferred pressures between 10 kPa and 30 kPa and did not perceive any difference in comfort for values below 30 kPa. The authors inferred that a good attachment pressure should be around 20 kPa. Pressures above 50 kPa, moreover, should be avoided, as they can affect blood circulation to the skin [65].

Technical

The suit has to fulfill all the technical requirements to allow it to be functional, durable and effective. These include aspects of the hardware as well as positioning of the sensors to allow the implementation of state-of-the-art Human-Robot-Interaction (HRI) control principles:

- Design-load bearing components with a safety factor of 2 to achieve durability.
- Choose transmission materials that have low backlash.
- Choose transmission materials with low friction.
- Locate the actuation stage far from the limb to reduce inertia of moving components.
- Locate sensors distally, to measure forces and positions after the transmission.

3.2.2 Modelling

Because of our choice of locating the tendon-driving motor distally, the dimensioning process of such motor requires to model the mapping between joint movement and motor torque. We did so using an inverse dynamics, second-order model of the elbow, and a simplified representation of the tendon-routing. The results provide us with guidelines to choose the power, torque and velocity of the actuator and estimate the magnitude of the forces being transmitted through the tendons. These

are used for choosing the hardware and materials that allow effective and safe use of the exosuit.

To evaluate the actuator's power requirements we use a bi-dimensional model of the elbow on the sagittal plane. The elbow is modelled as a hinge joint, with the forearm thus being a simple pendulum, as shown in Figure 3.3, and assuming the arm to be aligned with the direction of gravity.

Starting from the Lagrangian form one can derive the dynamics of the elbow in the joint space:

$$M\ddot{\theta} + C\dot{\theta} + N(\theta) = \tau \tag{3.1}$$

where M is the inertia of the forearm, C is defined as the Coriolis matrix and $N(\theta)$ is a column vector that takes into account gravitational forces. The vector τ expresses the external torques applied on the joints which, in our case, results from the force applied by the artificial tendons routed in the suit as shown in Figure 3.3. Although the suit is meant to work in parallel with its wearer's muscles, we hereby neglect the muscular torque and analyse the worst-case scenario where only the robot is providing energy.

A mapping from the tension in the tendons to the torque on the joints can be derived using geometrical considerations on the tendon's routing; referring to Figure 3.3, we can derive the extension function $h(\theta)$, projecting the elbow's joint angle to a corresponding displacement of the tendons:

$$h_f(\theta) = 2\sqrt{a^2 + b^2}\cos\left(\phi + \frac{\theta}{2}\right) - h_{f0} \tag{3.2}$$

$$h_e(\theta) = R\theta. \tag{3.3}$$

Where h_f is the extension function for the flexor and h_e for the extensor tendon, a is half the width of the arm, b is the distance of the anchor point from the joint's centre of rotation, $\phi = \arctan(a/b)$ and R is the radius of the joint. The constant h_{f0} assures that the extension functions are null when the arm is fully extended.

Using the principle of conservation of energy, the function $h(\theta) = [h_f(\theta), h_e(\theta)]^T$ can be used to find a Jacobian-like matrix $P(\theta)$, which we shall call *coupling matrix*, mapping tension in the tendons to torques on the joint:

$$\tau = P(\theta)f \tag{3.4}$$

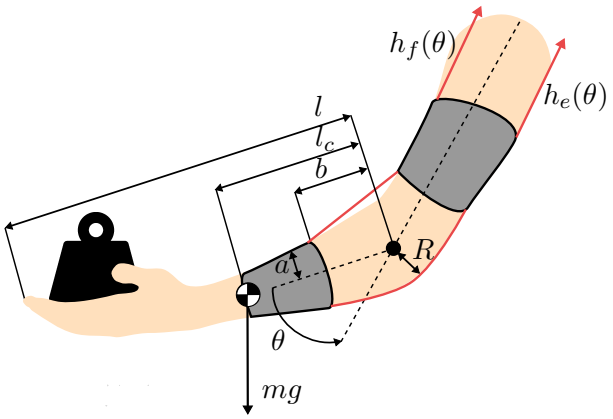

FIGURE 3.3: **Planar model of the elbow on the sagittal plane**

$$P(\theta) = \frac{\partial h}{\partial \theta}^T(\theta) = \left[-\sqrt{a^2+b^2}\sin\phi + \frac{\theta}{2}, R\right] \tag{3.5}$$

where $f = [f_f, f_e]$ is the tension on the flexing f_f and extending f_e tendons.

By substituting (3.4) in (3.1) we obtain:

$$M\ddot{\theta} + C\dot{\theta} + N = Pf, \tag{3.6}$$

where we have removed the dependency on θ for the sake of conciseness.

Finally, we include a term modelling losses due to friction, not negligible in Bowden cable systems. The main parameter affecting the entity of such losses is the bending angle of the outer housing. Assuming that the contact between the inner cable and the outer sheet can be modelled as the sliding of a cable over a fixed cylinder, the force transmission efficiency becomes:

$$f_{in}/f_{out} \approx e^{-\mu\phi}, \tag{3.7}$$

with μ being the friction coefficient between the cable and the outer sheet, ϕ the total wrap angle of the outer sheath of the Bowden cable, and f_{in}, f_{out} the tension in the cable before and after the transmission respectively. Assuming the actuator to be carried in a backpack, a reasonable and abundant estimate of the wrap angle is π. Using a teflon-steel static friction coefficient yields to an efficiency of $\approx 40\%$.

The requirements are summarised in Table 3.2.

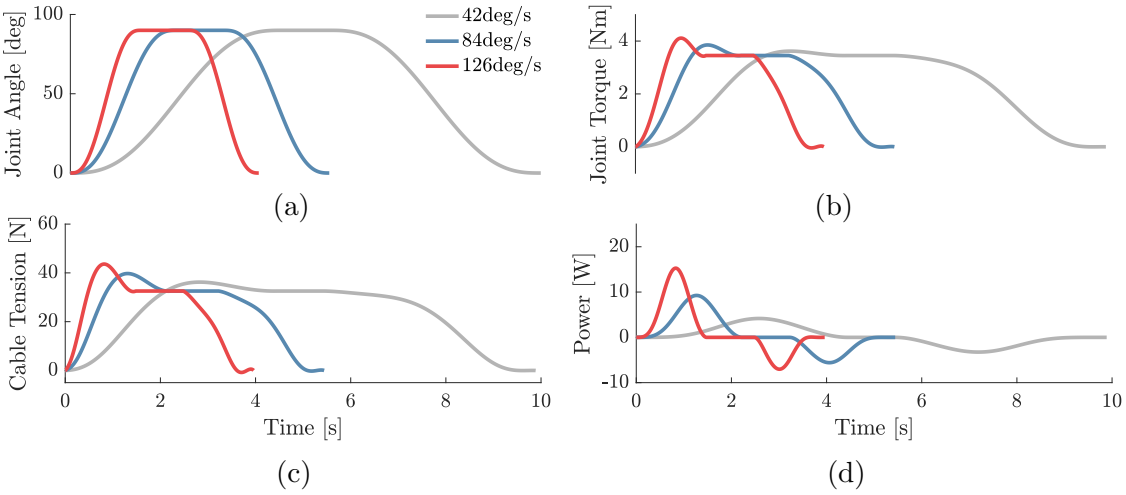

FIGURE 3.4: **Solution to the dynamics of the elbow joint for varying velocity of movement**. (a) Equation 3.6 was solved for minimum-jerk trajectories requiring 5,4,3 and 2 s to cover the whole range of motion of the elbow joint. (b) Torques on the elbow joint required to follow the corresponding trajectory of the joint. (c) Tension in the flexor tendon of the soft exosuit for varying velocity of the elbow joint. (d) Motor power consumption for varying velocities of the elbow joint, accounting for the losses in the transmission due to friction, as described by Equation 3.7.

3.3 Design description

3.3.1 Suit

The exosuit for assistance of the elbow joint presented in this thesis (shown in Figures 3.5.a,b) comprises of three fabric straps: one around the forearm (distal anchor point), one around the arm (proximal anchor point) and a shoulder harness, connected to the arm strap via adjustable webbing bands. Buckles, velcro straps and a Boa lacing system allow to tighten the suit.

A pair of Bowden cables transmits power from an actuation unit to the anchor points. The Bowden cables sheaths (Shimano SLR, ⌀ 5 mm) are attached to the arm strap, while their inner tendons (Dupont, Black Kevlar Fiber, 136 kg max load) to the forearm strap. When either of the two tendons is shortened, it pulls together the two anchor points, applying a flexing or extending moment on the elbow.

The shoulder harness is connected via inextensible webbing bands to the arm strap, covers the shoulder and encircles the chest; its purpose is to prevent the arm strap

TABLE 3.2: System requirements

Requirements	**C**haracteristics
Force/Motion:[59–61]	
Range of motion [deg]	146
Joint torque [N m]	4.45
Peak velocity [deg/s]	126
Cable tension [N]	100
Motor power [W]	50
Practical considerations:[62]	
Distal frame weight [kg]	0.7
Proximal pack weight [kg]	$\leq$2.5
Safety	Compliance Torque limit Speed limit Stop button
Size	50^{th} percentile healthy male
Comfort	Pressure peaks $\leq$ 30 kPa
Technical	Safety factor = 2 Low friction Low backlash Proximal motor Non collocated sensors

from migrating towards the center of the joint by relying on reaction forces from the shoulder and ribcage. The same is achieved for the forearm strap by tightening it with a boa lacing system, the conic shape of the forearm contributes to prevent slippage.

The proximal and chest straps were made by modifying a commercially available passive orthosis (Master-03, Reh4mat). Their substrate is made of a 3-layered fabric: an external layer used to attach hard components (buckles and webbing strips), an intermediate ethylene-vinyl acetate (EVA) foam to avoid peaks of pressure and an internal 3D polyamid structure to provide air permeability. The distal anchor point consists of a flexible plastic sheet, lined with ballistic nylon and covered by a 3 mm-thick layer of polyethylene (PE) sponge at the interface with the skin. A load cell (Futek, LCM300), secured on the distal anchor point, measures the tension in the flexing tendon and an absolute encoder (AMS, AS5047P, 1000 pulses/rev),

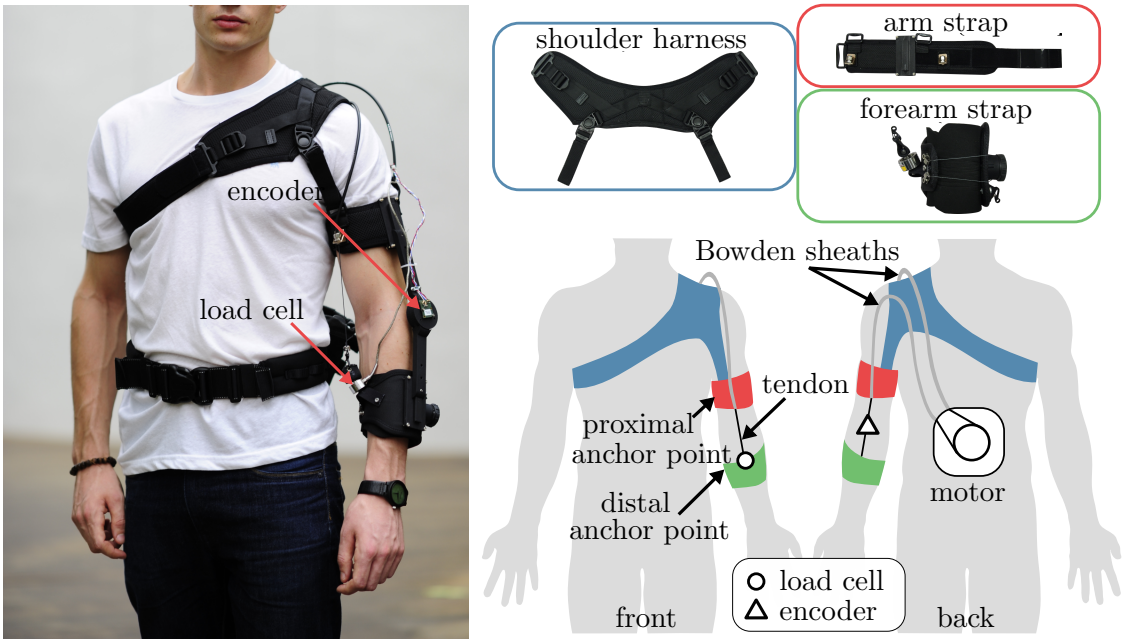

(a) (b)

FIGURE 3.5: **Design of the soft exosuit for the elbow.** The exosuit comprises three straps that wrap around the shoulder, arm and forearm, highlighted in blue, orange and green, respectively. The last two act as anchor points: the Bowden cables' outer sheath is attached to the arm strap and the inner tendons to the forearm strap. A load cell and an encoder sense the interaction force and the elbow position.

mounted on a 3D-printed joint (Shapeways, versatile plastic) between the arm and forearm straps, senses the angular position of the elbow. The plastic joint, featuring a rotational Degree of Freedom (DoF) at the elbow and a translational DoF at the distal anchor point, bears no loads and does not transmit torque. It thus serves the purpose of a goniometer without altering the fundamental characteristic of an exosuit: to rely on the structural integrity of the human joint to transmit forces between body segments.

3.3.2 Tendon-driving unit

The unit actuating the Bowden cables is shown in Figure 3.5.c. It consists of a brushless electric motor (Maxon, EC-i 40, 70 W) in series with a planetary gearhead (Maxon, GP 32, 55:1), capable of delivering up to 8.5 N m of continuous torque at the elbow joint (sufficient for activities of daily living [60]), and whose angular position is monitored by an incremental encoder (Scancon, 2RMHF, 5000 pulses/rev).

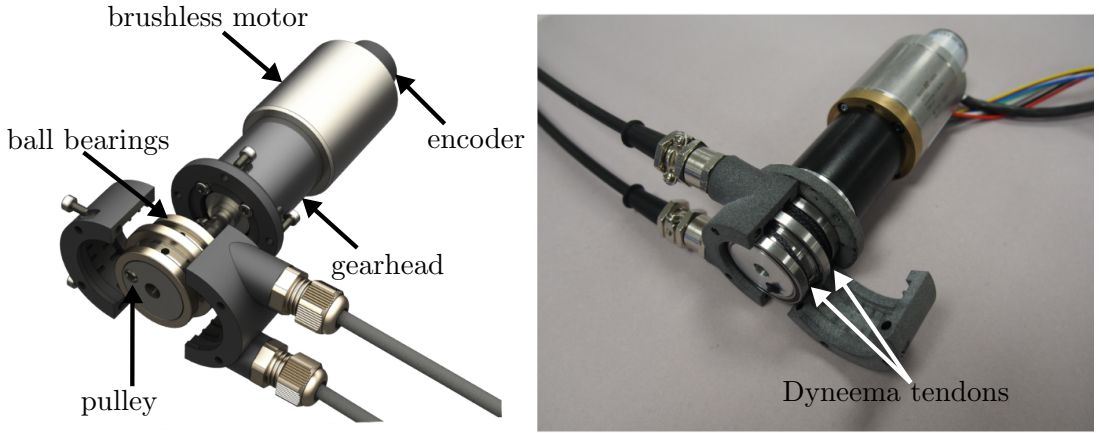

FIGURE 3.6: **Exploded view and photo of the actuation stage.**

The gearhead's output shaft drives a pulley around which the two tendons are wrapped in opposite directions, in an antagonistic fashion. The pulley is enclosed in a plastic casing; three ball bearings between the pulley and the plastic prevent the tendons from derailing when they are slack.

3.4 Electronics

The suit is controlled through a modular and scalable system architecture called FlexSEA, depicted in Figure 3.7, and positioned in a plastic casing, worn as a backpack. The FlexSEA controllers allow faster prototyping and easy scalability compared to commercially available motor drivers [66].

The system is composed of a low-level layer devoted to motor control and power management and a high-level layer for data storage, streaming and high-level control strategy settings. The low-level layer includes the FlexSEA Execute and the FlexSEA Battery boards.

The Execute board drives the brushless motor at a frequency of 10 kHz, taking care of motor commutation, data acquisition (motor encoder, stretch sensor and load cell) and it runs the gravity compensation control proposed in this work at a frequency of 1 kHz. The entire system is powered by a 22.2 V LiPo Battery, interfaced via a FlexSEA Battery board, that controls the battery's voltage level, preventing damages due to under-voltages and limiting the output current.

The high-level layer is composed by the FlexSEA Manage and the BeagleBone Black Wireless (BBBW) boards. We use the FlexSEA Manage simply as as a communication bridge between the Execute and the BBBW for this application, yet the Manage allows to connect up to 4 Execute boards, hence scaling the architecture for controlling more DOFs very efficiently.

The BBBW has two main functions: wireless streaming of data to a portable PC and management of control parameters.

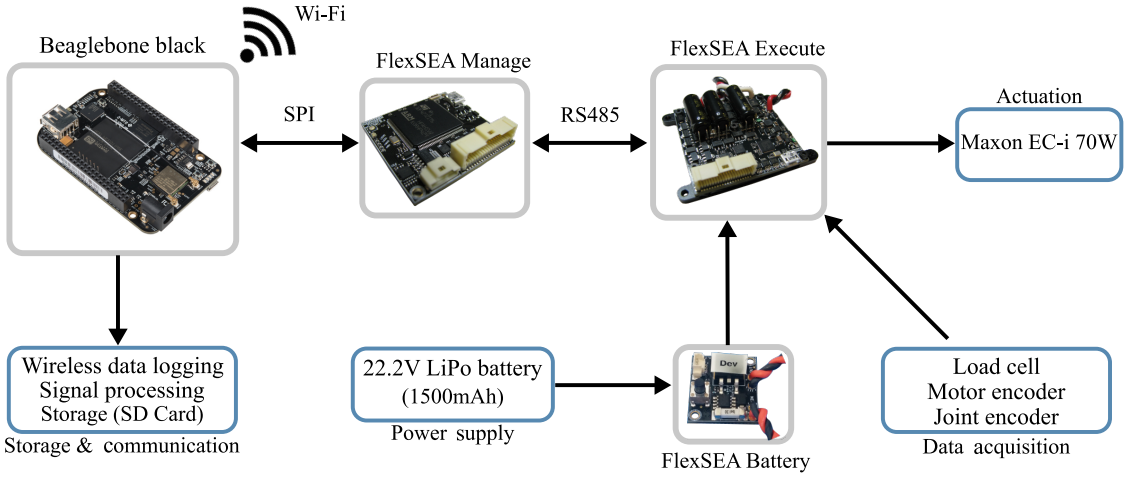

FIGURE 3.7: **Diagram showing the embedded modules used to control the soft exosuit.** The FlexSEA controllers, design specifically for wearable robotic applications, are modular boards that enable fast prototyping and easy scalability [66]. A commercially-available single board computer (Beaglebone Black Wireless) allows to wirelessly interface the exosuit with a portable PC, for data logging and tuning of control parameters.

3.5 Characterization

3.5.1 Suit stiffness

The suit's straps, the Bowden cables and the soft human tissues introduce a fair amount of elasticity in the transmission of power between the motor and the user's skeletal structure (Figure 3.8.a). Elastic interfaces absorb and release energy, affecting the phase and magnitude of the power transferred to the user [68]. Characterizing this stiffness is both important for quantitatively assessing the effect of design changes on the suit's performance and has valuable implications for control.

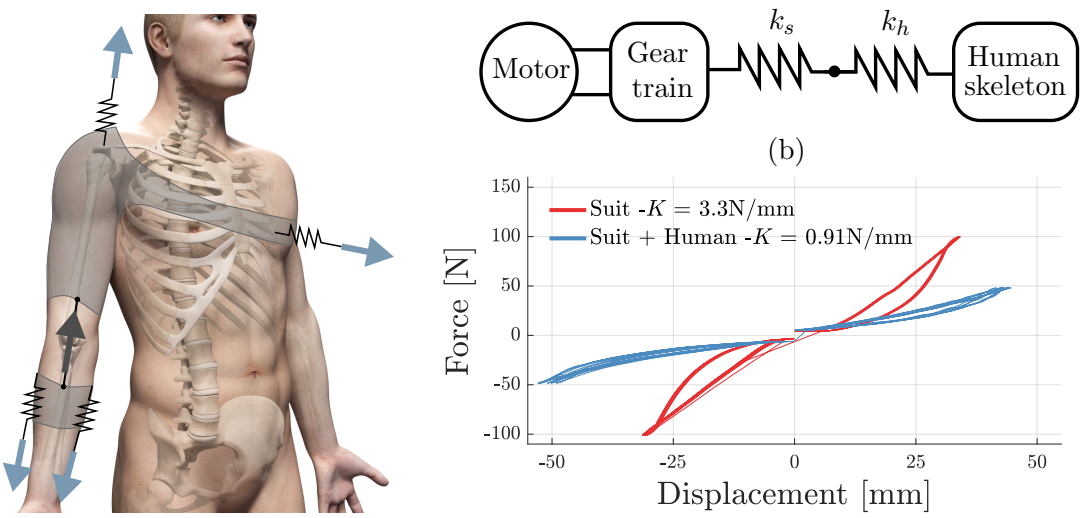

FIGURE 3.8: **Suit stiffness.** (a) Simplified schematics of the transmission of forces from the suit to the human body. Upon tensioning the suit, reaction forces from the body mostly occur at the distal anchor point, in the shear direction, on the shoulder and along the chest strap. All these points are not directly in contact with the bones. The soft underlying tissues introduce compliance. (b) Model of the transmission of forces from the motor to the human skeleton. The two main sources of elasticity are the suit and the human tissues, modelled here as two linear springs in series. This configuration closely resembles the working principle of Series Elastic Actuators (SEAs). (c) Suit's (red) and human+suit's (blue) stiffness, measured using the methodology describe in [67].

Quinlivan and colleagues proposed a method for assessing the stiffness of the exosuit and of the underlying human tissue [67]. The procedure consists in assuming the compliance between the motor and the user's skeletal structure can be modelled as two linear elastic elements in series (Figure 3.8.b), one given by the suit k_s, i.e. Bowden cables and fabric straps, and the other one accounting for the compliance of soft human tissues k_h. The hypotheses of linearity and pure elasticity are weak ones, but sufficiently approximate for the purpose of this analysis.

One can separate these two by first finding k_s alone, when the suit is worn by a rigid mannequin, and then estimating k_h from a similar analysis on human subjects. Figure 3.5.c shows a characterization of the exosuit's stiffness on a rigid mannequin (red) and on a subject (blue), using the methodology described in [67]. The stiffness can be derived by commanding the suit's motor to apply a linearly increasing force form 0 N to 100 N (mannequin) and 50 N (human) and back, on the flexing and extending tendons of the suit, and measuring its displacement with the encoder on the motor's axis. This was done on a rigid fiberglass mannequin (red) and on 5

human subjects (blue), performing 10 cycles of loading-unloading, with the elbow fully extended.

Force tracking was achieved using an indirect force control paradigm, described in Chapter 4. Data acquisition and high-level force control were implemented in Matlab Simulink (Mathworks, MA, USA) on a real-time acquisition board (Quanser QPIDe) at a sampling frequency of 1 kHz. Low-level velocity control was run on an EPOS2 50/5 motor controller (Maxon Motor, CH), at a refresh rate of 1 kHz.

The suit has a quasi-linear behaviour in the loading phase and a non-linear behaviour when unloaded, in both flexion and extension. A least-square linear approximation of its stiffness yielded a value of 3.3 N/mm on the mannequin and 0.91 N/mm as a mean over subjects, on the human body. This means that, in the tested configuration, k_s=3.3 N/mm and k_h=0.71 N/mm.

It is interesting to note that, since the two springs are in series, the equivalent resulting elasticity will be governed by the most compliant one. This has interesting implications for the design of the exosuit: although it is desirable, for efficiency and position-control performance, to have an as-stiff-as-possible suit in the direction of transmission of forces, any effort to do so will be invalidated by the low compliance of the underlying tissues.

While on one hand this series-elasticity is an undesirable property because it lowers transmission efficiency and position-control bandwidth, on the other it introduces well-known advantages in terms of safety and force control accuracy and stability [69].

3.5.2 Bowden cables

Bowden cables provide a flexible means of locating the motor away from the joint. This is a key feature of the exosuit and what allows it to be lightweight and ergonomic. However, Bowden cables introduce a range of non-linear phenomena in the transmission. These include losses due to friction, stick-slip phenomena, backlash and compliance. These non-linearities introduce significant tension losses across the cable and give rise to motion backlash, cable slack, and input-dependent stability of the servo system [70, 71]

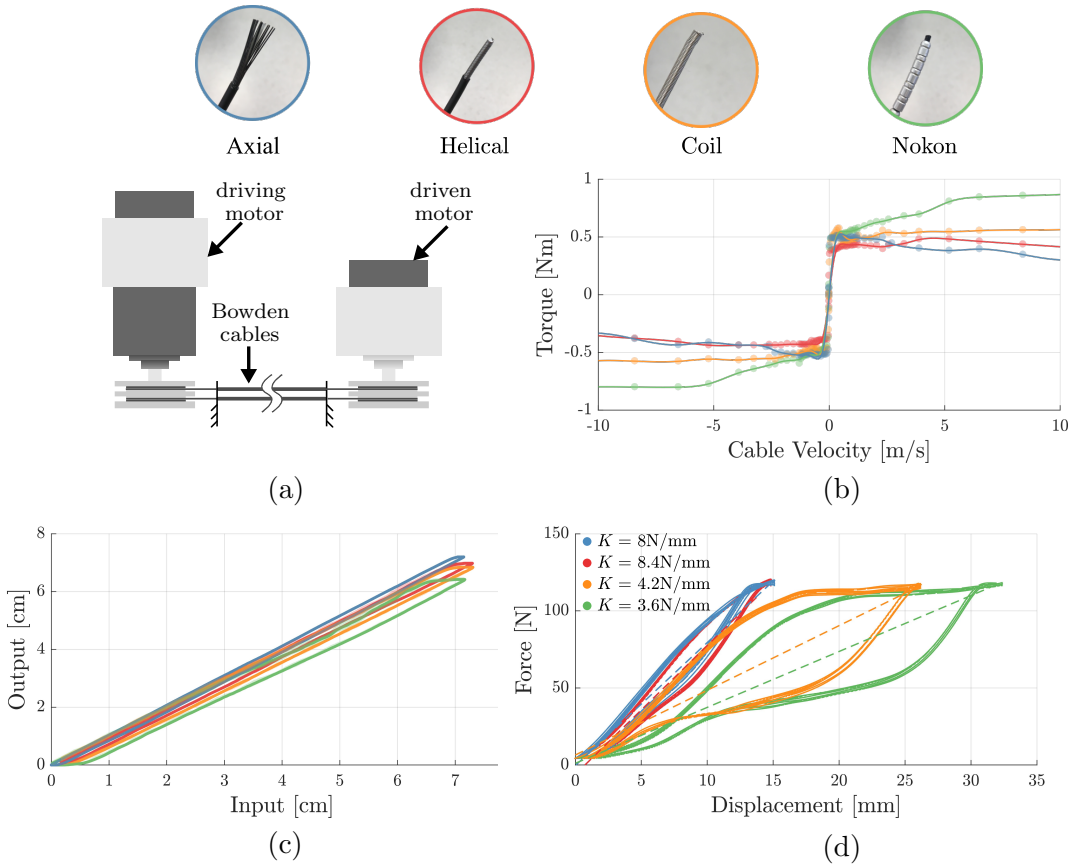

FIGURE 3.9: **Characterization of the friction, backlash and stiffness of different Bowden cables.**(a) Setup used to study the amount of friction and backlash of in the Bowden cables. A drivng motor was controlled in velocity for the friction study and position for the backlash one, while a driven motor applied a load of 50 N on the cables. To find stiffness, the driven motor was replaced with a load cell. (b) Friction curves for the Bowden cables, shown for the color-coded constructions above. (c) Backlash-hysteresis curves for a cyclical displacement of the cable of 7 cm. (d) Stiffness of the Bowden sheaths, measured as the relation between tension in the inner cables and displacement of the driving motor. The Bowden sheath construction with steel strands oriented along its axis exhibited the best performance.

A common approach, and one that our research group has previously explored [72, 73], consists in identifying the characteristics of such phenomena and compensating them in the implementation of the controller. A range of analytical methods have been proposed to model the nonlinear characteristics of Bowden cables [74]. These non-linearities, however, are known to be dependent on the total wrap angle of the outer sheaths of the Bowden cables that, in our application, continuously vary. This is true for both backlash hysteresis, friction and variations in stiffness. In previous work, we had addressed this issue rigorously with an adaptive controller

that learned and compensated for these phenomena continuously, during operation [72]. The resulting controller, although effective, was extremely complex. In this thesis we use a different approach (detailed in Chapter 4), and focus on optimizing the hardware.

We characterized four commercially available outer Bowden cables sheaths, shown in Figure 3.9, differing by the construction of the structural layer and the thickness of the inner Polytetrafluoroethylene (PTFE) lining. All cables had the same inner and outer diameters and were tested with a Dupont, Black Kevlar Fiber inner tendon. The four types of cables were characterized for friction, backlash and stiffness for a fixed wrap angle of the Bowden sheath and a fixed load on the inner tendon, with the aim of finding the one with the best performance, i.e. low backlash, low friction, low stick-slip phenomena and high stiffens [75].

The friction and backlash characterization was done using the setup shown in Figure 3.9.a: the Bowden cable guided the tendons from a driving to a driven pulley, both connected to DC motors (Maxon, EC-i 40, 50 W with a 5:1 reduction), equipped with incremental encoders on their axis. The wrap angle for the cables was 180 deg controlled through custom-designed 3D printed path guides. The driven motor was set to apply a fixed 50 N load on the tendons, to test a condition close to that of the application.

Friction was evaluated by controlling the driving motor in velocity, and measuring current ($\propto$ torque) on the motor's windings. This was done for 35 different velocities in each direction, held for 3 s each, equally distributed between 0 rpm and 6450 rpm, corresponding to a speed of the cable of up to 8.4 m/s. A similar experiment was performed to measure backlash, where the driving motor was controlled in position, to displace the tendon by 7 cm for 10 cycles.

Lastly, to compare the stiffness of the difference sheaths constructions, we replaced the driving motor with a more powerful Maxon, EC-i 40, 70 W with a 55:1 planetary gearhead, and the driven motor with a single axis load cell (Futek, LCM300), fixed on one side on the frame and on the other to the tendon. The motor was controlled to deliver 10 linearly-increasing loading and unloading cycles between 0 N and 120 N on the load cell, using the indirect force control paradigm detailed in Chapter 4. The displacement of the cable was measured by the encoder on the motor's axis. The inner velocity/position loop ran on a motor controller (Maxon, EPOS2 50/5)

and the outer loop on a real-time data acquisition board (Quanser, QPIDe), both at a sampling rate of 1 kHz.

Figure 3.9 shows the friction, backlash and stiffness results for the four tested types of Bowden cables constructions. Almost all sheaths presented a Coulomb-type friction profile, with a slightly higher static friction value and a typical Stribeck effect around zero velocity. The lowest values were found for the Bowden cable construction having strands of steel around the sheath's circumference, along its main axis. The backlash hysteresis profiles varied, with a difference between the input and output displacement of the cable ranging between 0.15 cm (axial construction) and 0.55 cm (nokon). Similarly, the sheath with the axial construction presented the highest stiffness.

3.5.3 Padding material and comfort

"*It is extraordinary to me that the most mature and old technology in the human timeline, the shoe, still gives us blisters. How can this be? We have no idea how to attach things to our bodies.*" [76]. These words clearly point out a critical yet underrated issue in wearable robots: designing a comfortable mechanical interface between the device and its wearer.

As the field of wearable robots rapidly grows and assistive devices promise to soon become part of our daily lives, it is key to face the challenge of finding a comfortable mechanical means to attach robots to the human body. This is all the more important for devices intended for users with sensory impairment, where the lack of feedback could lead to pressure ulcers or local blood flow obstruction.

Extensive research exists on the assessment and optimisation of the design of prosthetic sockets [77]; comfort is strongly correlated with the magnitude of pressure peaks and shear forces at the interface between the socket and the skin, although various other factors, such as temperature and perspiration, can play a role. Significantly less work exists for exoskeletons. De Rossi *et al.* proposed an apparatus to monitor the distribution of pressure at the human-robot interface of a lower-limb exoskeleton during gait training [78]. Using a similar approach, Levesque *et al.* identified areas exhibiting peaks of pressure on the attachment points of an active orthosis for gait assistance [79]; their findings suggest that the distribution

of pressure is affected more by the stiffness of the padding material than by its thickness.

This data-driven approach to guide design choices is a promising path: Quinlivan *et al.* used the same paradigm to optimise the topology and material composition of the attachment points of a soft exosuit for the lower limbs [67]. This work highlighted the importance of the geometry of the interface (larger areas lead to higher comfort) as well as advising the use of fabric materials that better conform to the human body.

Being for exoskeletons or exosuits, materials such as neoprene or polyethilene (PE) sponge are common choices for cushioning the human-robot interface, yet there is no data-supported knowledge to justify the choice of one over others. In this work, we evaluate the pressure distribution between the skin and the anchor points of a soft exosuit for different cushioning materials. We test foams and rubbers commonly used for padding sports equipment and orthoses and quantify their comfort by measuring peaks of pressure at the interface with the skin.

When the tendons of our exosuit are tensioned, to apply a torque on the elbow, the proximal and distal strap tend to migrate towards the center of the joint. To reduce the amount of movement, the proximal strap is connected via inextensible fabric to a harness that redistributes forces on the torso; the large contact area with the body ensures a comfortable wear. The distal strap is where the highest pressures are applied, hence where cushioning properties of different materials will be more evident.

The distribution of pressure around the forearm was acquired using a pressure mat (NexGen Ergonomics, BT5010, 28 cm×28 cm) consisting of an array of 256 pressure sensors, sampled at 100 Hz. The pressure mat was wrapped around the surface of the forearm and secured using double-sided tape to prevent displacement. One subject was asked to performed three sessions of three flexion/extension movements between 0 deg and 90 deg (0 deg being full extension) with the arm fixed on the side of the trunk, doffing and donning the exosuit between sessions. This was done for each of the five materials listed in Figure 3.10.b: each material was cut in a 3 mm-thick layer and used to line the internal surface of the distal strap. The exosuit provided an assistance equal and opposite to gravity, running the gravity-compensation algorithm described in Chapter 4.

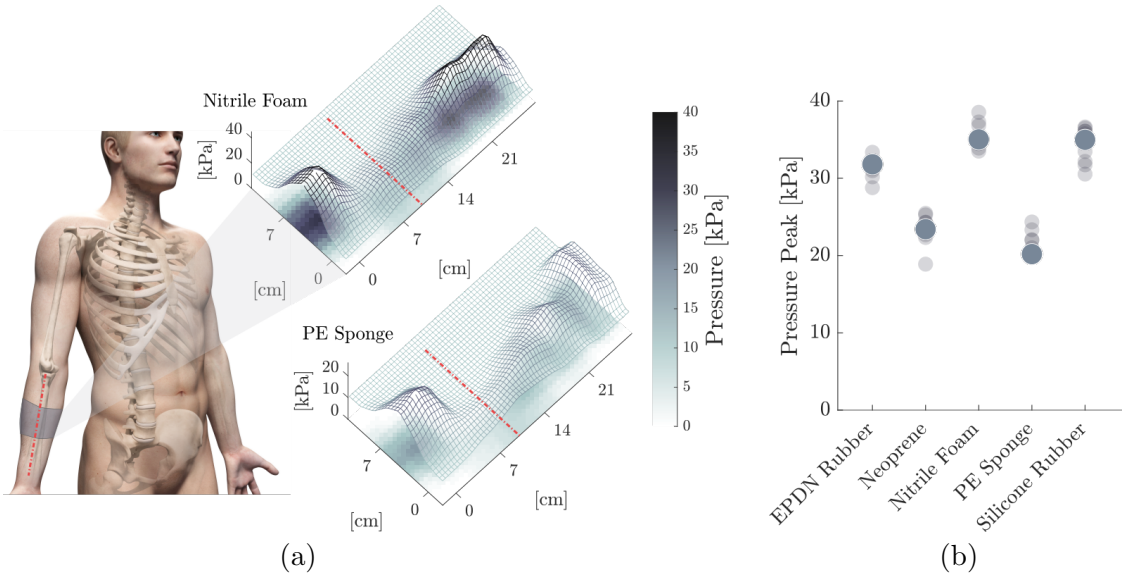

FIGURE 3.10: **Characterization of the pressure distribution at the human-suit interface.** The pressure at the interface between the body and the suit on the distal anchor point was measured with an array of 256 pressure sensors, with the elbow bent at 90 deg and its weight entirely supported by the suit. This was done with 5 different, commonly used, padding materials.

Unsurprisingly, the highest peaks in pressure were found when the elbow was flexed at 90 deg, i.e. when the component of gravity acting on the arm reaches its maximum value, on the posterior side of the forearm. Figure 3.10.a shows the distribution of pressure in this configuration when the distal strap was lined with nitrile foam (top) and with polyethylene sponge (bottom), the former showing higher peaks and a less homogeneous distribution. Figure 3.10.b shows the peak values of pressure for each of the nine repetition (transparent dots) and the mean over repetitions (opaque dots). PE sponge is the material exhibiting the best behaviour while rubber-based materials showed higher local peaks of pressure.

It is worth noting that obtained pressure profiles were due to the subject's weight only; it would be interesting to examine how they vary as the wearer lifts extra load. Moreover, a more thorough study to measure comfort would include an estimate of shear forces on the skin and examine how the force profiles change across subjects with different muscle tone. This data, correlated with physiological measures such as subcutaneous blood flow, could be used to drive the design of optimal interfaces for wearable robots and would provide interesting insights on their usability in daily life scenarios.

Table 3.3: System characteristics

	Characteristics	Requirement Achieved
Force/Motion:		
Range of motion [deg]	120-140[a]	✓
Joint torque [N m]	8.5	✓
Peak velocity [deg/s]	84	✗
Cable tension [N]	≈ 250	✓
Motor power [W]	70	✓
Practical considerations:		
Distal frame weight [kg]	0.71	✓
Proximal pack weight [kg]	2.2	✓
Safety	Compliance ≈ 0.91 N/mm	✓
	Torque limit	✓
	Speed limit	✓
	Stop button	✓
Size	M	✓
Comfort	≤30 kPa	✓
Technical	Safety factor = 2	✓
	Low friction	✓
	Low backlash	✓
	Proximal motor	✓
	Non collocated sensors	✓

[a]variation is caused by the placement of the anchor points.

3.6 Suit's characteristics

The characteristics of the suit are summarised in Table 3.3. By comparing it with Table 3.2, one can see that the requirement for speed was not achieved. This was noticeable only when testing the design on human subjects. A more thorough discussion on this point is highlighted in Chapter 4.

Chapter 4

Admittance controller for gravity compensation

This chapter presents the design of the controller for the soft exosuit. We start with an introduction to the control of compliant robots, highlighting the advantages and disadvantages of having elasticity in the transmission and justifying the choice of an admittance control scheme. We propose an indirect force control paradigm to both assist the user and allows the suit to move in concert with his/her movements. Finally, we evaluate the accuracy of the controller, the bandwidth of the human-suit system and the efficiency of the device.

4.1 Impact of gravity on post-stroke reaching

Reaching movements performed by stroke survivors exhibit an extreme sensitivity to mechanical loading [80]. This causes gravity-loaded reaching movements, very common in activities of daily living, to be uncoordinated and limited in speed and range of motion [81].

When the weight of the arm supported by an external device, most stroke survivors are able to perform reaching movements with surprising skill [82]. Figure 4.1 shows the results obtained by Sukal *et al.* [83], where the authors used a rigid admittance-controlled robotic arm to provide increasing levels of assistance to the paretic and non-paretic arms of chronic stroke patients, and asked them to reach as far as they

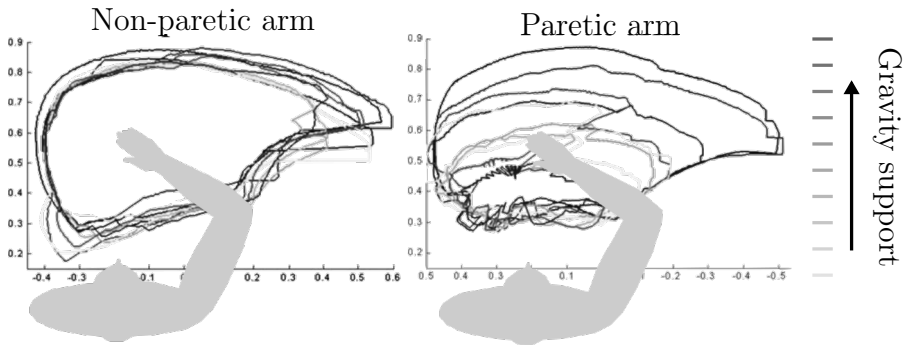

FIGURE 4.1: **Effect of gravitational support on reaching movements.** Comparison of the workspace of the healthy (left) and paretic (right) arm for varying level of gravity compensation, delivered through an admittance-controlled robot. The workspace of the paretic arm increases as the device increasingly supports the weight of the limb. Image adapted from [83].

could on the horizontal plane. While the healthy limb showed no difference across levels of assistance, the paretic limb's workspace was positively correlated with the level of support.

These results suggest that a simple gravity-compensating controller, implemented on a wearable device such as the exosuit presented in Chapter 3, could be enough to significantly broaden the range of tasks that he or she can perform. Over the technically more challenging options of compensating for inertia, velocity-dependent and gravity-related torques at the elbow joint, we thus decided to only address the last ones.

4.2 Control objectives

The control paradigm was designed for the dual purpose of:

- Providing assistance in daily activities by compensating for the gravitational force acting on the forearm.
- Not obstructing natural movements, i.e. allow the robot to move in concert with its wearer with minimal interaction force between the two.

The first objective requires the ability to track a position-dependent force profile equal and opposite to the gravitational force acting on the forearm.

The second objective requires transparency of the suit to the user's movements, in other words backdrivability. This cannot be achieved mechanically because the high reduction ratio of the motor's gearhead increases the reflected motor impedance and the Bowden cables make the transmission inefficient. We need to achieve backdrivability by control.

Before describing the design of the controller, we will provide a brief introduction of the control paradigms used for force control of compliant robots.

4.3 A brief introduction to compliant control

The antithesis between compliant and stiff control of robots only came about in the last twenty years [84],[85]. Traditional robotic devices, born for fast and precise tasks in assembly lines, were designed to be as stiff as possible, to increase their position/velocity control accuracy and bandwidth. These design choices, however, had negative consequences on their force-control performance: high stiffness caused high force modifications for small displacement errors, resulting in instability and unsafe interaction.

A substantial number of works, starting from the early 80s, proposed to achieve safety in physical HRI by means of active force controllers. Hogan's impedance controller [86] and Salisbury's stiffness control [87] are probably the most well-known attempts of getting a heavy, rigid, electro-mechanical system to behave gently as it interacts with the environment. Despite leading to pioneering results, these early studies also highlighted the limitations of "virtual" compliance: the impedance characteristics are limited in bandwidth by the performance of the controller and, since the hardware is intrinsically rigid, they are not robust to failure [88].

Later, Pratt *et al.* proposed to intentionally introduce mechanical compliance in the design [69]. Placing an elastic element between the actuator and the load effectively decouples the actuator's rotor inertia from the links, whenever an impact occurs. The authors indeed showed that, using this paradigm, one can increase shock tolerance and reduce inadvertent damage to the environment. Furthermore, Series Elastic Actuators (SEA) feature improved stability and accuracy of force control compared to rigid transmissions. Indirect force controllers, encompassing impedance and admittance architectures, are a common choice for compliant robots

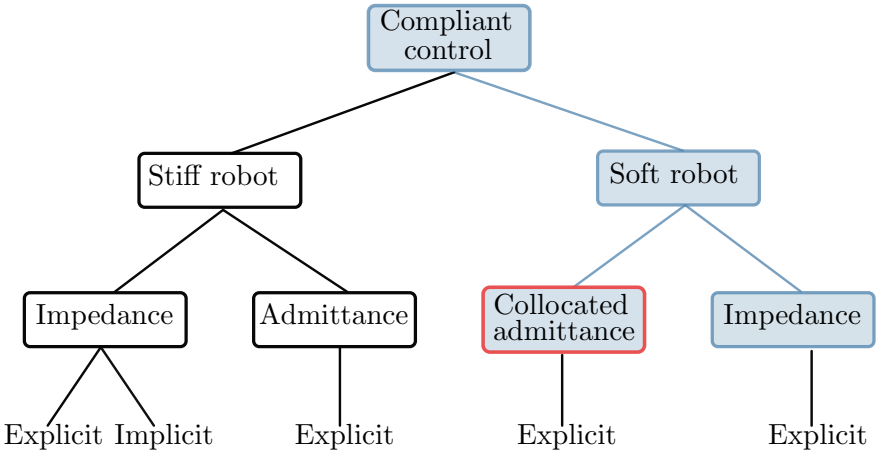

FIGURE 4.2: **Compliant control.** Compliant control for soft and stiff robots, using the taxonomy formulated in [89]. Compliant control and indirect force control are used as synonyms. *Explicit* and *implicit* refer, respectively, to the need or not of a sensor to measure the interaction force between the robot and the environment. The blocks highlighted in blue indicate the chosen controller. Image adapted from [89].

to safely interact with human beings [89]. This is because imposing a relation between force and velocity, unlike direct force paradigms, allows to control the power transfer between the device and its user [86].

The taxonomy described in [89] and represented in Figure 4.2, nicely sums up the options for indirect force control of compliant robots (path highlighted in blue). A compliant transmission always requires a force sensor at the interface between the robot and the environment/user, to observe what is happening between the two (this is not the case in rigid backdrivable transmissions, where one can infer the interaction force from the current on the motor's windings, e.g. [86]).

Both the impedance and admittance controllers are viable options but the former is more prone to stability issues, whilst the latter is more robust thanks to the inner position/velocity-control loop.

4.4 Admittance control for the rich and lazy

In [90], the same research group that introduced SEAs proposed to control a SEA-powered legged robot with an admittance control scheme that closed the internal velocity/position loop on the motor's sensor (collocated) rather than on the joint's. The authors found that a high gain for this internal loop allowed to stably reject

non-linearities in the transmission, such as static friction-related effects and backlash, while allowing the outer force control loop to operate at a slower refresh rate.

This type of admittance control, baptized by Calanca and colleagues [89] "collocated admittance control", allows to use a high-gain position/velocity feedback loop instead of complex backlash- and friction- compensating models (such as the one we used in [72]). This "lazy" approach is not principled buy pragmatic and effective.

Paradoxically, moreover, this method works better with a highly reduced actuator, because its non-backdrivability reduces the effect of external forces (e.g. friction) on the inner position/velocity loop. It thus nicely agrees with the high torque requirements of the application.

4.5 Controller design

The controller we propose for the soft exosuit for the elbow is shown in Figure 4.3.a It comprises an outer torque loop and an inner velocity loop. The outer loop (indicated by the red arrow in Figure 4.3.a) is responsible for tracking a position-dependent torque profile at the elbow, equal and opposite to gravity, and makes use of the model of the elbow presented in Chapter 3:

$$\tau_g = mgl_c \sin\theta, \tag{4.1}$$

where, with reference to Figure 4.3.b, θ is the elbow angle, obtained from an incremental encoder positioned on the joint (0 deg corresponding to the elbow being fully extended on the side of the trunk), m the mass of the forearm, l_c the distance of the forearm's and hand's centre of mass from the axis of rotation of the elbow and $g = 9.81\,\mathrm{m/s^2}$ the gravitational acceleration.

The assistive torque is estimated from the tension measured by load cell on the suit's tendons. Figure 3.3.b shows a schematics of the suit's tendon routing. Using trigonometric relations, one can derive the mapping from a displacement of either tendon to a joint rotation; we call these extension functions, $h_f(\theta)$ for the flexor

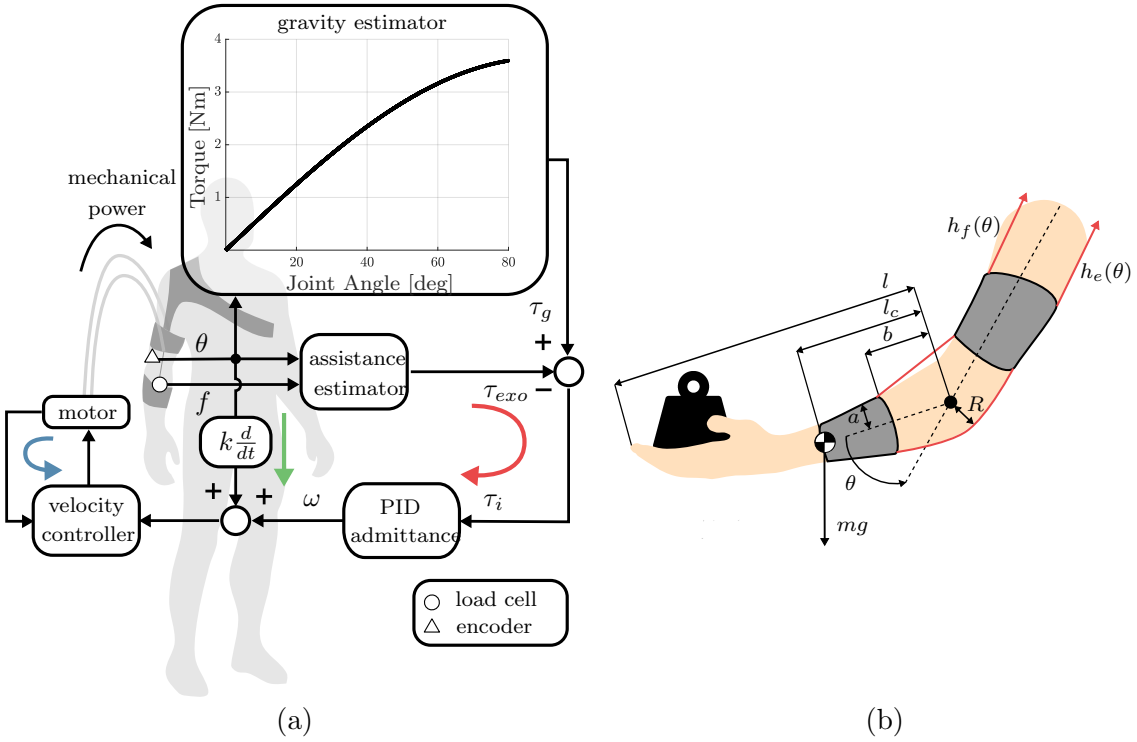

(a) (b)

FIGURE 4.3: **Schematics of the admittance controller for transparency and gravity compensation.** An outer torque loop (red) tracks a reference profile equal and opposite to gravity, computing a motion reference as an interaction torque is sensed, according to the admittance specified by a PID controller. The inner velocity loop (light blue) is tuned to be as stiff as possible, to reject force disturbances like stiction and backlash. The green arrow indicates a positive feedback path, introduced to improve transparency.

and $h_e(\theta)$ for the extensor:

$$h_f(\theta) = 2\sqrt{a^2+b^2}\cos\left(\tan^{-1}\left(\frac{a}{b}\right)+\frac{\theta}{2}\right)-2b \tag{4.2}$$

$$h_e(\theta) = R\theta \tag{4.3}$$

where a is half of the width of the arm, b is the distance from the joint centre of rotation to the anchor points and R is the radius of the elbow joint.

From the two extension functions $h(\theta)$ we can compute the position-dependent moment arm of the cables' tension on the elbow's axis of rotation:

$$P(\theta) = \frac{\partial h}{\partial \theta}^T(\theta) = \left[-\sqrt{a^2+b^2}\sin\left(\phi+\frac{\theta}{2}\right), R\right] \tag{4.4}$$

where $h = \begin{bmatrix} h_f(\theta) & h_e(\theta) \end{bmatrix}^T$ represents the vector of cable extensions. The estimated assistive torque delivered at the joint is obtained by the equation:

$$\tau_{exo} = P(\theta) f \tag{4.5}$$

where f is the measured cable tensions obtained by the load cell.

Note that the null-space of $P(\theta)$ is given by the span of all vectors of the form $\left[R/(\sqrt{a^2+b^2}\sin(\phi+\theta/2), 1\right]^T$, this condition, however, implies co-contraction of both of the suit's tendons, which cannot be achieved with one motor in the current configuration. This model assumes that the position of the anchor points is fixed. It neglects deformation of the fabric and soft tissues upon the application of a force from the tendons.

The difference between τ_g, calculated from Equation 4.1, and τ_{exo}, calculated from Equation 4.1 , is converted in a velocity for the motor, ω_d, by an admittance of the form (in the Laplace domain):

$$Y(s) = \frac{\omega_d}{\tau_g - \tau_{exo}} = P + \frac{I}{s} + Ds, \tag{4.6}$$

with the P, I and D constants governing the characteristics of the relation between the interaction force and the motor's velocity [91].

A low-level, PI velocity loop (blue arrow in Figure 3.3.a) tracks the desired velocity on the motor's axis. Note that this speed loop is closed on the motor's sensor rather than on the elbow's. This approach, known as collocated admittance control [89], has been shown to robustly deal with force disturbances such as stiction and backlash, while guaranteeing stability even for low sampling rates of the high-level feedback loop [90].

Finally, a positive feedback term is added to the desired velocity (shown in Figure 3.3.a in green), to increase the controller's sensitivity to the user's movement: the faster the user moves, the faster the motor will. This strategy is commonly used to compensate for stick-slip friction phenomena, but it here facilitates initiation of movement, making the exosuit more transparent [19]. The final desired velocity,

tracked by the low-level motor driver, has the form:

$$\omega_d(s) = \underbrace{P(\tau_g - \tau_{exo}) + \frac{I}{s}(\tau_g - \tau_{exo}) + Ds(\tau_g - \tau_{exo})}_{\text{PID Admittance}} + \underbrace{ks\theta}_{\text{Positive feedback}} . \quad (4.7)$$

With τ_g being the gravitational torque acting on the joint, τ_{exo} the assistive torque delivered by the suit, k the positive feedback gain and θ the joint angle.

The distance of the center of mass of the forearm and hand from the axis of rotation of the elbow, the mass of the hand and forearm and the radius of elbow are all derived from the body mass and height of the suit's wearer, using anthropometric tables [62, 92].

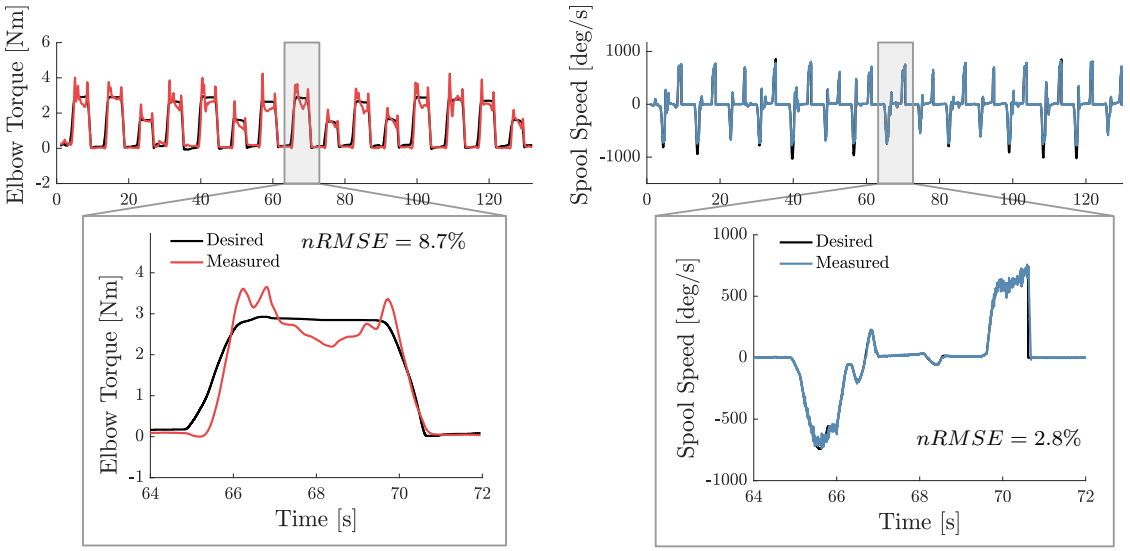

FIGURE 4.4: **Tracking accuracy of the collocated admittance controller.** (a) Accuracy of the outer torque loop in tracking a desired profile during motion of the elbow joint. The root mean square error (RMSE) is 8.7% of the range of the desired torque. (b) Accuracy of the inner velocity loop. The RMSE is 2.8% of the range of the desired velocity.

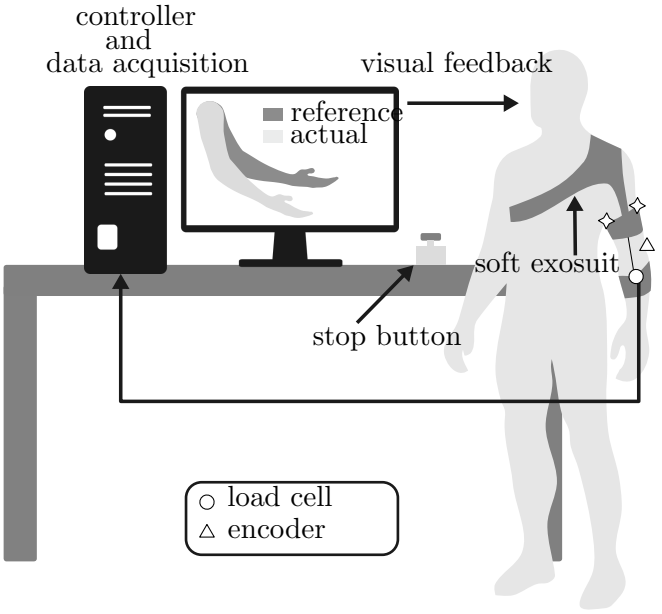

FIGURE 4.5: **Experimental setup.** Subjects were asked to follow a reference trajectory displayed on a screen in the form of a moving elbow, the position of their own arm was superimposed to provide visual feedback. This was done in both the powered and unpowered conditions, while monitoring the elbow angle and interaction force.

4.6 Control performance

4.6.1 Accuracy

To evaluate the control accuracy, we performed a preliminary testing on 2 subjects. The experimental setup is shown in Figure 4.5. Participants, wearing the exosuit on their left arm, had to follow a reference movement performed by a dummy character on a screen. The position of their own elbow was displayed as a superimposed translucent replica of the reference one to provide visual feedback. To ensure that they were moving at the desired velocity, participants were asked to match the movement of the character on the screen as accurately as possible.

The reference motion consisted of series of Minimum Jerk Trajectories (MJT), known to correspond well to the movements of healthy subjects [93], at a peak velocity of 84 deg/s.

The accuracy of the admittance controller in tracking the position-dependent gravity profile is fundamental for the performance of the suit.

Figure 4.4 shows the desired and measured profiles of both layers of the admittance controller. Figure 4.4.a displays the tracking accuracy of the outer torque loop (orange in Figure 3.3.a), for one subject, moving with assistance from the exosuit at movements with a peak velocity of 84 deg/s.

The reference trajectory is a position-dependent estimate of the torque acting on the elbow because of the weight of the forearm. The controller shows overshoots in the rising transient region and before the downwards motion. The RMSE, averaged over 2 subjects, repetitions and velocities, was found to be 8.7 % of the range of desired torques.

Figure 4.4.b, shows the accuracy of the inner velocity loop (blue arrow in Figure 3.3.a), tracking the speed of the pulley on the motor's shaft, for the same repetitions. This PID was tuned to be as stiff as possible, to stably reject nonlinearities in the transmission. The RMSE, over subjects and velocities, was found to be 2.8 % of the range of desired motor speeds.

4.6.2 Bandwidth

To identify the controller's bandwidth, the same 2 subjects who performed the experiment detailed in Section 4.6.1 were asked to perform a dynamic task, using the same protocol described in Section 4.6.1 but following sinusoidal trajectories in wide range and with finer intervals of velocities. Each subject performed the task in two conditions: without receiving assistance from the device (unpowered) and with assistance (powered).

The reference trajectory consisted in a sinusoidal signal of the form:

$$\theta_d(t) = A_0 + A\sin(2\pi f(t)t) \tag{4.8}$$

with $A_0 = \mathrm{A} = 40\,\mathrm{deg}$, chosen to cover a range of motion typical of ADLs, and f being a step-wise varying frequency in increasing steps of 0.05 Hz, between 0.05 Hz and 0.9 Hz. These values were chosen as they correspond to movements with a peak velocity between 12.5 deg/s and 226 deg/s, equivalent to 10% to 180% of the speed of the elbow in daily tasks [61]. Each frequency value was held for 20 s; the first 5 s of each window where discarded to allow evaluation of the response

at "steady state". We collected kinematic data (AMS, AS5047P, 1000 pulses/rev) and tension on the exosuits' flexing tendon (Futek, LCM300).

Figure 4.6.a shows the reference, unpowered and powered trajectories for one subject and eight different velocities of movement. In the unpowered case, the participant could easily follow the reference signal. Such was not the case for powered movements, showing a net deterioration in tracking accuracy above 75 deg/s. For each frequency/velocity of the powered case we evaluated the ratio between the Fourier coefficients of the first harmonic of the measured and desired elbow angles:

$$H(f_0) = \frac{C_1(\theta_m)}{C_1(\theta_d)}. \tag{4.9}$$

The magnitude and phase of $H(f_0)$ were calculated to derive a Bode plot of the human-suit's position tracking accuracy, shown in Figure 4.6.b. Finally, to display the effect of velocity on the level of assistance provided by the device, we estimated the biological torque exerted by the wearer in percentage of the total torque required for movement ($\tau_{bio}/\tau_{total} \times 100$, where the human torque is estimated using the procedure described in Chapter 5). This is shown in Figure 4.6.c.

Our system has a bandwidth, defined as the first frequency where the gain drops below -3 dB of its steady-state value, of 0.35 Hz, corresponding to a peak velocity of movement of 88 deg/s. This is highlighted in red in Figures 4.6.b, where it corresponds to an average phase of 40 deg, $\approx$0.3 s of delay. In Figure 4.6.c, the drop in performance is clear, with the biological torque increasing to values above 70% of the total torque for speeds above the bandwidth.

4.6.3 Power consumption

Figure 4.7 shows the typical appearance of the electrical power consumed by the motor and the output power delivered at the elbow joint for a flexion/extension movement of the elbow. The gray shaded area shows the mechanical power delivered by the exosuit at the elbow, computed as the product between the assistive torque of the exosuit and the rotational speed of the elbow: $P_{elbow} = \tau_{exo}\dot{\theta}$. This quantity reaches a maximum of 4 W and has a symmetrical behaviour in the ascending and descending phases. The electrical power consumed by the motor, computed as $P_{motor} = IV$, with I and V being the current and voltage on the

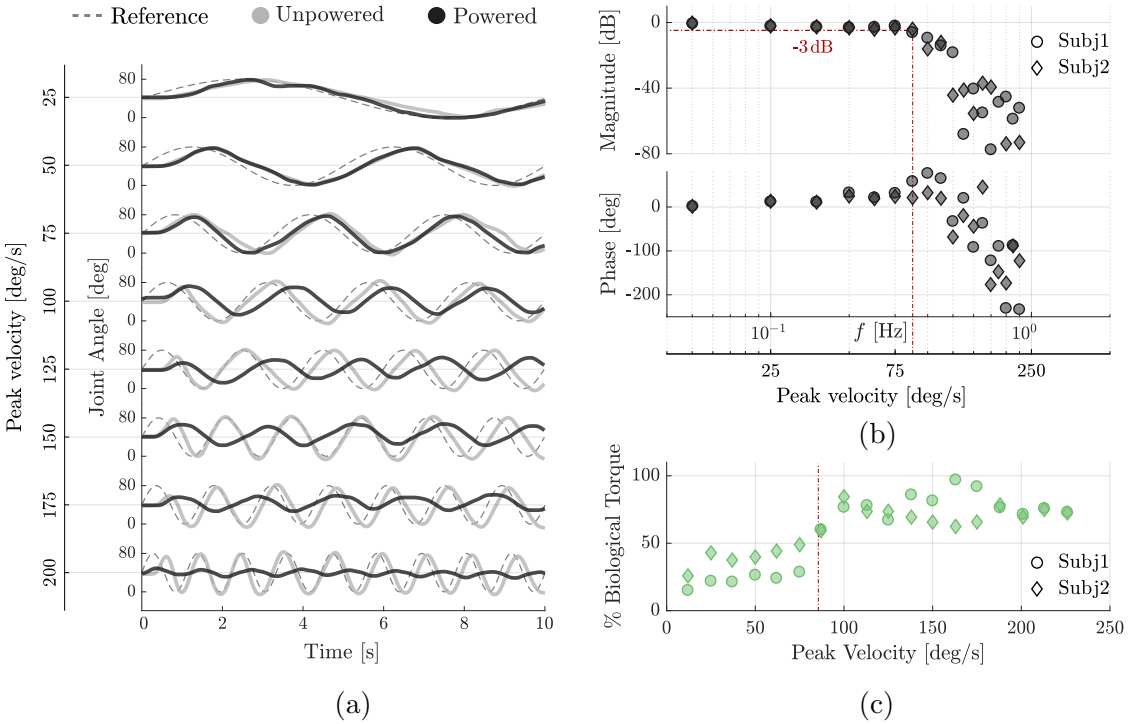

FIGURE 4.6: **Tracking and assistive performance of the suit for varying movement velocities.** (a) Reference (dashed), unpowered (gray) and powered (black) trajectories of the elbow for 8 of the 18 tested velocities of movement, shown for 10 s and one subject. (b) Bode plot of the estimated transfer function in Equation 4.9, between the measured and desired elbow position, in the powered condition. The human-suit system has a bandwidth of 0.35 Hz, highlighted by the red dashed line. Different markers correspond to different subjects. (c) Biological torque, in percentage of the total torque required for movement ($\tau_h/\tau_{total} \times 100$). Above the bandwidth (red dashed line), the effort that the wearer needs to exert to move increases steeply.

motor's windings, is shown in grey. It reaches a peak around 15 W just before motion inversion, it then drops to zero and shows a small negative contribution in the descending phase, induced by the counter-electromotive force due to gravity. The big mismatch between P_{elbow} and P_{motor} highlights the low efficiency of the device, an average over repetitions and subjects just below 20%.

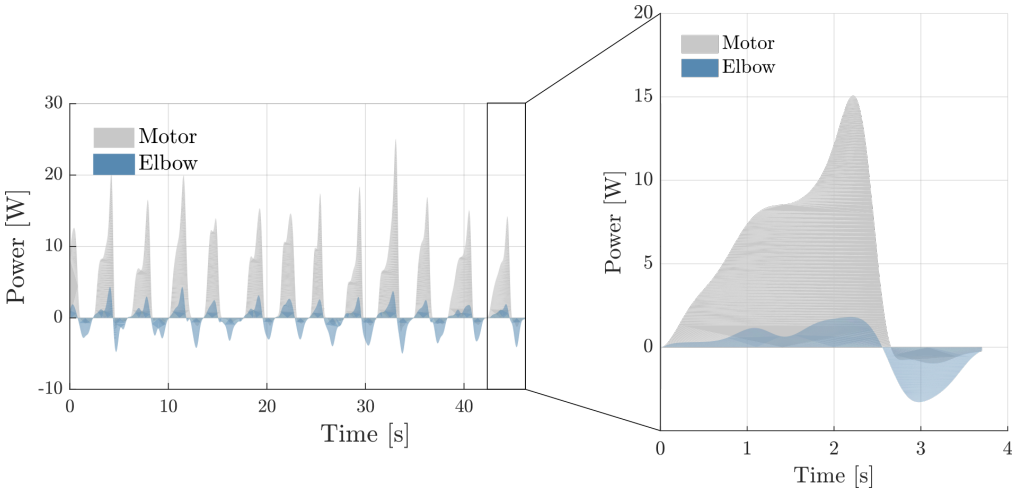

FIGURE 4.7: **Electrical power consumed by the motor and mechanical power delivered at the elbow joint.** Typical power profile at the elbow and on the motor's windings, for sinusoidal movements of the joint, for one subject. The electrical power consumed by the motor, shown in gray, reaches peaks between 15-20 W, when the elbow is at 90 deg, and small negative values in the descending phase. The power delivered at the elbow is a fraction of the one consumed and slightly out of phase, due to losses and viscoelasticity in the transmission.

4.7 Closing remarks

The admittance controller proposed in this Chapter showed to have the valuable ability to deal with friction and backlash in the transmission, as shown by the good tracking accuracy of the velocity loop, without the need for complex feedforward models. The lower performance of the force controller was expected and is probably caused by the non-linear characteristics of the suit and human tissue compliance.

The presence of friction, backlash and non-linear compliance in the transmission resulted, however, in a low bandwidth (0.35 Hz at an amplitude of 40 deg) and low efficiency (≈20%). The first approach to improve performance would be through hardware changes. A good starting point is the work from Schiele and colleagues [75], where the authors give some practical suggestions to improve efficiency and force-rendering performance of Bowden cable actuators:

– Use friction couples with a very small friction coefficient, PTFE on PTFE is well suited. In our device, we did use PTFE coating on the inner lining of the Bowden sheath, but not on the cable, made of braided Dyneema wire.

- Use friction couples whose coefficient of friction increases with speed. This avoids stick-slip phenomena and would not only improve efficiency but also force rendering bandwidth. Again, the best choice would be PTFE on PTFE, which we did not have.

- Use cables and sleeves with high stiffness. In Chapter 3, Section 3.5, we tested the stiffness of Bowden sheaths with different constructions and chose the one with the highest stiffness. When compared to a 7×7 stainless steel wire rope, braided Dyneema (used here) has a stiffness only 8% lower but weighs 80% less.

- Forces from the suit to the human body should be transmitted along paths that are as stiff as possible. In this work, we used inextensible webbing bands as load paths but we did not optimize the choice of materials. The work from Quinlivan *et al.* [67] shows an elegant procedure to choose the best garments and orientation of the fabric fibers to increase stiffness. The authors also suggest to try to load bony prominents of the human body and pre-compress soft tissues, to reduce compliance of the human-suit interface.

- Finally, choosing a motor with a higher nominal torque would allow to use a gearhead with a smaller reduction ratio, hence higher efficiency.

Further improvements could be achieved through enhancements of the controller. Lee *et al.* [94] showed how including a stiffness model of the suit and of the limb being assisted (the thigh in their case) improved the bandwidth of an admittance controller very similar to the one presented here, by over 100%. A motor with higher nominal speed would also be needed, in our case.

The performance of the outer torque loop is, moreover, strongly dependent on the gains of the admittance block, whose values, in this study, were tuned heuristically. This was done for each subject during a familiarisation phase, prior testing the performance of the device. In [91], the authors propose a similar PID admittance controller for a 7-DoF upper extremity exoskeleton. Their parameters regulation procedure consists of a method similar to the Ziegler-Nichols and Cohen-Coon methods, where the control parameters are tuned based on the identified characteristics of the plant. This, however, requires knowledge of the mechanical impedance of the human arm, which is known to continuously vary depending on the task being performed [95, 96] and across subjects.

A different and fairly new approach consists in automatically tuning the control parameters online, so as to maximise a performance (or safety) index of the exosuit. Recently published results suggest that this process could be addressed systematically and automated through optimization techniques. Zhang and colleagues [97] have shown how a control paradigm that modulates the assistance characteristics, in order to minimize the metabolic cost of human walking, can accommodate the large diversity among subjects and significantly improve performance. Ding *et al.* [98] have shown equally encouraging results using a Bayesian optimization technique to modulate the force profile of a soft exosuit to assist hip flexion. This gives us reason to believe that identifying a suitable cost function for the device presented here and using it to optimize its control parameters, could lead to improved safety, quality of assistance and intuitiveness of use.

The major drawbacks identified in this preliminary evaluation of the performance of the device are the low bandwidth and efficiency.

The suit has an efficiency below 20%. This was, to some degree, expected, due to the high reduction ratio of the motor's gearhead, friction losses in Bowden cables and viscoelastic properties of the suit and human tissue. The suit has a bandwidth corresponding to a peak velocity of of the joint 88 deg/s; we expect this to affect the kinetics and kinematics of natural human movement. This evalutation, as well as an in-depth analysis of the activation of the muscles working in parallel with the suit, will be the topic of Chapter 5.

Chapter 5

Physiological and kinematic effects on human movements

This chapter examines the effect of the exosuit on the kinematics and kinetics of human movements and on the pattern of activation of the muscles involved in flexing and extending the elbow, directly addressing the three hypotheses outlined in Chapter 1. The validation is done on eight subjects in a static and dynamic task. The former to verify the effectiveness of the exosuit in delaying the onset of fatigue and the latter to assess its transparency. The chapter ends with a discussion on the implications of our findings for the use of the suit in ADLs and a comparison with similar state-of-the-art devices.

5.1 Experimental protocol

The aim of the evaluation procedure was to assess the effect of the exosuit on human kinematics and biomechanics. To do so, we compared smoothness and accuracy of movement, biological torque and muscular activation patterns of healthy subjects performing controlled motions of the elbow, with and without assistance from the suit. The testing was done on 8 male subjects (average age 29.2 ± 1.4) presenting no evidence or known history of skeletal or neurological diseases, and exhibiting intact joint range of motion and muscle strength. At the beginning of each experimental session the participants were informed of the procedure and they signed an informed

consent. The procedures, in agreement with the Declaration of Helsinki, were approved by the Institutional Review Board at Nanyang Technological University.

The experimental setup is shown in Figure 5.1. Participants, wearing the exosuit on their left arm, had to follow a reference movement performed by a dummy character on a screen. The position of their own elbow was displayed as a superimposed translucent replica of the reference one to provide visual feedback. To ensure that they were moving at the desired velocity, participants were asked to match the movement of the character on the screen as accurately as possible.

This was done by each subject in two conditions: with and without assistance from the device, we shall refer to these as *powered* and *unpowered* conditions, respectively. In the latter case the exosuit's tendons were unhooked from the distal anchor point and the motor's power source was turned off. The sequence of the two conditions was randomly assigned to each participant to mitigate potential order effects. In the powered condition, subjects were asked to relax and rely on the suit to support their limb's weight.

The reference motion consisted of series of Minimum Jerk Trajectories (MJT), known to correspond well to the movements of healthy subjects [93], at varying peak velocities, chosen to be fractions of the average elbow speed in activities of daily living (ADLs), i.e. 126 deg/s [61]. The evaluation comprised three sessions: a familiarisation phase, a dynamic and an isometric task.

5.1.1 Familiarisation

The familiarisation was performed with assistance from the exosuit so that the participant could get accustomed to using the device and we could fine-tune the gains of the PID admittance controller. The participant was asked for his weight and height, used to evaluate the geometrical and physiological parameters used in Equations 6.6-6.7 and 5.1, from anthropometric tables [62, 92].

The reference motion consisted in a series of MJTs between 0 deg and 30 deg, 60 deg or 80 deg, each amplitude repeated 8 times in a random order, for a total of 24 movements. A typical reference signal is shown in Figure 6.12.a. The peak velocity of movement was chosen to be 50% of the average elbow speed in ADLs. Neural control of muscles was inferred by recording surface EMG.

5.1.2 Dynamic task

The dynamic task was used to assess the effectiveness of the exosuit in both shadowing the wearer's movements and compensating for gravitational forces.

Subjects were asked to hold a mass in their hand and follow the reference trajectory displayed on the screen; this was done both with and without assistance from the exosuit and for three different velocities of movement, for a total of 6 sessions. All sessions of the same condition were performed on the same day, with a 30 min break between them. Powered and unpowered bouts were conducted on separate days to avoid fatigue. The mass consisted in a 1 kg plate, used to increase muscular activation in both conditions and enhance the signal-to-noise ratio of the data collected using surface electromyography.

The reference MJT motion was the same as the one for the familiarisation phase (an example of which can be seen in Figure 6.12.a) but performed in three different sessions at three different peak velocities: 42 deg/s, 84 deg/s and 126 deg/s, corresponding to 33%, 67% and 100% of the average elbow speed in ADLs.

We recorded the angular position of the elbow, the tension on the exosuit's flexing tendon and the electromyography (EMG) of the biceps brachii and the long head of the triceps brachii, responsible for flexing and extending the elbow, respectively. The skin was cleaned and the electrodes (Delsys Trigno IM) were placed according to the SENIAM standards [99]. At the beginning of each session we performed a manual test for maximum voluntary contraction (MVC), subsequently used to normalise the muscular activity, allowing comparison across subjects. The test was repeated two times per muscle, with a break in-between to avoid fatigue. All data was acquired at a sampling frequency of 1 kHz through a Quanser QPIDe acquisition board.

5.1.3 Isometric Task

The goal of the isometric task was to assess the impact of the exosuit on muscle fatigue.

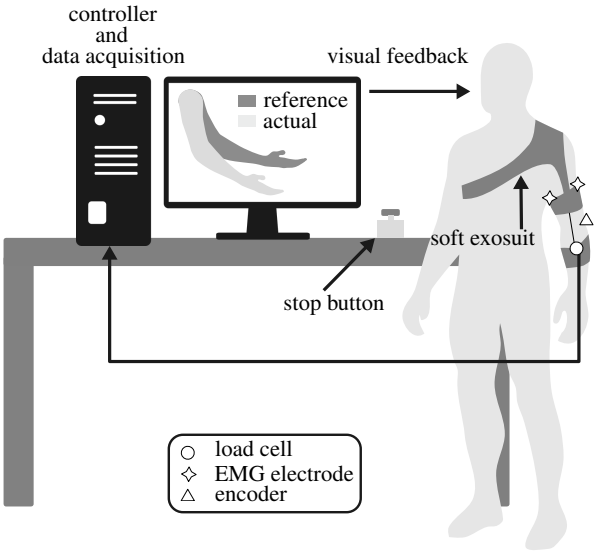

FIGURE 5.1: **Experimental setup.** Subjects were asked to follow a reference trajectory displayed on a screen in the form of a moving elbow, the position of their own arm was superimposed to provide visual feedback. This was done in both the powered and unpowered conditions, while monitoring the elbow angle, the interaction force (only powered) and EMG activity of two antagonistic muscles driving the joint.

While holding a load, subjects were asked to repeatedly maintain the elbow in a fixed position. The load was chosen to be a mass equivalent to 3% of the participant's body weight, corresponding to approximately 15% of his MVC, held at 90 deg for three fatiguing repetitions of 40 s each, separated by 20 s of rest. This was done both for the powered and unpowered condition, in a randomized order and on different days. Although fatiguing protocols often involve higher loads and isometric contractions until voluntary exhaustion [100], our suit was not designed to transmit heavy weights to the human body. This combination of magnitude and timing of exercise was chosen as a reasonable compromise between intensity and comfort.

We recorded EMG of the biceps brachii and the long head of the triceps brachii using the same procedure adopted for the dynamic task. One subject was dropped out of the fatigue evaluation due to incorrect placement of the electrodes.

5.2 Data Analysis

Raw data from the suit's absolute encoder and load cell was low-pass filtered (second order Butterworth filter, 10 Hz cut-off frequency) and segmented to isolate the 24 movements comprising each session.

The accuracy of movement was quantified by evaluating the coefficient of determination (r^2) between the measured and reference trajectory. Time delays between the reference and measured trajectories were estimated by finding the time lag corresponding to a peak in the cross-correlation between the two signals.

Smooth movements are a characteristic feature of healthy, efficient and well-trained motor behaviour [101] and an external assistive device should not make them less so. To quantify kinematic smoothness, we used the SPectral ARC length (SPARC) index proposed in [102]. This required an additional event-based segmentation to isolate epochs where subjects were actually moving from those of static holding, which we did using a lower threshold on the absolute velocity of 2.5 deg/s. The SPARC index was estimated on the norm of the elbow's speed.

The measured force on the flexing tendon was mapped to a torque on the joint using Equation 6.7, this was used as an estimate of the assistive moment delivered by the exosuit, τ_{exo}. The total torque required to perform the movement was derived from the inverse dynamics of the human elbow, represented as a simple pendulum using a second order model of the form:

$$I\ddot{\theta} + B\dot{\theta} + \tau_g = \tau, \tag{5.1}$$

with I being the moment of inertia of the forearm and hand, B takes into account the viscosity of the elbow joint (we used a value of 0.2 Nms/rad according to the values reported in [103]) and τ_g is the gravity-dependent torque, presented in Equation 6.6. The norm of the difference between the total and assistive torque, $\tau_{bio} = \tau - \tau_{exo}$, was used to estimate the remaining biological torque exerted by the subject to perform the movement or hold the position. The absolute value of the biological torque $|\tau_{bio}|$ was used as a cost index (the higher the worse) of the performance of the device.

The output EMG signal of the Delsys Trigno system (pre-conditioned with a band-pass Butterworth filter between 20 Hz and 450 Hz) was processed to extract its linear average envelope using the procedure suggested in [104]: this included noise filtering, rectification, smoothening using a moving-average filter (0.2 s window) and normalisation by the MVC. The root mean square (RMS) of the processed EMG signal was used as index of the level of activation of a muscle.

Finally, the EMG data gathered from the isometric task was used to evaluate the effect of the exosuit on the onset of fatigue. Myoelectric manifestations of muscle fatigue appear both in the time and frequency domain as an increase in the EMG amplitude or as a shift towards lower frequencies of the signal's power spectral density function [105]. We used the median frequency (MNF) of the EMG's power spectrum and the average rectified value (ARV) of its amplitude as indexes of fatigue, evaluated on epochs of 3 s during the last isometric repetition. The rate of change of these values during the 40 s of isometric contraction were used to quantify fatigue. We calculated their slope by fitting a first order model with a least square method: a steeper positive slope for the ARV and a steeper negative one for the MNF indicate a faster onset of fatigue.

5.2.1 Statistical analysis

We checked that the metrics were normally distributed using a Shapiro-Wilk test with a significance level of α =0.05. All metrics were normally distributed except for the elbow's smoothness (SPARC index) and coefficient of determination (r^2) between the reference and measured trajectories.

Non normally-distributed metrics were evaluated by a non-parametric Wilcoxon signed-rank test between the powered and unpowered conditions, our null hypothesis being that both samples came from distributions with equal mean. Normally-distributed metrics were statistically compared with a paired t-test ($\alpha = 0.05$) between the powered and unpowered conditions. Outliers were removed before any further analysis using a Thompson Tau test.

Reported values and measurements from here onwards, in both graphs and text, are presented as mean $\pm$ standard error of the mean (SEM).

5.3 Results

5.3.1 The exosuit reduces movement accuracy and smoothness

Figure 6.12 shows the effect of the exosuit on the trajectories of the elbow. As shown in Figure 6.12.b, as the velocity of movement increased, the tracking accuracy of the powered condition worsened when compared to the unpowered one. The average accuracy, measured by the coefficient of determination between the measured and reference trajectories, for the powered and unpowered conditions were 0.91 ± 0.02 and 0.80 ± 0.06, respectively. A Wilcoxon signed-rank test between the two confirmed that wearing the exosuit significantly reduces the ability to track a reference trajectory ($p = 8 \times 10^{-5}$).

This deterioration in tracking accuracy is a consequence of both a delay introduced by the suit in the initiation of movement and its inability to track high velocities. The former effect is shown in Figure 5.3.a, highlighting that the suit offset reaction times by approximately 200 ms, independently of movement speed. Figure 5.3.b shows that wearing the suit slowed down human movements. Although this was observed overall, averaging over velocities and subjects, it did not apply to low velocities (42 deg/s), where the opposite was true.

Similarly, the smoothness of movement was affected by the exosuit's assistance, with the difference in SPARC index [102] between the two conditions increasing for increasing movement velocity. The overall smoothness, averaged over velocities and subjects, was -1.76 ± 0.10 (unpowered) and -1.82 ± 0.14 (powered). The latter being significantly lower than the former ($p = 2 \times 10^{-13}$).

5.3.2 The exosuit reduces muscular effort

As the suit provided a force against gravity to support the weight of the forearm, it reduced the amount of effort that the flexor muscle needed to exert ($p = 5 \times 10^{-15}$). Figure 6.14.a shows a representative case of the activity (raw and its envelope) of the biceps brachii and long head of the triceps brachii during five consecutive movements of the elbow, in both the powered and unpowered conditions.

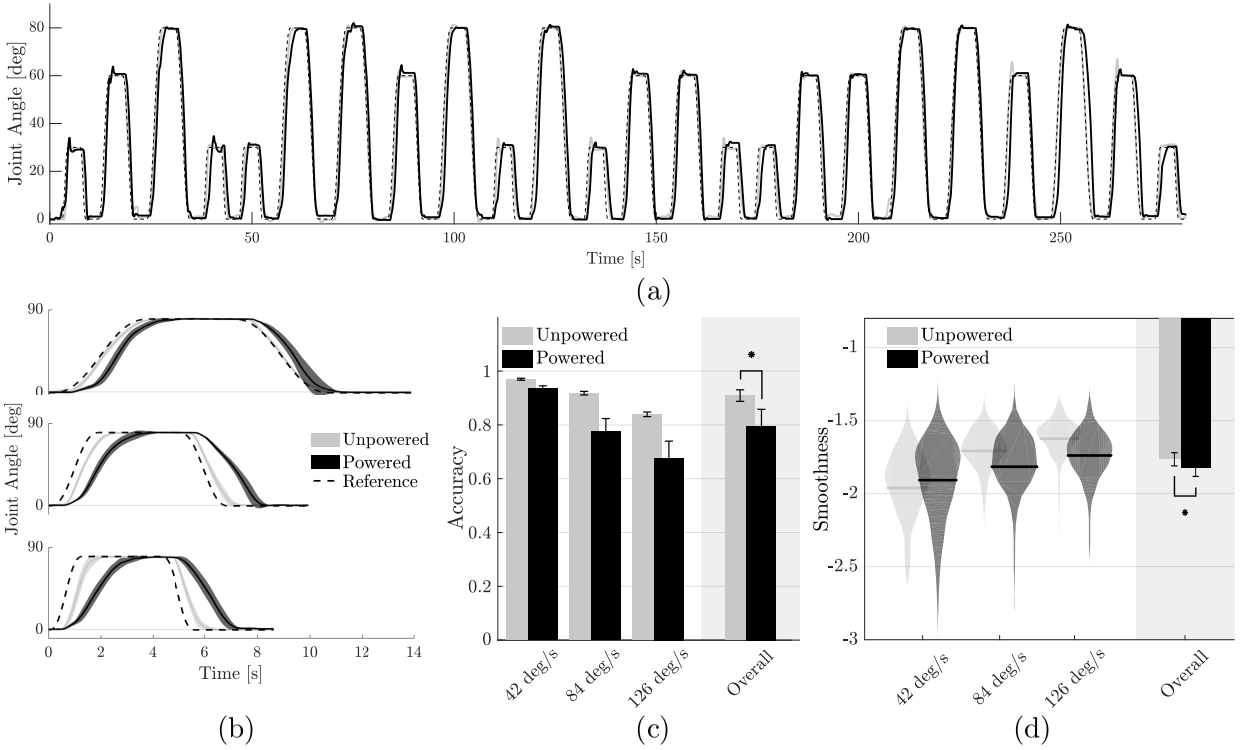

FIGURE 5.2: **Effect on joint kinematics.** (a) Typical sequence of flexion/extension movements performed by a participant in a session with a peak velocity of 42 deg/s. Shaded areas indicate the standard deviation around the mean trajectory. (b) Trajectories for the unpowered and powered conditions, averaged over repetitions, for one subject and at the three tested velocities (from top to bottom: 42, 84 and 126 deg/s); as the velocity increases, the accuracy of the powered condition decreases. (c) Average accuracy, measured through the coefficient of determination, r^2, between the reference and measured trajectory of the elbow in the unpowered and powered condition. The overall mean, averaged over subjects and velocities, indicate that the assistance from the exosuit significantly ($p = 8\times10^{-5}$) reduces a subjects's capacity to follow a reference motion. (d) A similar trend was found for the smoothness of movement, measured with the SPARC index. Assistance from the exosuit significantly reduces movement smoothness (-3.4%, $p = 2\times10^{-13}$). Error bars show the standard error of the mean.

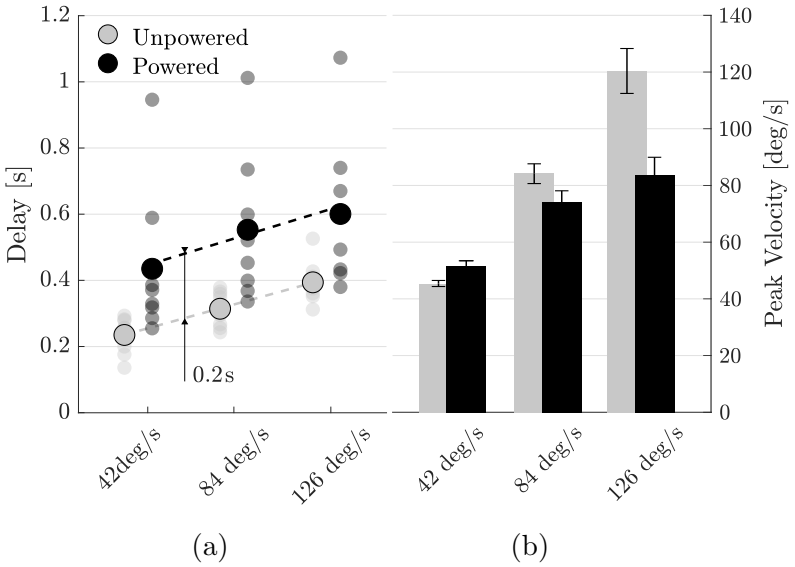

FIGURE 5.3: **Effect of the exosuit on delay and peak velocity of movement.** (a) Wearing the exosuit introduced a time lag between the reference trajectory and the wearer's movement. The average delay, over subjects, is 200 ms higher than the one observed in the unpowered condition, independently of the target velocity. (b) Assistance from the exosuit slowed down human movement for velocities higher than 42 deg/s. This is most most probably a corollary of the limited bandwidth of the device.

The net change in the biceps brachii muscular effort (Figure 6.14.b), evaluated as the difference in the EMG's RMS between the powered and unpowered cases, was significantly smaller than 0 for all velocities ($p = 1 \times 10^{-3}$ for 42 deg/s, $p = 1 \times 10^{-3}$ for 84 deg/s, $p = 8 \times 10^{-3}$ for 126 deg/s). Such was not the case for the triceps brachii, whose activity's net change between the two conditions cannot be said to differ from 0.

Figure 6.14.c shows the change in activity of the biceps brachii expressed as percentage of its activity in the unpowered condition. Similarly to what happened to the accuracy and smoothness of movement (Figure 6.12), the performance of the suit degraded for higher velocities. Wearing the exosuit resulted in a significant reduction of the biceps muscle effort, averaged over subjects and velocities, of $64.8 \pm 7.66\%$ ($p = 5 \times 10^{-15}$).

5.3.3 The exosuit reduces the biological torque

Figure 5.5.a shows the total torque required to perform the movement (grey), the one provided by the exosuit (black) and the estimated biological torque (in

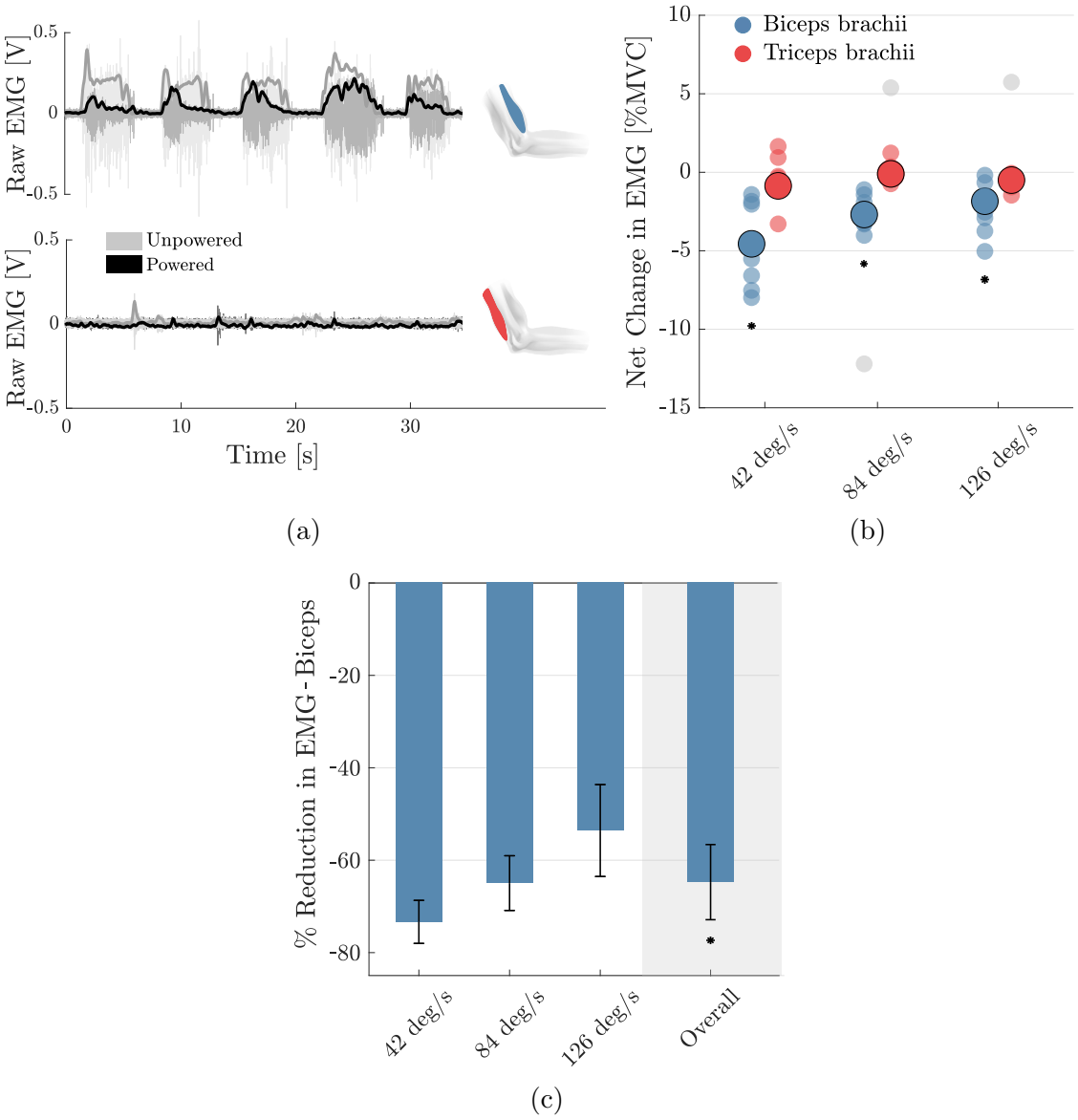

FIGURE 5.4: **Changes in muscular activation**. (a) Raw signal and envelope of the electromyography (EMG) of the biceps brachii and long head of the triceps brachii during five consecutive movements, performed in the powered (black) and unpowered (grey) conditions. (b) Net change (powered - unpowered) of the root mean square of the EMG signal of both evaluated muscles, for the three velocities. Translucent circles are the values for each individual subject, opaque contoured circles indicate the mean over subjects. Circles in grey are outliers, identified through a Thomson tau analysis. Asterisks indicate significant difference from 0. (c) Change in the activity of the biceps brachii, expressed as percentage of its activity in the unpowered condition (net change/unpowered). Assistance from the exosuit singificantly reduces muscular effort (64.8±7.66 %, $p = 5{\times}10^{-15}$). Error bars show the standard error of the mean.

green), for one subject, averaged over repetitions for the three tested velocities of movement. The exosuit supports large part of the total torque but introduces negative biological moments, especially when initiating the downwards motion.

Figure 5.5.b shows the average over subjects and repetitions of the total, the exosuit's and the biological torque in the powered condition (in the unpowered condition $\tau_{bio} = \tau_{total}$). The figure shows that when the exosuit is assisting the subject, the biological torque is only a fraction of the total one but, as the velocity increases, the wearer needs to exert higher positive and negative torques.

The overall gain, shown in Figure 5.5.c, was, nevertheless, favorable, with the percentage change of the absolute biological torque ($|\tau_{bio}|$) between the powered and unpowered conditions being significantly lower than 0 for all individual velocities ($p = 3 \times 10^{-6}$ for 42 deg/s, $p = 4 \times 10^{-5}$ for 84 deg/s, $p = 3 \times 10^{-4}$ for 126 deg/s) and overall ($-59.20 \pm 5.58\%$, $p = 9 \times 10^{-14}$).

5.3.4 The exosuit delays the onset of fatigue

The isometric contraction task, performed with aid from the exosuit, showed a slower onset of fatigue in the biceps brachii compared to the unpowered condition ($p = 0.03$ for the ARV and $p = 0.01$ for the MNF).

Figure 5.6.a-b show the raw and envelope of the biceps' EMG signal, and the trend of the average rectified value (ARV) and median frequency of the EMG's spectrum (MNF) for both the powered and unpowered conditions of one representative subject. Values over the 40 s contraction window are reported in percentage of the initial value, discarding the first 3 s after reaching the target position of the elbow. A steeper positive slope for the ARV and a steeper negative one for the MNF indicate a faster onset of fatigue.

The mean slope and its standard error over subjects are shown, for both metrics and conditions, in Figure 5.6.c

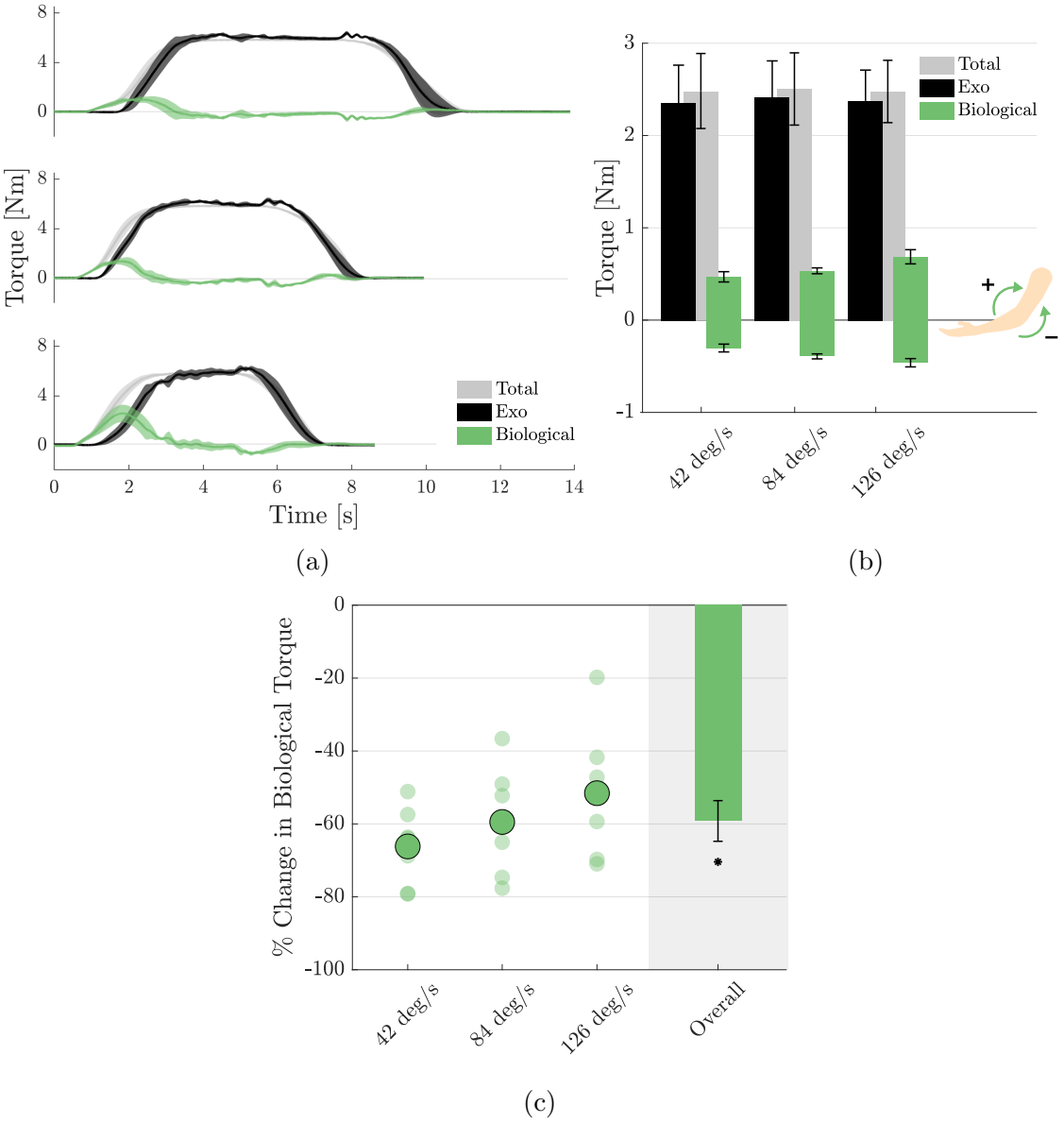

FIGURE 5.5: **Changes in biological torque.** (a) Total, assistive torque provided by the exosuit and biological torque (total-exo) for one subject, averaged over repetitions, for all three velocities of movement (from top to bottom: 42, 84 and 126 deg/s). As the velocity of movement increases, the magnitude of the biological torque increases, mostly around the transient regions. Shaded areas indicate the standard deviation around the mean. (b) Average over subjects of the total, assistive and biological torques. The exosuit compensates for most of the positive (flexing) torque but introduces a negative (extending) component. (d) Change in biological torque, expressed as percentage of the total torque in the unpowered condition (|biological powered| /total unpowered). Translucent circles are the values for each individual subject, opaque contoured circles indicate the mean over subjects. Asterisks indicate significant difference from 0. Wearing the exosuit significantly reduces the magnitude of the torque that the wearer needs to exert to move (-59.20± 5.58%, $p = 9\times10^{-14}$). Error bars show the standard error of the mean.

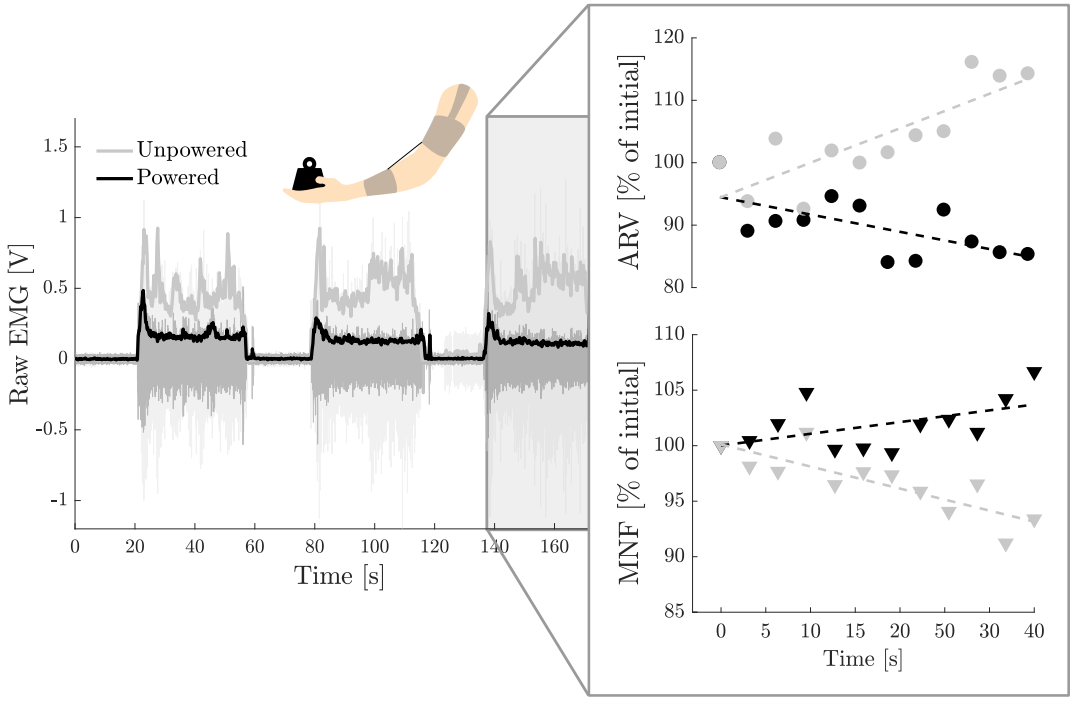

(a) (b)

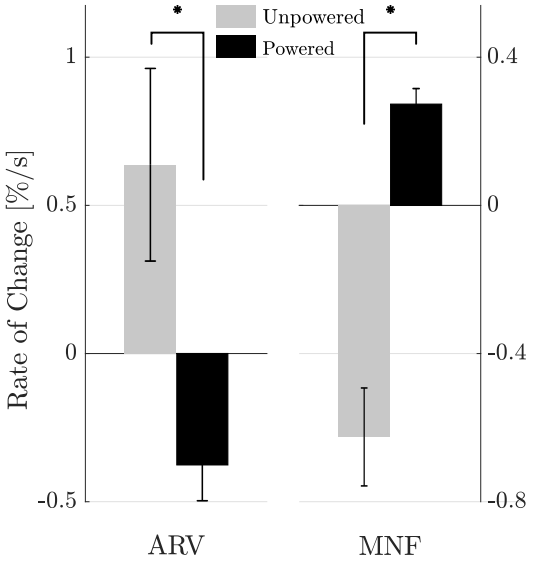

(c)

FIGURE 5.6: **Fatigue analysis.** (a) Raw signal and envelope of the electromyography (EMG) of the biceps brachii of one subject, during the isometric task, for both the unpowered and powered condition. (b) Trend of the average rectified value (ARV) and median frequency (MNF) of the EMG signal of one subject, during the last isometric contraction. Indexes are expressed in percentage of their initial value. A steeper positive slope for the ARV and a steeper negative one for the MNF indicate a faster onset of fatigue. (c) The slope of the ARV and MNF, averaged over subjects. Both indexes confirm that wearing the exosuit significantly reduces the onset of fatigue ($p = 0.03$ for the ARV and $p = 0.01$ for the MNF). Error bars show the standard error of the mean.

5.4 Discussion

5.4.1 On the changes in muscular contraction

Moving with assistance from the powered exosuit lowered the muscular effort by an average of $64.8 \pm 7.66\%$. This is probably a direct corollary of the observed significant reduction in biological torque between the powered and unpowered conditions.

These findings are in line with what we detected in a preliminary evaluation of the exosuit on two subjects, described in Chiaradia *et al.* [106], and show a higher benefit when compared to our very first evaluation of an assistive sleeve, reported in Dinh *et al.* [72].

The results in [72] (48.5% reduction in muscular effort) are only indicatively comparable to the ones presented here. The difference is partly caused by a refinement of the hardware and partly by considering that the control approach presented in Dinh *et al.* was aimed at assisting impaired subjects and designed to automatically tailor the level of assistance to the ability of movement of its wearer.

A systematic comparison of our work with existing literature is not yet possible because of the absence of a standard assessment procedure. Figure 5.7, however, highlights recent works that specifically report biomechanical and muscular effects of wearing a soft exosuit on joints that, like the elbow, are involved in gross lifting tasks. The figure puts emphasis on sample size and population type.

Four of the studies listed in Figure 5.7 use the reduction in magnitude of the EMG activity as a performance index. Kim *et al.* [107] report changes in muscular activation when wearing a cable-driven exosuit assisting shoulder and elbow flexion. During a static task, one subject showed an average of 49.4% and 68% reduction in the biceps brachii and the anterior deltoid, respectively.

Similarly, O'Neill *et al.* [43] present a wearable robot for the shoulder that uses soft textile pneumatic actuators to assist the joint in abduction and horizontal flexion/extension. The device, evaluated on three healthy participants, reduced the activity of the medial deltoid (63.89%) and infraspinatus muscles (34.03%) when

abducting the shoulder and that of the pectoralis major (23.20%) and posterior deltoid (70.09%) during horizontal flexion/extension.

Abe *et al.* present a suit made of pressurised muscle textile; they evaluated it on one subject and reported a reduction in the EMG activity of the biceps brachii of 33% and an increase in that of the triceps brachii of 35% [108].

Li and colleagues [109] use a paradigm similar to the one presented here to assist healthy subjects and stroke patients in flexing the shoulder and elbow. They recorded a reduction in the activity of the biceps brachii of a healthy individual of 58.17% and an increase in the range of motion of chronic stroke patients of up to 174%.

Two more studies evaluate the effect of exosuits on the movements of the upper limbs of impaired participants. Dinh *et al.* [72] use the residual EMG activity of a severe brachial plexus injury patient to initiate a flexing movement of the elbow. Kadivar *et al.* [110] explore the feasibility of introducing a similar device for the shoulder and elbow in a rehabilitation procedure of a traumatic brain injury patient. None of these two studies, though, report changes in muscular activity.

It is worth highlighting that all the results listed in Figure 5.7 were obtained with a procedure fundamentally different from the one used in this study: the admittance controller that we propose allowed the suit to continuously move in concert with its wearer while delivering an assistive torque. The other studies listed here lacked an intention-detection strategy. The robot was triggered to apply a predefined torque or trajectory, regardless of the intention of the wearer: during the evaluation the subject was simply asked to relax.

5.4.2 On the changes in biological torque

Moving with the exosuit reduced the biological torque by an average of $59.20 \pm 5.58\%$. The device could compensate the forearm's weight nearly entirely while holding a static position but the wearer still had to make a significant effort at initiation of movement (see the positive peaks of biological torque in Figure 5.5.a). This limitation was most likely caused by the flexing tendon slacking when the arm was fully extended; assistance was not delivered at initiation of movement until the slack was recovered. A simple solution to this problem could be to pre-tension the

tendons. This, however, might negatively impact on comfort, especially during prolonged use.

Moving with the exosuit increased the extending biological torque at the elbow compared to the unpowered condition (+0.39 N m). Participants needed to slightly push to initiate the downwards motion when the elbow was flexed (see the peaks of negative torque in Figure 5.5.a). This unwanted interaction torque was caused by the impedance of the controller and can be used as an index of the transparency of the exosuit: increasing the admittance of the controller would reduce this effect but would make the device less stable.

Surprisingly, the increase in negative torque was not accompanied by a significant increase in the activity of the extensor muscle. One plausible explanation could be the subtle change in the activation of the triceps brachii was not sufficient in magnitude to be detected with surface EMG. Further investigations, looking, for example, at the muscular response while holding heavier weights, could help to clarify this point.

During isometric tasks our exosuit delayed the onset of fatigue. This result is most likely a corollary of the observed reduction in biological torque. A similar finding is described in [52], where a cable-driven suit for the shoulder is shown to reduce the fatigue in the anterior and medial deltoid of five healthy subjects. Unfortunately, a quantitative comparison here is not possible because of the different metrics used to assess fatigue in [52].

5.4.3 On the changes in kinematics

Moving with assistance from the exosuit significantly reduced the accuracy of movement. This deterioration in accuracy was caused by the powered movements being slower than the unpowered ones. Figure 6.12.b shows a clear delay between the reference and measured trajectory of the elbow in the powered condition, quantified in Figure 5.3.a. Wearing the exosuit introduced a delay in the reaction time of approximately 200 ms. An analysis of the peak velocities of the elbow between the two conditions (Figure 5.3.b) confirms these observations: wearing the exosuit reduces the peak velocity of the elbow by an average of 9.4±4.4%. This slowing down of movements is consistent with previous findings investigating the effects of

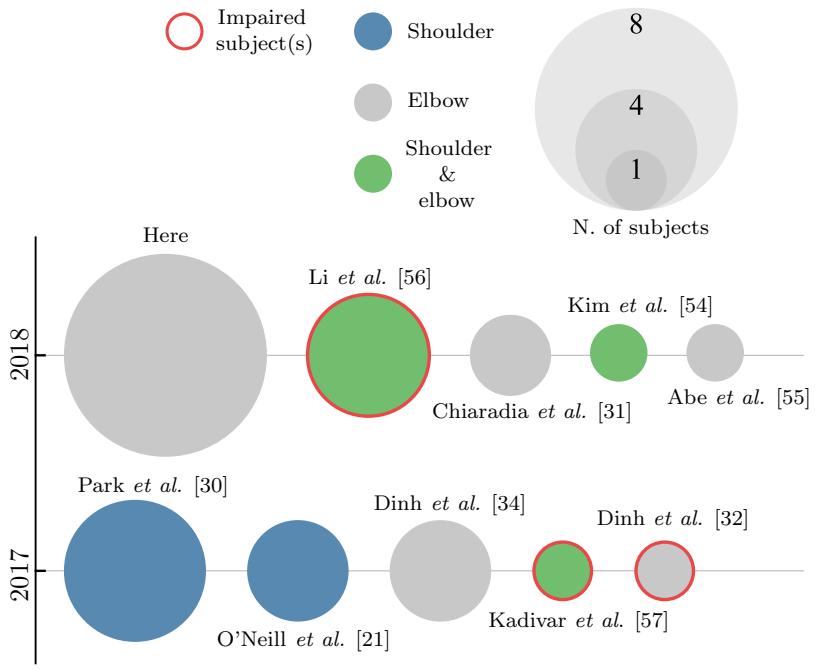

FIGURE 5.7: **Studies evaluating the effect of soft wearable robots on the biomechanics of the upper limbs.**

interactions with an exoskeleton on human motion [111], but its underlying cause is not entirely clear. We think that one or a combination of two mechanisms may be at play here: (1) Desmurget *et al.* [112] have shown that movements constrained by contact with an external body (in this case the exosuit), involve a fundamentally different control strategy from unconstrained movements, which can affect their duration. (2) Movements are slowed down by technological limitations of the device: deformation and migration of the fabric, friction and backlash in the Bowden cables and slack in the tendons introduce latency and affect the transient behaviour of the controller.

There is compelling evidence that smooth movements are characteristic of efficient and well-trained motor behaviour [101] and an assistive device should not alter this. Yet we found that wearing the exosuit significantly reduced movement smoothness. Encouragingly, the difference between the mean values of the SPARC index was fairly low: -1.76 ± 0.10 (unpowered) and -1.82 ± 0.14 (powered), corresponding to only a 3.4% drop.

Unfortunately, no investigation performing such assessment on soft exosuits exists in literature, but our results echo the findings from Jarassé [113] and Pirondini

[114], reporting an increase in movement jerk and number of peaks, respectively, when subjects were assisted by a rigid exoskeleton.

The deterioration in smoothness and accuracy of movement are both imperfections in the transparency of the exosuit. They suggest that care should be taken if using the device as an assessment tool, since powered movements may not reflect the characteristics of natural movements. It should be noted, however, that participants used the device for less than 10 min, in total. It would be interesting to verify if additional training results in a mitigation of these unwanted effects. Previous studies confirm that the initial disruption of natural kinematics of movement, often seen when one first wears an assistive robotic apparatus, progressively diminishes as the subject learns to use the device [115].

The time lag, introduced by the suit, between the intention and the initiation of movement, may affect one's feeling of being in control of his/her own actions, known as sense of agency. Previous work has shown that a longer interval between actions and their effects is associated with a lower sense of agency [116]. This idea applies to the temporal relation between motor and sensory signals too: temporally matched intended movements and proprioceptive feedback seem to be essential for promoting intuitive control and body-ownership [117]. Investigating how the kinematic imperfections of the suit impact on the user's subjective perception of the device would be of great interest. This is especially true for clinical applications, where the strong connection between the robot and body perception, often termed "embodiment", is a crucial factor for functional recovery [118].

5.4.4 Limitations of the experimental protocol

Finally, we should spend a word on the device's safety. Because of the intrinsic compliance of its transmission, the suit benefits from the features of traditional series elastic actuators: its elasticity decouples the actuator's rotor inertia from the limb, should an impact occur, and the low impedance is preserved even in case of failure. The low mass of the device, moreover, practically eliminates inadvertent damage to the environment. The admittance control adds an additional layer of safety. This is because by imposing the relation between force and velocity, unlike direct force or position control schemes, allows to constrain the power transfer between the device and its user [86]. The major limitation lies in the low efficiency

of the actuation stage, caused by the high reduction ratio needed to deliver the range of forces required by the suit. This results in low backdrivability when power is off.

Although this study demonstrates encouraging results, we acknowledge that there are a number of limitations to this work. Firstly, this study involved a small and relative young cohort of participants; this reduces the strength of the statistical findings. The participants, moreover, were all males of similar height (178±0.8 cm) and weight (77.8±2.1 kg). This choice was forced by the size of the available prototype of the exosuit. We have no reason to believe that the results would change for a female population or for individuals of different physical structure, if they wore a suitably-sized device.

In this study, the baseline condition for comparison was an unpowered condition and not a no-suit condition. We chose this configuration to reduce the length of testing sessions and to avoid doffing and donning the suit during bouts, which could have led to increased variability in the kinematic data.The wearable component, attached to the forearm, moreover, weighs only 170 g, distributed close to the center of the elbow joint; becuase of this, we speculate that the unpowered condition would differ very little from a no-suit condition.

Another limitation of our study is that the current version of the exosuit uses a quadrature encoder, mounted on a 3D printed link, to measure the elbow angle. The linkage structure transmits no torques and bears no loads, but it only measures the true elbow angle if aligned with the biological joint. We took care of ensuring this was the case during the donning procedure but we cannot exclude that movement of the fabric may have slightly shifted its position during operation. We believe that two of the outliers in Figure 6.14.b may have been caused by incorrect measurement of the joint angle. We estimated that migration of one of the anchor points, along the main axis of the forearm/arm, between 3 mm-9 mm, can result in a maximum error in measuring the joint angle between 8 deg-14 deg. We did not observe systematic displacement for the range of forces used in this study. However, for the sake of robustness, it would be appropriate to replace the encoder with a more robust sensing strategy (e.g. inertial measurement units).

In order to evaluate the effects of the device solely on elbow movements, we performed the experiment in a very controlled setting. Subjects were asked to keep

the arm aligned with gravity, only move the forearm and the range of motion was limited to 90 deg for safety. We have no reason to doubt that the results obtained in this study will not generalize to functional movements, but further investigations are needed to verify this hypothesis.

The present study only evaluated the performance of the exosuit when assisting its wearer in lifting a single, relatively low weight. The dynamic tasks were performed with a 1 kg mass, held in the participants' hand, and the static task, used to assess fatigue, were performed with a load equal to 3% of the wearers' body mass. It would be interesting to investigate the performance of the device for varying loads. We expect the limiting factor here to be comfort rather than the maximum rated torque of the actuation stage.

Last, the admittance controller used anthropometric data to estimate the assistive torque required by each participant, based on their body mass and height; because of physiological differences among subjects, a fine tuning of the parameters, performed in the familiarization phase, was required to personalize the controller. The tuning was based on qualitative feedback from the participant and was by no means optimal.

Recently published results suggest that such individualization process could be addressed systematically and automated through optimization techniques. Zhang and colleagues [97] have shown how a control paradigm that modulates the assistance characteristics, in order to minimize the metabolic cost of human walking, can accommodate the large diversity among subjects and significantly improve performance. Ding *et al.* [98] have shown equally encouraging results using a Bayesian optimization technique to modulate the force profile of a soft exosuit to assist hip flexion. This gives us reason to believe that identifying a suitable cost function for the device presented here and using it to optimize its control parameters, could lead to improved quality of assistance and intuitiveness of use.

5.5 Conclusion

An analysis of the biomechanical and kinematic effects of the soft exosuit presented in Chapter 3 and controlled using the paradigm describe in Chapter 4, tested on healthy subjects, showed that: (1) the device is not exactly transparent, affecting

the speed and accuracy of movements; (2) it works in parallel with the human muscles, significantly reducing their magnitude of activation in dynamic movements; (3) assistance from the exosuit in static tasks delays the onset of muscular fatigue.

Chapter 6

Addressing the curse of dimensionality in wearable robots

The size, weight and power consumption of wearable robots rapidly scale with their number of active degrees of freedom. While various underactuation strategies have been proposed, most of them impose hard constrains on the kinetics and kinematics of the device. In this chapter, we propose a paradigm to independently control multiple degrees of freedom using a set of modular components, all tapping power from a single motor. Each module consists of three electromagnetic clutches, controlled to convert a constant unidirectional motion in an arbitrary output trajectory. We detail the design and functioning principle of each module and propose a principled approach to control the velocity and position of its output. The device is characterized in free space and under loading conditions. Finally, this Chapter's digression is reconnected to the topic of the thesis by evaluating the proposed actuation scheme to drive the soft exosuit for the elbow joint, using the methodology proposed in Chapter 5. We compare the new actuation design with the performance obtained using a traditional DC motor and an unpowered-exosuit condition.

6.1 Introduction

One of the earliest attempts to develop a wearable robotic device to assist human motion, dating back to 1967, failed because of the excessive weight and size of the system [119]. Since then, advancements in material science, power supplies and

computing power have fundamentally broadened the boundaries of what we can achieve.

Exoskeletons have been used for a plethora of applications, ranging from performance augmentation in industry [120] to neuro-rehabilitation in medicine [121]. Despite exciting achievements, there are still substantial technical limitations preventing wearable powered devices from becoming a ubiquitous part of our daily lives. Among others, power requirements and weight of the actuation stage play a key role, confining most of the existing exoskeletons to research laboratories or specialized clinics.

A significant step forwards in this direction has been recently taken by using fabric and polymers to transmit forces and torques to the human body. Soft materials limit the magnitude and accuracy of assistive forces but allow to engineer lighter, less power-demanding and svelter exoskeletons, resembling our everyday clothes more than the rigid machines portrayed by science-fiction movies [53].

Although fundamental research is being carried out to design efficient, controllable and robust new actuators [122], most exosuits are powered by traditional electric motors, transferring power to the joints through flexible transmissions [40]. Using one motor to assist each Degrees of Freedom (DoF) of the human body is the most common design choice. However, this strategy is easily scalable to complex systems: the human arm alone has at least 7 DoFs and the complexity, size and weight of a device using such a high number of motors would make it impractical.

A common way to address this problem is to use fewer motors than DoF: underactuation strategies include differential mechanism [123], mechanical implementation of kinematic synergies [124] and routing of the driving cables along multiple joints [125]. However, these approaches impose hard constrains on the kinetics and/or kinematics of the wearer, allowing only a finite number of predefined moving patterns. This idea is conceptually shown in Figure 6.1.a, where multiple DoF are mechanically coupled to be driven by a single motor.

An interesting, yet less investigated, method involves using a set of modules, each one moving a DoFs, that all tap mechanical energy from a single drive. In literature, this paradigm is known as One-To-Many (OTP) [126], Unidrive [127] or Single-Motor-Driven (SMD) system [128].

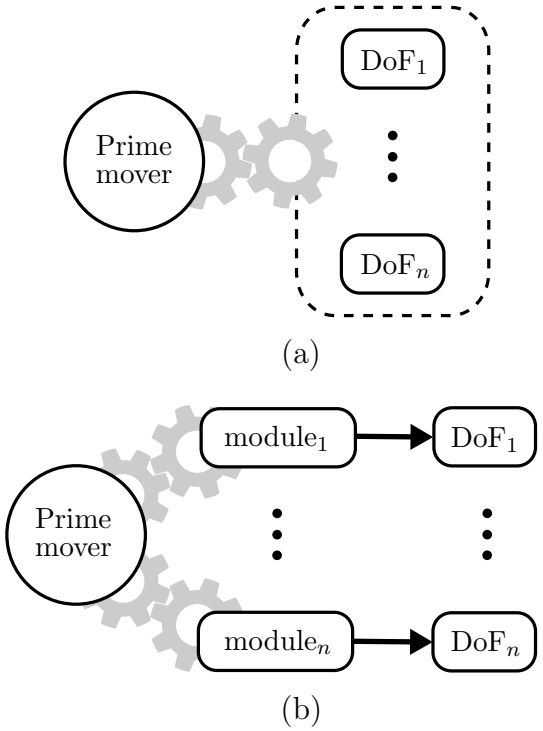

FIGURE 6.1: **Underactuation mechanisms and One-To-Many (OTM) paradigm.** (a) Typical underactuated mechanisms rely on some form of mechanical coupling between degrees of freedom (DoF), imposing a hard constrain on the kinematics and/or dynamics of the system. (b) The OTM paradigm consists in actuating many DoF, each tapping power from the same drive but controlled independently by a local module.

The idea of having a prime mover delivering motion to many subunits is gracefully illustrated in Dante Alighieri's picture of the structure of the universe: he imagined the existence of an outer rotating spheric "sky" that generates energy and transfers it trough its motion to its inner circles, each rotating at a fraction of its speed:

"Non suo moto per altro distinto,
ma li altri son mensurati da questo,
s come diece da mezzo e da quinto." [1]

A One-To-Many transmission is the mechanical equivalent of this idea: one electric motor, that we shall call prime mover, transfers power to many modules, each driving a DoF. This paradigm is shown in Figure 6.1.b. The prime mover rotates at a constant speed and the trajectory of each DoF is modulated locally by its corresponding module. Such a setup, unlike underactuation mechanisms, allows

[1] "Its motion is not measured by another, but all the others are by this, as ten is measured by its half and by its fifth."[129]

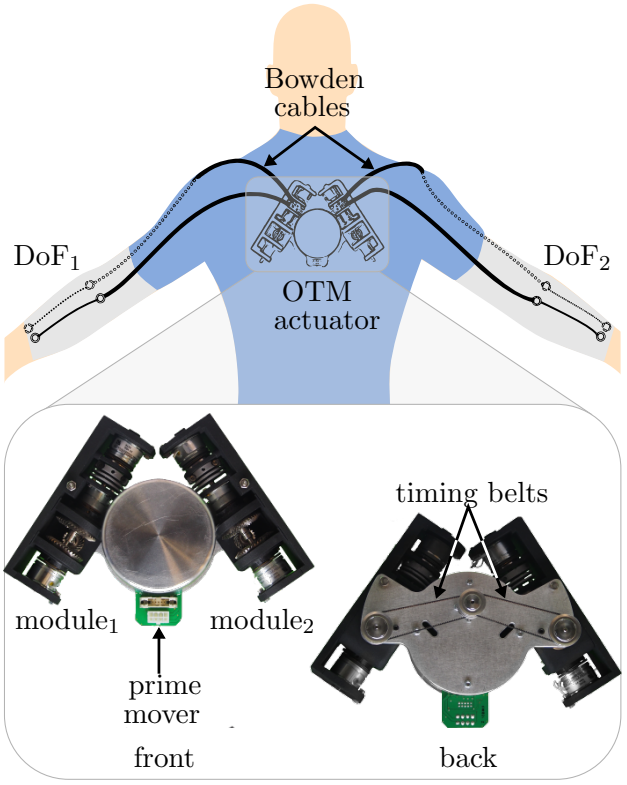

FIGURE 6.2: **OTM actuator to power two elbow exosuits with one electric motor.** This system, that we proposed in [131], consists in one prime mover, transmitting power to two clutchable DOF Modules connected to two elbow exosuits via Bowden cables. Each module independently controls the position of its corresponding DoF.

independent control of each DoF and scales nicely with increasingly complex systems.

The challenge when designing an OTM system comes down to engineering a module that is smaller and less power-consuming than a motor but can control the position, velocity and/or torque of a joint just as well.

Performance-wise, Infinite variable transmissions (IVT), allowing to continuously modulate their transmission ratio within a range of positive and negative values, are the ideal candidates for an OTM module. The input velocity remains constant while the output velocity of each DoF can be modulated and even reversed by changing the transmission ratio of each IVT. The recently-published work from Kembaum *et al.* proposed a novel compact design [130], but traditionally, the size and mass of IVTs would not justify their use over a simple additional motor.

Hunt *et al.* proposed an OTM system where each module consisted of a linear spring and a clutchable ratchet, the former used to store energy and the latter to selectively release it [126].

The group led by Kermani [132, 133], proposed a mechanism employing magneto-rheological (MR) clutches to design a 2 DoF manipulator for safe human-robot interaction. A single electric motor was placed a the base of the robot, providing power to both joints, while three MR clutches were controlled to limit the output torque's magnitude and direction at each joint. The authors showed that this Distributed Active-Semi Active (DASA) actuation paradigm can achieve smooth and accurate tracking of joint positions while benefiting from key advantages of MR clutches such as backdrivability and low impedance.

Finally, a handful of research groups have presented designs based on a similar and powerful principle: the module consists of at least two gears, constantly rotating in opposite directions, and the output is coupled with either one of them using ElectroMagnetic (EM) clutches, or locked using a brake [127, 134]. The group led by Xie was probably one of the first to propose such arrangement to drive a 9 DoF robotic hand [128] and a 6 DoF serial manipulator [135] with a single electric motor.

The encouraging results of OTM systems, applied to drive manipulators and robotic hands, led us to investigate their feasibility in the field of wearable assistive devices, increasingly in need of novel, efficient actuation paradigms. We previously proposed an OTM system, consisting of 2 clutchable modules, to actuate the tendons driving a soft exosuit for the elbow joints [131], shown in Figure 6.2.

In this Chapter, we propose a refined version of our module's design and present a PID-modulated Pulse-Width Modulation (PWM) controller to finely adjust the velocity of each DoF. We characterise the system on a test-bench and then use it as the low-level layer of an admittance-based scheme to control our soft exosuit.

The performance of the new actuation unit is finally compared to that of a traditional DC motor by assessing their impact on kinetics and kinematics of human movement. This human-in-the-loop validation highlights the limitations of our approach and points out avenues for improvement.

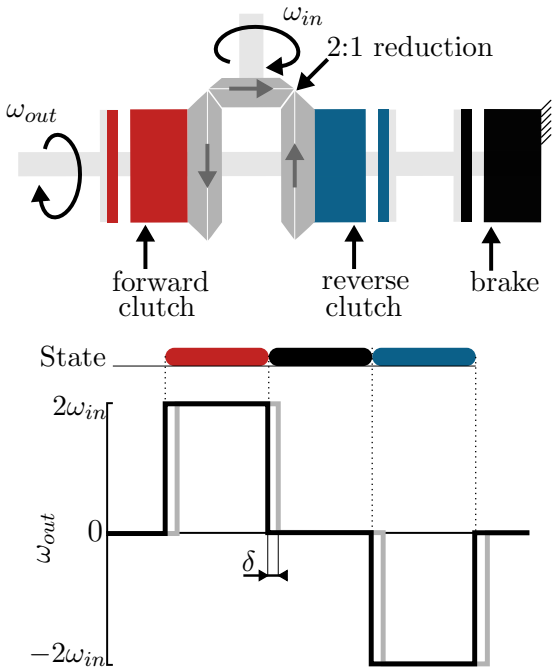

FIGURE 6.3: **Working principle of a DOF module.** ElectroMagnetic (EM) clutches are used to convert a unidirectional input to a bidirectional output by coupling an output shaft with either one of two counter-rotating gears; a brake locks the output in place. Black lines in the plot show the ideal behaviour of the clutches, gray lines the actual one, caused by a delay in engagement and disengagement of the armature and rotor.

TABLE 6.1: Possible states of the module

State	Forward clutch	Reverse clutch	Brake
Free	OFF	OFF	OFF
Forward	ON	OFF	OFF
Reverse	OFF	ON	OFF
Lock	OFF	OFF	ON

6.2 OTM Design and Control

The working principle of the clutchable OTM module is shown in Figure 6.3. The device consists of 3 EM clutches (SO11, Inertia Dynamics, 5 W) used for coupling the output to either a forward-rotating gear (red), a reverse-rotating gear (blue) or to lock it (black). Depending on which clutch is engaged, the module works in 4 possible states:

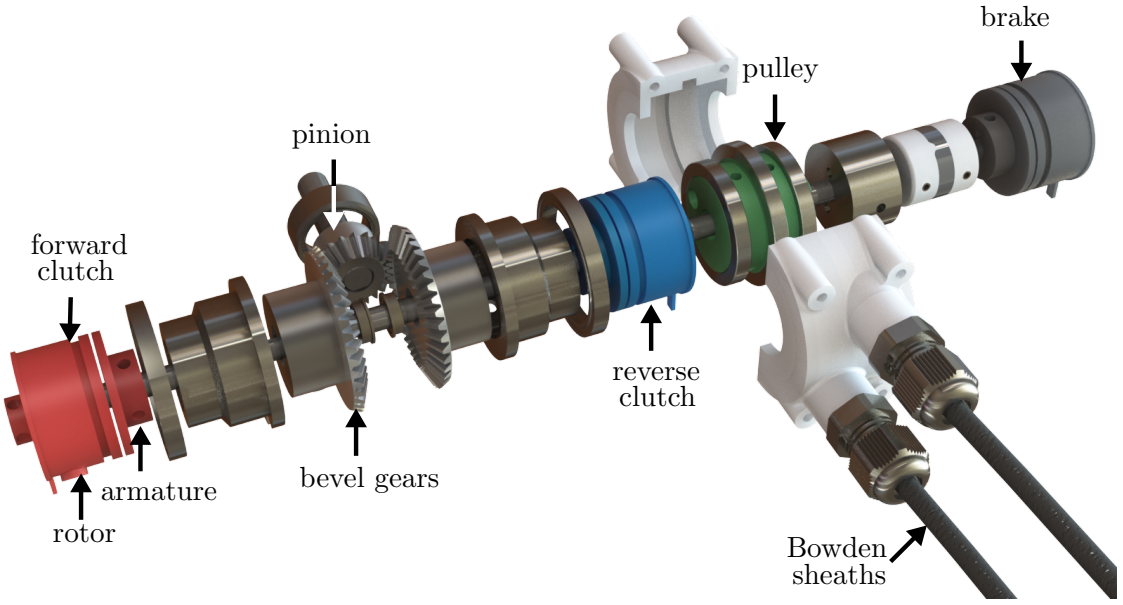

FIGURE 6.4: **Mechanical design of a One-To-Many (OTM) module.** Each module receives power from the prime mover through a pinion, connected to two, opposite-facing, bevel gears that rotate in opposite directions. Each bevel gear can be coupled to the passing countershaft by engaging an ElectroMagnetic (EM) clutch, selectively rotating it in either direction. A third EM clutch can connect the countershaft to the frame, acting as a break. The shaft drives a pulley housing the antagonistic Bowden cables that actuate the soft exosuit.

- Free: when all the clutches are disengaged, the output velocity at the pulley is undefined, the output is back-drivable.
- Lock: when the brake is engaged.
- Forward: when the "forward" clutch is engaged, the output velocity equals the input velocity times the reduction ratio between the input and output ports.
- Reverse: when the "reverse" clutch is engaged, the output velocity equals the reverse of the input velocity times the reduction ratio between the input and output ports.

Table 6.1 summarizes the states of the module, where the engagement of each clutch is represented by a binary variable. Any other pattern of activation is avoided as it would result in mechanical stall of the prime mover.

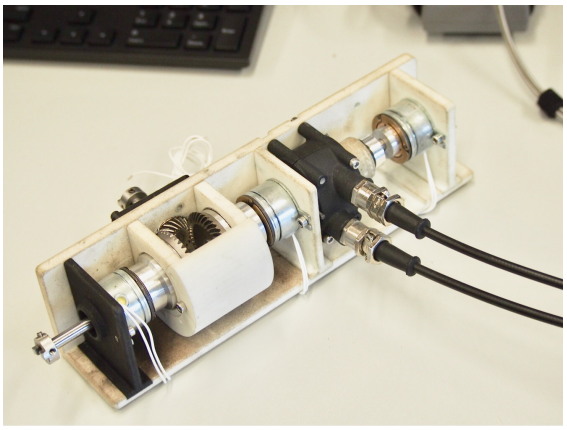

FIGURE 6.5: **Assembled of a single DOF Module.**

6.2.1 Mechanical Design

Figure 6.4 shows an exploded view of the functional components of the module. A pinion is continuously rotated by the prime mover and meshes orthogonally with two bevel gears facing each other. Thanks to this arrangements, the bevel gears rotate in opposite directions. An aluminium link couples each gear to the armature of an EM clutch, whose rotor is rigidly linked to a passing countershaft. When power is applied to either one of the EM clutches, the armature is coupled to the rotor, thus effectively linking the countershaft to either one of the gears. A third, identical clutch, acts as a brake, locking the countershaft in a static position by coupling it with the frame. A flexible coupling joins the countershaft to a pulley (the output of the module); the pulley houses two cables wrapped in opposite directions and is used to transmit motion to the exosuit through flexible Bowden cables. Figure 6.5 shows a photograph of an assembled module, enclosed in a 3D printed casing.

6.2.2 Control

Figure 6.3 shows that the module has 3 working states: forward, reverse and brake. In [131], we proposed a heuristic control approach that consisted in a feedback state machine to keep the measured trajectory as close as possible to a reference profile. This strategy, although being simple, presented fundamental limitations in accuracy and stability.

In this work, we propose a more principled paradigm to control this discrete system, based on the work of [127]. The controller is based on Pulse Width Modulation (PWM) of the three discrete states of the OTM, regulated by a feedback PI controller, to continuously adjust the average velocity of the module's output. The non-linear PI controller translates a difference between the desired and actual velocity of the module to a rectangular pulse signal, having value -1 (reverse clutch), 0 (brake) or 1 (forward clutch), whose duration in time is dependent on the magnitude of the error.

In the next sections we describe how a tracking error is converted to a discrete control signal for the clutches for an ideal PWM-regulated system.

Using a state-space representation, we can describe a non-linear PWM-controlled system with the following equations:

$$\begin{cases} \frac{dx}{dt} = u(t)\omega_{in} \\ y(t) = x(t) \\ e(t) = r(t) - y(t) \\ u(t) = PWM(e(t_k)) \end{cases}$$

where

- $u(t)$ is the control signal for the clutches, bonded to have values -1,0 or 1.
- $x(t)$, the state variable; in out case, the angular position of the module's pulley, θ.
- $e(t)$ is the error between the reference $r(t)$ and the output $y(t)$.
- ω_{in} is the fixed input velocity of the module.
- t_k represents the instant of initiation of the k-th PWM period (Figure 6.6, top).
- $PWM(e(t_k))$ is the PWM control operator, defined as:

$$PWM = \begin{cases} \text{sgn}(e(t_k)) & \text{for } t_k \leq t \leq t_k + \alpha \\ 0 & \text{elsewhere} \end{cases} \tag{6.1}$$

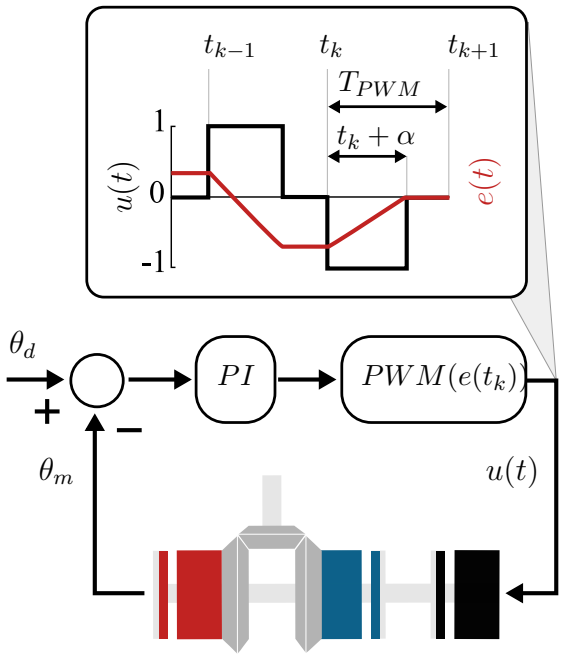

FIGURE 6.6: **PI-regulated PWM control of the clutchable module.** The error between the desired and measured position of the countershaft is passed through a traditional PI controller in cascade with the PWM function defined in Equation 6.1. This sets the control signal to 1 or -1 for a fraction of the PWM period that depends on the magnitude of the error. 1 engages the forward clutch, -1 the reverse clutch and 0 the brake.

where we have used $\alpha = \tau(e(t_k))T_{PWM}$, for simplifying the notation, with $\tau(e(t_k))$ being the duty ratio function and T_{PWM} the period of the PWM signal.

The PWM operator basically sets the control signal to 1, 0 or -1 for a period of time defined by $\tau(e(t_k))$.

This duty ratio function, $\tau(e(t_k))$, needs to output a value between 0 and 1, representing the ratio for which the control signal will be equal to the sign of the error. Sira-Ramirez suggests the following as a good choice for non-linear systems [136]:

$$\tau(e(t_k)) = \begin{cases} \beta|e(t_k)| & \text{for } |e(t_k)| \leq 1/\beta \\ 1 & \text{for } |e(t_k)| > 1/\beta, \end{cases} \tag{6.2}$$

that makes the duty ratio proportional to the magnitude of the error if the error is relatively small (smaller than a threshold $1/\beta$) and saturates it to 1 if the magnitude of the error is larger than the threshold.

The big assumption of this controller is that the clutches behave like ideal switches, i.e. the output velocity of the module instantaneously equals a multiple of the input velocity when the clutch is engaged (Figure 6.3, black). In practice, this is not the case: the clutches have an intrinsic delay when engaging (shown in gray in Figure 6.3) and the velocity of the output decays in an exponential-like fashion when the clutch is disengaged [127].

[137] and colleagues have shown that such phenomenon can be mitigated with the addition of an integral feedback term. Adding this to Equation 6.2 makes the output of the duty ratio function, in the region $|e(t_k)| \leq 1/\beta$, proportional not only on the magnitude of the error but also to its history, effectively behaving like a non-linear PI controller.

6.2.3 Performance

We characterised the performance of the DOF module for varying control parameters and tested its limits in speed and torque transmission.

Specifically, we evaluated the ability of the controller to modulate the output velocity for varying PMW periods T_{PWM}, we tested its ramp response and bandwidth for varying input velocities of the prime mover and, lastly, its maximum load rating. The DOF module was equipped with an incremental encoder (AMS, AS5047P, 1000 pulses/rev), monitoring the position of the cable pulley.

6.2.3.1 Velocity modulation

Figure 6.7 shows the ability of the PWM controller to adjust the velocity of the module as its duty cycle changes. The plot shows the normalised velocity (ω_{out}/ω_{in}), for varying duty ratio of the PWM signal, where the duty ratio expresses the percentage of time in T_{PWM}, where the control signal is non-zero, i.e. 1 or -1. Lines of different color represent different frequencies of the PWM signal.

The T_{PWM} should be set as small as possible, to ensure stability, but bigger than the time delay δ, necessary for the clutches to physically engage once powered. Indeed, very high frequencies of the PWM do not result in a higher ability to modulate the output velocity. This is caused by the intrinsic delay, δ, necessary

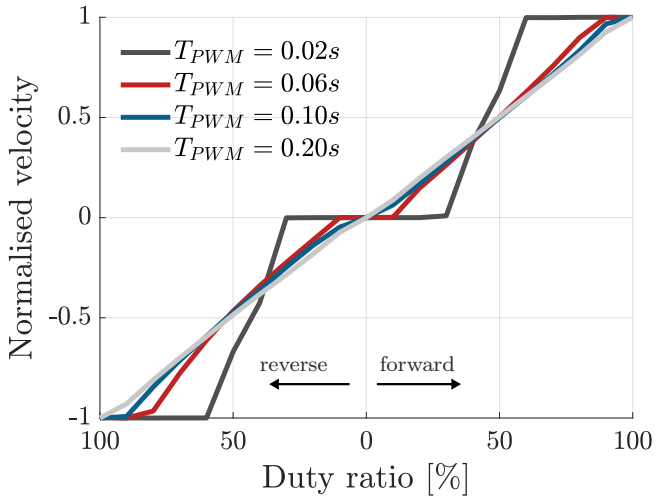

FIGURE 6.7: **Choosing the period of the PWM signal.** Velocity of the output shaft, normalised by the input speed, versus the duty ratio of the PWM signal controlling the forward and reverse clutches. Different colors show different PWM frequencies. For high frequency, low and high duty ratios do not affect the output velocity.

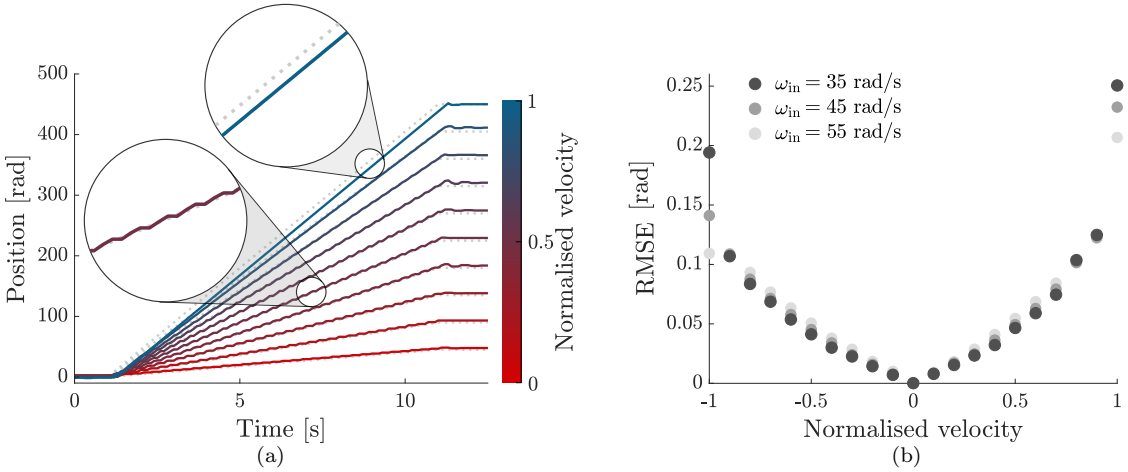

FIGURE 6.8: **Ramp response.** (a) Tracking performance of the DOF module with the PI-regulated PWM control. Ramp response for velocities between 10% and 100% of the input velocity. (b) RMSE between the desired and measured positions of the module's output, for desired output velocities between -ω_{in} and ω_{in} (x-axis) and different input velocities (grayscale). The behaviour of the controller is symmetric, with increasing error for higher absolute velocities.

for the rotor and the armature of the EM clutches to engage upon the application of power. We chose $T_{PWM} = 0.20\,\text{s}$, being the highest PWM frequency showing a near-linear trend.

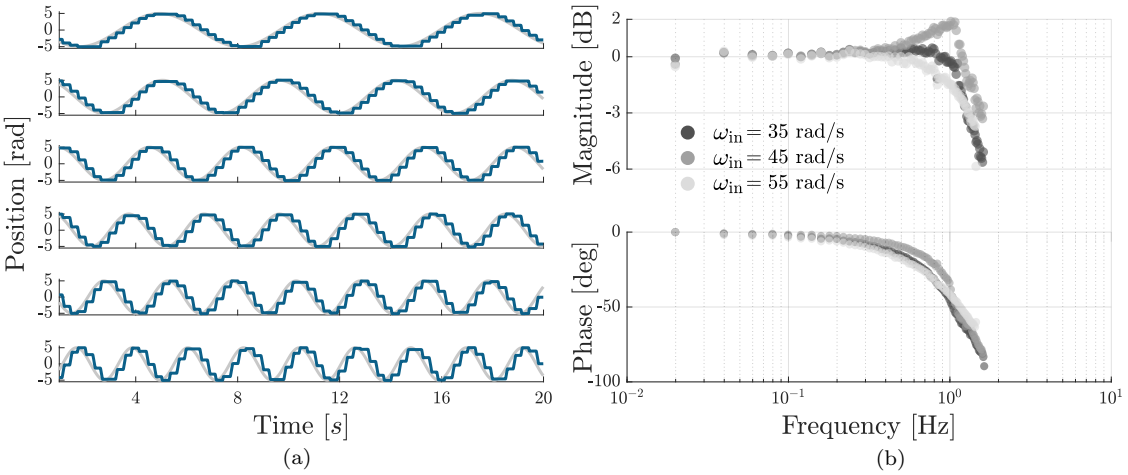

FIGURE 6.9: **Sinusolidal tracking and Bode plot.** (a) Sinusoidal tracking accuracy of the OTM module with the PI-regulated PWM control described in Section 6.2.2, shown for six equally-spaced frequencies, between 0.15 Hz and 0.4 Hz. (b) Bode plot of the transfer function between desired and measured position of the module's output, shown for three different velocities of the prime mover. The system has a cut-off frequency of 1.26 Hz, 1.51 Hz and 1.30 Hz, for a speed of the prime mover of 35 rad/s, 45 rad/s and 55 rad/s, respectively.

6.2.3.2 Ramp Response

Figure 6.8.a shows the tracking ability of our PID-modulated PWM controller to track a ramp position profile of increasing slope, between 10% and 100% of the input velocity, in steps of 10%. The experiment was repeated for three fixed input velocities and showed a consistent behaviour, with the tracking ability of the controller deteriorating as the normalised speed approached one.

6.2.3.3 Bandwidth

Figure 6.9 shows the tracking of sinusoidal trajectories and Bode plot of the module with the controller proposed in Section 6.2.2. The module was commanded to follow a sinusoidal trajectory of the form:

$$\theta^d_{out}(t) = A \sin(2\pi f_0 t) \tag{6.3}$$

with A corresponding to the amplitude required for a flexion/extension motion of the elbow of 90 deg and a frequency f_0 evaluated between 0.01 Hz and 1.51 Hz, in incremental steps of 0.02 Hz. For each frequency we collected data for 20 s at a sampling rate of 1 kHz; the first second was discarded for further analysis

TABLE 6.2: Technical Specifications

Characteristics	**Values**		
Module			
Weight [Kg]	0.534		
Dimensions [cm]	$15 \times 6 \times 5$		
	35 rad/s	45 rad/s	55 rad/s
Bandwidth [Hz]	1.26	1.51	1.30
Assembly			
DOF	2		
Weight [Kg]	2.2		
Dimensions [cm]	$26 \times 18 \times 12$		
Motor Power [W]	90		
Max Torque [a] [Nm]	3.4		
Max Velocity[a] [deg/s]	424		

[a]at the elbow joint

to evaluate the performance of the system at steady-state. This procedure was repeated for three different input velocities of the prime mover 35 rad/s, 45 rad/s and 55 rad/s.

For each frequency we performed an analysis in the Fourier domain to evaluate the amplitude ratio and the phase lag between the desired $s(t)$ and the measured θ_{out} signal. The n^{th} complex coefficient of the Fourier series has the form:

$$C_n = \frac{f_0}{N} \int_0^{\frac{N}{f_0}} s(t) e^{-j2\pi n f_0 t} dt \tag{6.4}$$

where f_0 is the sampling rate and N is the number of cycles whereby the signal is repeated. For each driving frequency we evaluated the response as the ratio between the coefficients of the fundamental frequency of the measured and desired signals:

$$H(f_0) = \frac{C_1^{measured}}{C_1^{desired}}. \tag{6.5}$$

Figure 6.9.b shows a Bode plot of the system, representing the transfer function between the measured and desired position of the module. The device and controller show a cut-off frequency of 1.26 Hz, 1.51 Hz and 1.30 Hz, for a speed of the prime mover of 35 rad/s, 45 rad/s and 55 rad/s respectively. We chose a velocity of 45 rad/s for all following tests.

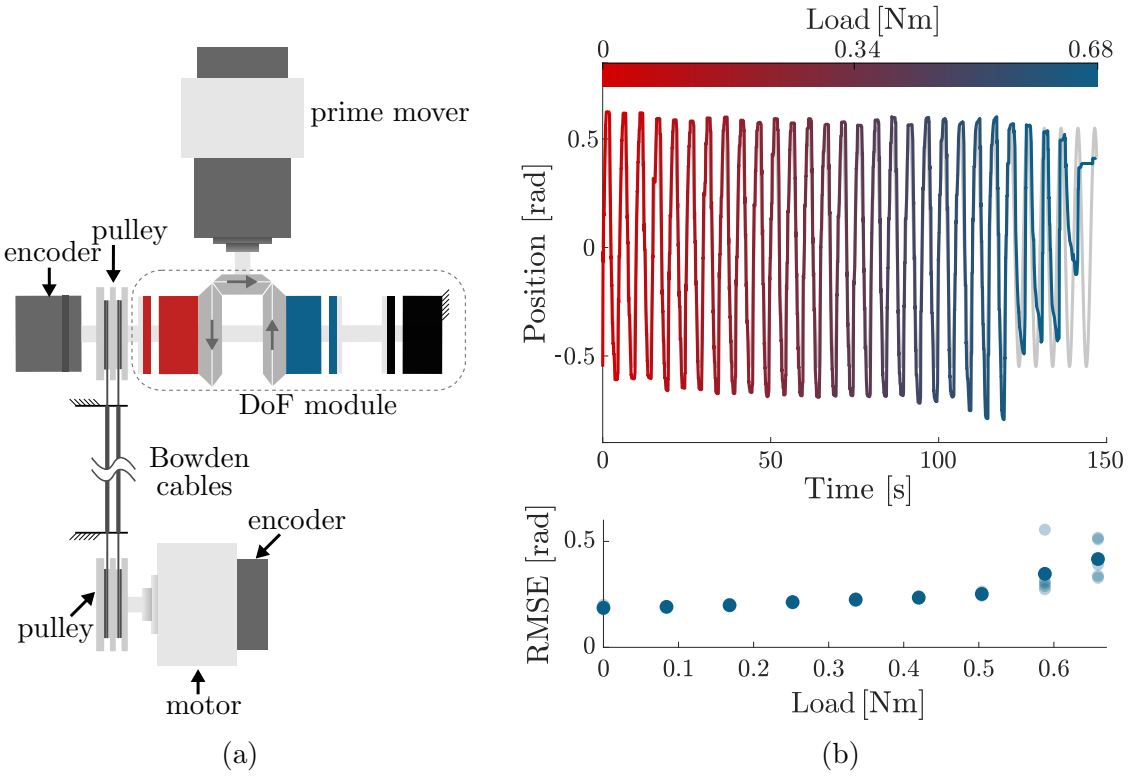

FIGURE 6.10: **Performance testing under load.** (a) Testbench used for assessing the performance of the DoF while moving a load. The Bowden cables, driven by the module, were attached to a second DC motor that applied a resistve torque. (b) Tracking accuracy of the OTM module, controlled with the PI-regulated PWM controller, under increasing load. The top plot shows the desired (gray) and measured (coloured) position of the module's output as the load increases between 0 N m and 0.68 N m. The clutches start to slip just before 0.6 N m, as quantified by the increase in RMSE shown in the bottom plot.

6.2.3.4 Loaded behaviour

Finally, we tested the tracking accuracy of the module in the presence of a load. For this testing, we attached the Bowden cables on a second pulley, driven by a DC motor (Maxon EC-i 40, 70W, 3.7:1 reduction ratio), to apply a load on the end-effector (shown in Figure 6.10.a).

The module was set to follow a sinusoidal trajectory while the load linearly increased between 0 N m and 0.68 N m (maximum rated torque for the EM clutches). The test was repeated 5 times. Indeed, the clutches started slipping, causing a steep deterioration in tracking accuracy, around 0.6 N m (Figure 6.10.b). This is lower than their rated value, probably due to friction losses in the transmission.

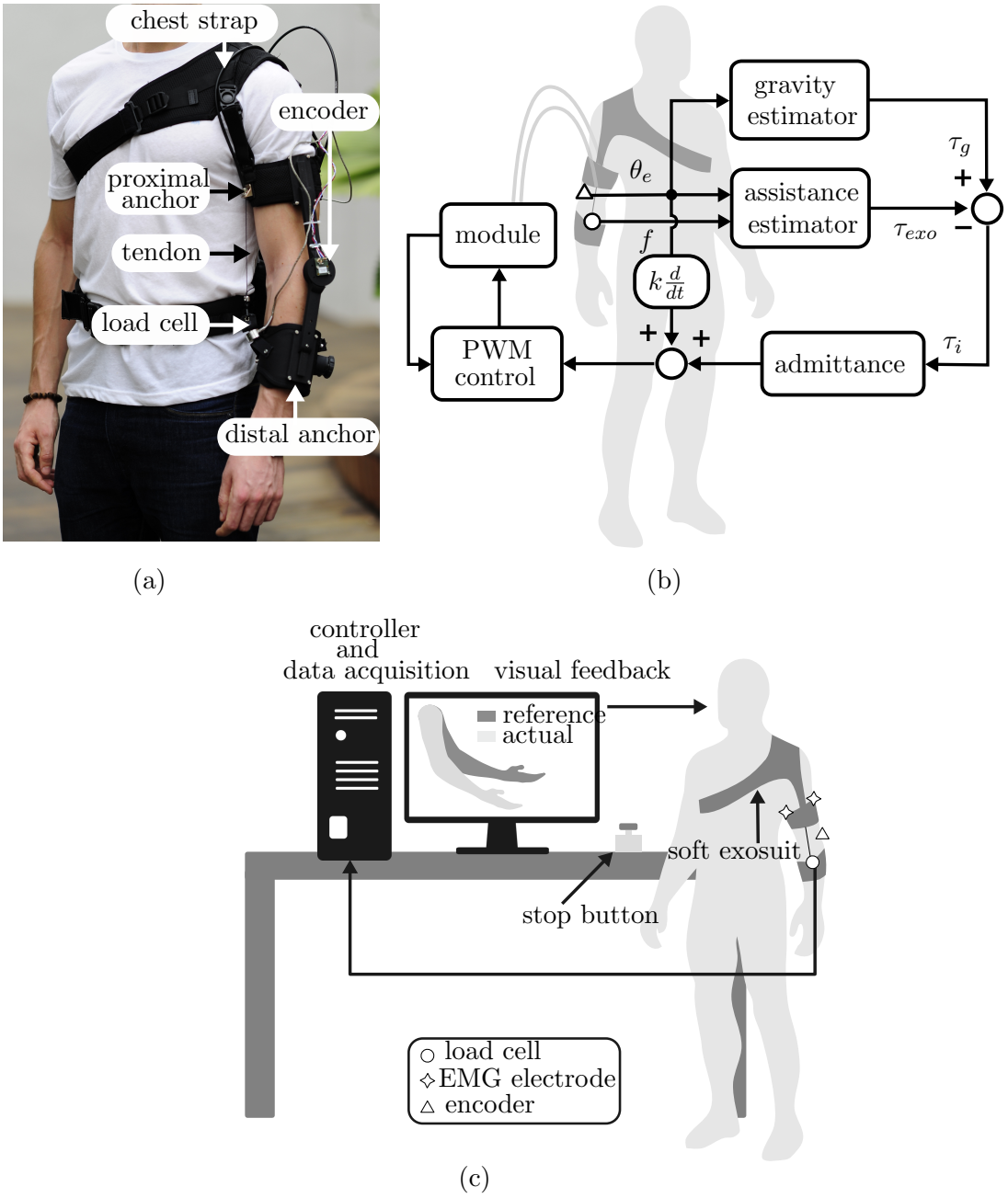

FIGURE 6.11: **Soft tendon-driven exosuit for the elbow joint.** The suit is driven by Bowden cables, that allow to locate the actuation stage far from the limb.

Table 6.2 summarizes the technical characteristics of our OTM module assembly shown in Figure 6.2, where the maximum rated torque and velocity have been mapped to the elbow joint.

6.3 Testing on Human Movements

To test the feasibility of the OTM mechanism for assistive purposes, we compared the performance of an exosuit driven by the OTM mechanism to that of the exosuit driven by a traditional DC motor. The performance of the device was assessed through its effect on the the kinematics and muscular activity of its wearer.

6.3.1 Exosuit design and control

The exosuit used for testing this paradigm is thoroughly described in Chapter 3, using the control presented in Chapter 4. For the ease of reading, we here give an overview of its working principle.

The suit is shown in Figure 6.11.a. The device consists of a frame of soft material that wraps around the arm and forearm and transmits torque to the elbow through artificial tendons. A pair of Bowden cables transmits power from the actuation unit to the joint.

The suit is equipped with a force sensor (Futek, LCM300), secured on the distal anchor point, that measures the tension in the flexing tendon, and an absolute encoder (AMS, AS5047P, 1000 pulses/rev), mounted on a 3D-printed joint between the arm and forearm straps, that monitors the angular position of the joint.

The device provides assistance to its wearer through an admittance-based controller, detailed in Chapter 4. The control paradigm is designed to have the dual purpose of compensating for gravitational forces acting on the forearm and allowing the exosuit to move in concert with its wearer.

A schematic diagram of the controller is shown in Figure 6.11.b. It comprises an outer torque loop and an inner position loop. The former is responsible for tracking the position-dependent torque profile at the elbow, equal and opposite to gravity. A PID-admittance converts the error between the desired and assistive torque at the elbow to a position reference for the actuation stage.

The torque acting on the elbow joint as a result of gravity is estimated using a simple single-joint model and assuming that the arm is adducted on the side of the

trunk:

$$\tau_g = mgl_c \sin\theta_e, \tag{6.6}$$

with m being the combined mass of the forearm and hand, l_c the distance of the center of gravity of the forearm and hand from the center of rotation of the elbow joint, g the acceleration of gravity and θ_e the elbow angle, assumed to be zero in the fully-extended configuration.

The assistive torque is estimated by multiplying the tension measured by the load cell, f, by its moment arm $P(\theta_e)$ (refer to [138] for a full formulation):

$$\tau_{exo} = P(\theta_e)f. \tag{6.7}$$

Using the notation shown in Figure 6.11.c, the difference between τ_g and τ_{exo} is converted to a reference position for the actuation stage, by a specified admittance. The admittance assumes the form of a PID controller [91]:

$$Y(s) = \frac{\theta_e}{\tau_g - \tau_{exo}} = P + \frac{I}{s} + Ds, \tag{6.8}$$

with the P, I and D constants governing the characteristics of the relation between the interaction force and the exosuit's kinematics. An additional positive feedback term, proportional to the speed of the elbow joint, increases the sensitivity of the device to its wearer's movements.

6.3.2 Experiments and data analysis

The aim of this experiment was to compare the effect on human movements of the exosuit driven by an OTM module to that of the exosuit driven by a traditional DC motor. We included a third condition, consisting in unpowered movements, to have a physiological baseline. In all three conditions, we evaluated smoothness and accuracy of movement, biological torque and muscular activation patterns of a healthy subject performing controlled movements of the elbow. The experimental procedure ia similar to the one we describe in Chapter 5, to quantify the effects of a soft wearable exosuit on movements of the upper limbs.

The testing was done on one male subject presenting no evidence or known history of skeletal or neurological diseases, and exhibiting intact joint range of motion and

muscle strength. The participant had to follow a reference movement performed by a dummy character on a screen. The position of his own elbow was displayed as a superimposed replica of the reference one to provide visual feedback. In the unpowered condition, the exosuit's tendons were unhooked from the distal anchor point and the motor's power source was turned off.

The reference motion consisted of series of 10 Minimum Jerk Trajectories (MJT), known to correspond well to the movements of healthy subjects [93], with amplitude of 80 deg and a peak velocity of 60 deg/s, corresponding to approximately 50% of the average speed in activities of daily living [61].

Raw data from the suit's absolute encoder and load cell was low-pass filtered (second order Butterworth filter, 10 Hz cut-off frequency) and segmented to isolate the 10 movements comprising each condition. The accuracy of movement was quantified by evaluating the Root Mean Square Error (RMSE) between the measured and reference trajectory.

To quantify kinematic smoothness, we used the SPectral ARC length (SPARC) index proposed in [102]. The SPARC index was estimated on the norm of the elbow's speed.

The measured force on the flexing tendon was mapped to a torque on the joint using Equation 6.7, this was used as an estimate of the assistive moment delivered by the exosuit, τ_{exo}. The total torque, τ, required to perform the movement was derived from the inverse dynamics of the human elbow, represented as a simple pendulum using a second order model. The difference between the total and assistive torque,

$$\tau_{bio} = \tau - \tau_{exo}, \tag{6.9}$$

was used to estimate the biological torque exerted by the subject to perform the movement or hold the position.

The output EMG signal of the Delsys Trigno system was processed to extract its linear average envelope using the procedure suggested in [104]. The Root Mean Square (RMS) of the processed EMG signal was used as an index of the level of activation of a muscle.

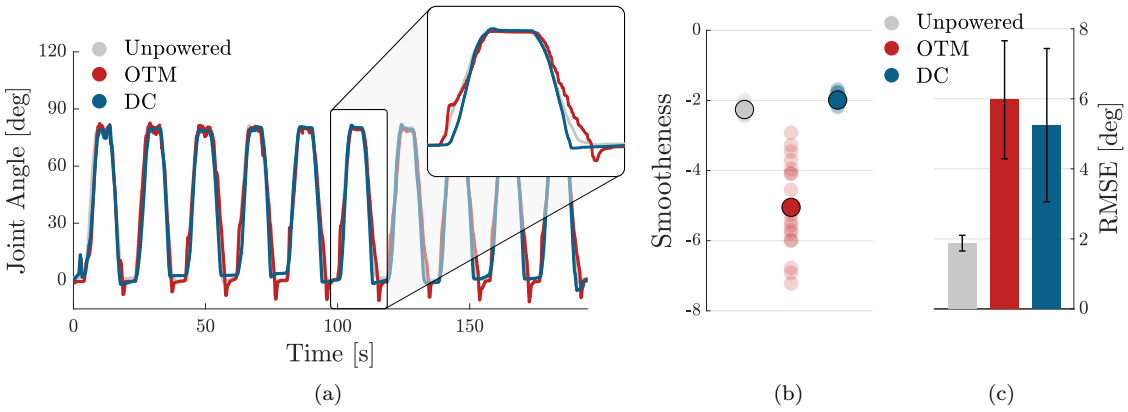

FIGURE 6.12: **Characteristics of the kinematics of the elbow joint for the three tested conditions.** (a) Trajectories of the elbow when wearing the exosuit in the three tested conditions: unpowered (gray), powered by the OTM module (red) and powered by a traditional DC motor (blue). (b) Smoothness of movements as measured by the SPARC coefficient in the three tested conditions. Translucent dots are individual values over the 20 sub-movements of the task, while opaque dots show their mean. (c) Accuracy in tracking the reference trajectory, measured by calculating the RMSE, for the three conditions. Movements assisted by the OTM module have similar accuracy to movements assisted by a traditional DC motor.

6.3.3 Results

Figure 6.12 compares the characteristics of the elbow's trajectory for the three tested conditions. In (a), the zoomed-in area shows the overlapping trajectories for the unpowered (gray), powered by an OTM module (red) and powered by a DC (blue) cases: the second condition clearly being more jerky than movements with the DC motor. This is confirmed by a quantitative analysis of the smoothness of movement, evaluated through the SPARC index and shown in Figure 6.12.b.

Figure 6.12.c shows the mean and standard error of the mean of the root mean square error between the reference MJT trajectory and the measured one, in the three conditions. When assisted by the exosuit, whether using the OTM module or a traditional DC motor, movements are less accurate. A smaller difference in mean values exists between the OTM and DC motor cases. An analysis of the forces transmitted by the exosuit during movement gives further insight on the performance of the OTM module. Figure 6.13 shows the profile and average values of the biological torque, calculated using Equation 6.9. In the unpowered case, the entire moment required for movement is exerted by the subject; in the OTM case,

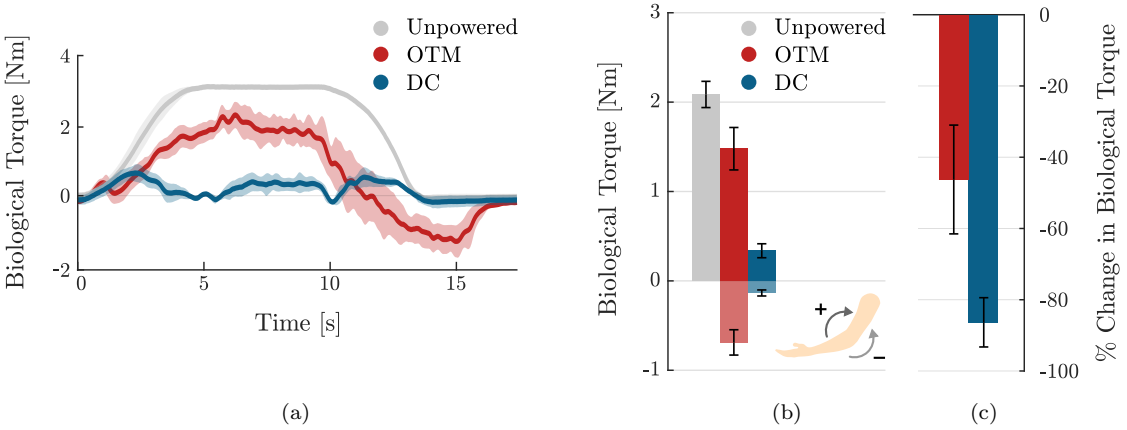

FIGURE 6.13: **Comparison of the biological torque among the three tested conditions.** (a) Average (solid) and standard deviation across repetitions of the biological torque profiles for the unpowered (gray) condition, for the powered by an OTM module (red) and powered by a traditional DC motor (blue). (b) Mean and standard error of the biological torque, averaged across repetitions, for the three tested conditions. (c) Change in the overall biological torque required for lifting the arm when assisted by the exosuit. Values are in percentage change of the unpowered case.

the positive torque required for movement is reduces, but the exosuit introduces a substantial negative component in the descending phase (Figure 6.9.a).

Figure 6.9.b shows the mean and standard error of the mean, for the positive and negative biological torques exerted in the three conditions. Wearing the exosuit introduces a negative component, required to initiate the downwards motion, both when powered by the DC motor and OTM module. In the latter case, however, the magnitude of negative torque is substantially higher. Overall, the OTM reduces the biological torque at the joint of 46.2%, compared to the unpowered condition, while the DC motor achieves an average -86.3% change.

Finally, Figure 6.14 analyses the activity of the two major antagonistic muscles involved in delivering power to the elbow joint, namely the biceps brachii and the long head of the triceps brachii. An average and standard deviation of the profile of activation of these muscles is shown in Figure 6.14.a, for the three conditions.

When the suit is unpowered, the biceps brachii reaches a peak activation of 7% of his MVC, while the triceps muscles is relaxed for most of the duration of the movement. When the exosuit, powered by a traditional DC motor, assists its wearer, the activation of the biceps muscles is substantially reduced, with a peak activation during the transient lifting phase. When the device is powered by the

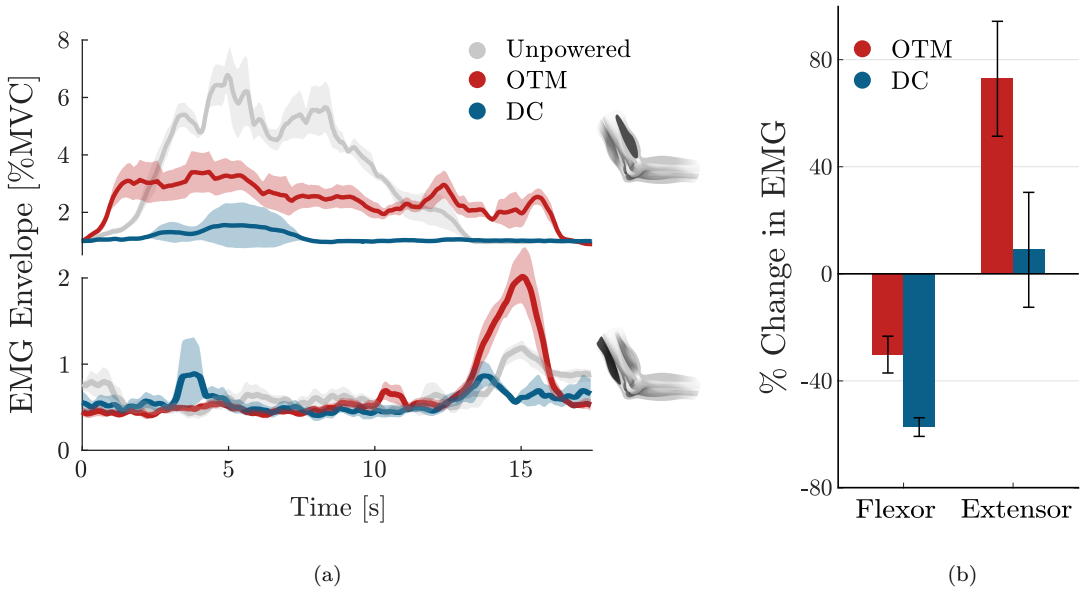

(a) (b)

FIGURE 6.14: **Muscular activation of the biceps brachii and long head of the triceps brachii.** (a) Average (solid) and standard deviation (shaded) across repetitions of the muscular activation profile during one lifting repetition of the forearm, shown for the unpowered condition (gray), for the exosuit powered by the OTM condition (red) and the exosuit powered by a traditional DC motor (blue). (b) Percentage change in the RMS of the muscular activity of the antagonistic muscles, averaged over repetitions.

OTM module, the agonist muscle's activity is lower than the unpowered condition but presents a slightly different activation pattern, while the triceps shows a peak during the descending phase.

Figure 6.14.b shows the average over repetitions and time, of the RMS of the activity of both muscles for the OTM and DC conditions, expressed in percentage change of the unpowered case. Using a traditional DC motor to actuate the exosuit reduces the activation of the biceps muscle by 57.1% and increases that of the triceps muscle of 8.84%. When the OTM powered the suit, the activation of the biceps muscle was reduced by an average 30% while its antagonist increased by 74%.

6.4 Discussion

Power consumption, weight and size of wearable robots have a fundamental impact on their performance. Soft exosuits, adopting clothing-like materials instead

of rigid frames, represent a significant step towards making assistive wearable devices ubiquitous in the near future. Yet, because of the unparalleled complexity of our bodies' biomechanics, we are bounded to either use a high number of motors or underactuation solutions that constrain the natural kinematics of human movements.

The implementation of an actuator that can exploit, in a power-efficient manner, the torque generated by a single motor to drive multiple DoF would cut down cost, weight and size of the actuation module, reducing the complexity of the control and increasing the overall autonomy of device.

In this study we presented the design and control, and proposed a human-in-the-loop validation of a clutchable modular unit to implement the OTM paradigm for a soft exosuit. The following subsections discuss the implications of our findings first by looking purely at the technical performance of the device and then evaluating its effects on human biomechanics.

6.4.1 On the performance of the PWM controller

Figure 6.7 shows that as the frequency of the PWM controller increases, the output velocity stays null for low duty cycles and saturates to the input velocity earlier, effectively reducing the range of duty cycle where one can modulate the output velocity. This effect is caused by the delay δ, necessary for the armature and rotor of the EM clutches to engage/disengage upon the application of power. Our results are consistent with the observations of [127], who found a similar behaviour with wrap-spring clutches: when increasing the PWM frequency, the period T_{PWM} decreases and, for small duty-ratios, Δt becomes smaller than δ, effectively causing the clutch never to engage. For high duty ratios, on the other hand, the disengagement time, $T_{PWM} - \Delta t$ is smaller than the minimum time required for the clutch to disengage, causing a permanent engagement.

The bandwidth of each module, with a PI-regulated PWM controller, varied for input velocities of 35 rad/s, 45 rad/s and 55 rad/s, with the maximum 1.51 Hz obtained for 45 rad/s. This result echoes our previous findings, where [131] tested the same device for higher input velocity and found a saturation effect of its bandwidth for higher velocities of the prime mover. This suggests that the limiting dynamic

at high frequencies is not given by the rotating speed of the prime mover but by the engaging dynamics of the clutches [127].

Assuming a sinusoidal motion of the elbow with a peak to peak movement of 90 deg, 1.51 Hz corresponds to a maximum velocity of the joint of 426 deg/s, which is sufficient for everyday tasks such as drinking from a glass (269 deg/s), eating with a spoon (126 deg/s) and pouring from a bottle (92 deg/s), but not for more demanding working tasks such as hammering (842 deg/s) [61].

The maximum load that each module can handle is bounded by the maximum rated torque of the EM clutches. This can be mapped, using Equation 6.7, to an estimated average torque at the elbow joint of 3.4 N m, which is just above the torque required to keep an the average human male forearm in a static posture of 90 deg.

It is worth comparing the performance achieved here with EM clutches with the results reported in [132], using Magneto-rheological ones. Yadmellat and colleagues present custom-built clutches, each able to transmit a maximum torque of 15 N m and shown to accurately track a 2 Hz sinusoidal trajectory. Their clutches weigh 2.2 kg each, with a volume of over 650 cm^2 but, unlike EM cluthces, allow to achieve a smooth and continuous regulation of the output torque, solving the problem of jerky movements typical of discrete systems.

6.4.2 On the effect on human movements

It is increasingly important to evaluate novel wearable assistive technologies based on their effect on the end-user. We believe that this human-in-the-loop validation approach can provide important insights on the limitations and advantages of the innovation, allowing a data-driven design process.

In this work, we compared the performance of of the OTM module with that of a traditional DC motor by looking at its effect on the kinematics and physiology of healthy movements.

Overall, when driven by the OTM module, the assistive device provided fewer benefits in terms of muscular activation and had a more marked effect on movement kinematics than when driven by a traditional DC motor. Specifically, wearing

the exosuit powered by the OTM module resulted in more jerky movements, as measured by the SPARC index. This is probably a direct consequence of the discrete nature of the mechanism, driving the assisted joint with small step-like motions along the desired trajectory (see Figure 6.8 or Figure 6.9). These fast-changing dynamics are filtered by the compliant transmission between the pulley and the joint but still affect the wearer's movement. We believe that switching to particle-based megneto-rheological clutches, that allow a continuous modulation of the torque being transferred between their input and output shafts, would attenuate or even solve this problem. Previous studies support this proposition [132].

Movements assisted by the OTM module resulted in an overall 46.2% reduction in biological torque, versus an 86.3% reduction achieved with a traditional DC motor, when compared to the unpowered case. This poorer performance of the OTM module is partly caused by: (1) the upper torque limit of the EM clutches, restraining the magnitude of assistance that the actuation can provide; (2) the lower bandwidth of the module, that does not allow it to move fast enough to accommodate the user's intention. This last point is clearly visible in Figure 6.13, in red, where the biological torque shows a significant negative peak during the descending phase of the joint: the user had to push down against the exosuit to extend the elbow.

A corollary of the increase in negative torque, when using the OTM actuation module, is an increase in the activation of the long head of the triceps brachii. Figure 6.14.a shows a peak in the activation of the extensor muscle (bottom plot, in red), of up to 2% of the MVC, during the descending phase of movement. This peak is present also in the other two conditions, but with much smaller amplitude. Overall, the activity of the triceps brachii increased notably when wearing the exosuit powered by the OTM module, while the biceps brachii was reduced by 30%, when compared to the unpowered condition.

It is useful to compare the technical characteristics of the proposed OTM system with the traditional approach of using one motor per elbow. In the latter case one would require at least a 70 W motor with an appropriate reduction stage and a motor controller per DoF, which would result in no more than 600 g and 560 cm^3 per DoF (e.g. Maxon EC-i 40, 70 W, 2-stage planetary gearhead and an ESCON 50/5 module motor driver). Figure 6.15 shows how the volume and weight of the actuation stage scale with increasing DoF, for a typical one-to-one paradigm and

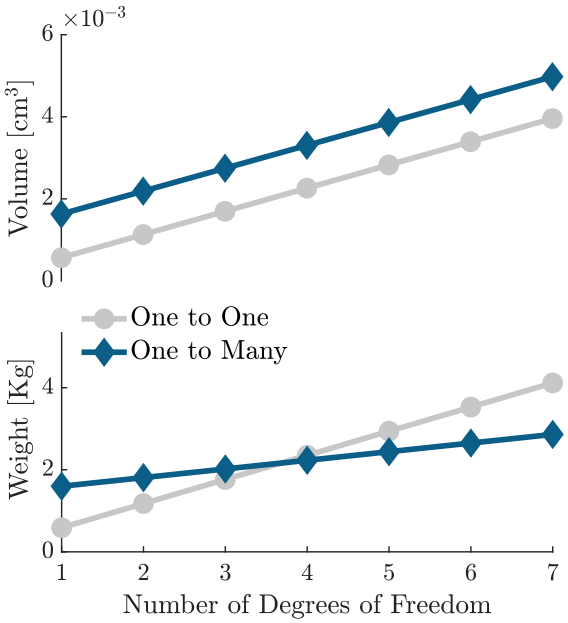

FIGURE 6.15: **Scalability of the OTM design proposed herein, compared to a traditional one-to-one approach.** Volume and weight of the actuation strategy using an OTM paradigm, compared to a setup having similar torque and velocity rating but using one electric motor per DoF.

for the OTM strategy proposed here. With the current hardware, the actuation stage would weigh less only for 4 or more DoF. It is worth highlighting, however, that the OTM system only requires one motor controller overall and three simple relay switches per DoF, thus reducing the cost and idle power consumption of the electronics compared to the traditional approach. There is, moreover, ample room for improvement of the size and weight of the OTM modules. In the present work we explored the potential of an OTM module and compared its performance with a direct drive DC motor, using a wearable device as a test bench for human testing. The DC motor showed higher benefits in assisting human kinematics thanks to its higher bandwidth and smoother motion. However, the OTM paradigm lends itself well to scalable applications, that require independent control of multiple DoFs. This is a common problem in wearable technology, where the complexity of human biomechanics results in an increase in weight, power consumption and control intricacy of the device. If on one side the OTM startegy showed limitations in trajectory tracking, on the other, multiple OTM modules can be driven using a single drive and their control strategy might be optimized reducing the task manifold.

The OTM paradigm was tested only on one human participant. This was done

because the focus of the evaluation was on the technical capabilities of the device rather than its effect of human movement. However, we acknowledge that testing on a larger group of subject might reveal subtle yet critical insights into the feasibility of using this technology for human motion assistance on which. This would be an interesting point to address for future work.

In our experiment we used a wearable device for upper limb, and it is known that replicating the dexterity of a human arm is a complex task; we believe that with further improvement on the hardware design, the OTM paradigm has the potential to allow independent control of multiple DoF in a power- and size-effective manner. A different result, for example, might be obtained for well-defined tasks with periodic velocity profiles such as walking, where joint coordination can be achieved by means of synergistic and intermittent assistance on each leg [125].

Chapter 7

Conclusion and outlook

7.1 General conclusion

This thesis presented the design, control and validation of a soft robotic exosuit for the elbow. The robot was designed as a mobile tool for rehabilitation and asssitance in ADLs for subjects with neuromuscular disorders.

In the Introduction to our work, in Chapter 1, we listed our main objectives and presented three hypotheses, regarding the feasibility of using a soft device to assist movements of the upper limbs. These objectives were addressed in the main work packages of the thesis, with Chapter 5 directly seeking an answer to our research questions. The following sections list again the aims of each Chapter, with concluding remarks on whether these they were achieved.

7.2 Major contributions

7.2.1 Design principles

Aim: Design of the exosuit – Design and realization of a soft, lightweight and comfortable robotic garment, able to support and assist arm movements.

The Chapter described the process of designing the suit, with a thorough description of the actuation stage and the wearable component. The procedure included identifying some of the major technical and practical requirements of the device, achieved by a combination of scrutinizing biomechanical and ergonomic studies on human movements and proposing a simple dynamic model of the elbow. The suit was then characterized to verify that it matched the previously-stated requirements. We did reach most of them, except for the bandwidth of the suit, found to be lower than the one rewuired for ADLs. This is a technical problem that could be solved by choosing a different actuation stage.

This Chapter only tells part of the story of the design, presenting it as a rigorous data- and requirement-driven, rigorous process. In reality, maybe because of the novelty of the system, maybe because of my inexperience (more likely), it was more of a painful trial-and-error procedure.

7.2.2 Controller

Aim: Control of the exosuit – Implementation of a control paradigm that allows the suit to move in concert with its wearer, while providing, in whole or in part, the power needed to perform the task.

This Chapter detailed the choice and working principle of the algorithm used to provide gravity compensation assistance to the exosuit's user. Unlike existing paradigms and our previous works [72], the controller stands out for simplicity and robustness. This Chapter also presents a preliminary evaluation of the accuracy and bandwidth of the controller. The experimental data gathered was used to assess the efficiency of the device.

The proposed paradigm indeed allowed the suit to provide part of the power required to perform a task but allowed the suit to move in concert with its wearer only for movements up to 88 deg/s. Although this is acceptable for most of the ADLs, it is below the set requirements of the device.

7.2.3 Effects on human movements

Aim: Validation of the exosuit – Design of an experimental protocol and performance indexes to evaluate the bio-mechanical and physiological response of the suit's wearer. This work package directly addresses H1-H3.

With H1-H3 being:

- **H1**: We hypothesize that an exosuit working in parallel with the human muscles can reduce the effort that its wearer needs to exert to perform the movement and hold a position.
- **H2**: We hypothesize that an exosuit working in parallel with the human muscles can delay the onset of fatigue.
- **H3**: We speculate that the low inertia and intrinsic compliance of the suit will allow its wearer to move without significantly affecting his/her natural kinematics.

The work described in this Chapter is, to our knowledge, the first that evaluates the effect of a soft exosuit on the characteristics of human movement of the upper limbs. The proposed experimental protocol comprised a thorough assessment of the kinematic (delay, peak velocity of movement, smoothness and accuracy of movement), dynamic (estimate of the change in biological torque) and physiological (muscular activation pattern) changes caused by the assistance from the exosuit.

These indexes provide useful insights in how an assistive device affects natural movements, with implications for their use in rehabilitation, assistance and augmentation. Moreover, they could be used as a benchmark to evaluate the impact of hardware and software changes on the performance of the device. While similar studies have been carried out for locomotion, the authors are unaware of comparable work for the upper limbs, where most of the existing devices are validated using control strategies that do not account for the wearer's intention.

In this Chapter, we also showed that H1 can indeed be accepted; by working in parallel with the human muscles, the tendon-driven exosuit reduces the amount of

biological torque required for movement and, as a corollary, diminishes the activation of the involved muscles. H2 was verified in a static task, where we found a significant reduction in parameters measuring the onset of muscular fatigue, when subjects wore the device. Finally, wearing the exosuit did alter the kinematics of movement, affecting smoothness, accuracy and delay in initiating a movement. H3 is to be rejected. We think that better results could, however, be achieved by choosing an actuator with a higher velocity rating.

7.2.4 The One-to-Many actuator

Chapter 6 was a technical challenge to try to address one of the major obstacles that prevents wearable assistive devices from becoming a ubiquitous part of our daily life. Our aim here was to design an actuation paradigm that allowed to exploit the mechanical power generated by one electric motor to independently drive multiple DoFs.

We thoroughly tested the technical performance and proposed a controller for a module that employs electromagnetic clutches to convert a unidirectional motion from the main drive in an arbitrary trajectory. We compared the performance of the suit, powered using this paradigm, with its performance using a simple DC motor, using the methodology outlined in Chapter 5.

Assistance using the one-to-many actuator resulted in a deterioration of movement smoothness and accuracy, a reduction in assistive torque and abnormal patterns of co-contraction of the antagonistic muscles when compared to the DC case. However, the overall effect was beneficial when compared to a no-exosuit case. This work highlighted the need for technical improvement in this technology but showed its promising potential in mobile wearable technology.

7.3 Open questions and future work

One main weakness of this work is that the exosuit and the proposed controller were only evaluated on a cohort of young, healthy participants. Although the obtained results are positive, we can only speculate on the outcome that such a technology could have on a population of subjects with neuromuscular impairments. It would

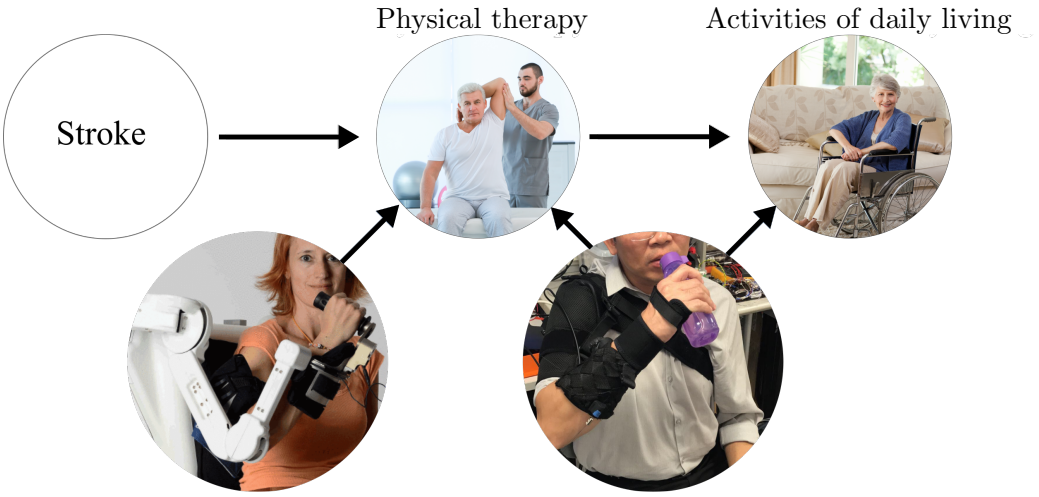

FIGURE 7.1: **Clinical testing.** Unlike rigid robots, that, because of their complexity are confined to specialized clinics and hospitals, exosuits would allow training and assistance at home, in a daily environment.

be interesting to examine the effects on patients with different pathologies and at a different stage of recovery. The work outlined in this thesis set a basis for addressing this question but did not venture in that direction.

While extensive work has been done to prove the effectiveness of rigid robots as automated tools for rehabilitation, it would be interesting to test the effect of the exosuit for the same purpose. Unlike rigid robots, exosuits would allow training and assistance at home, in a daily environment, thanks to their portability (this idea is shown in Figure 7.1). This work was started in the context of this thesis, by formulating the following hypotheses and preparing an experimental protocol for addressing them.

- We hypothesize that exosuits, like rigid robots, can be used as tools for clinical rehabilitation of stroke patients. We have partially started to address this idea in Appendix A.2.
- We hypothesize that exosuit-training better generalizes to ADLs: While rigid exoskeletons primarily allow for training only in virtual environments due to their size and weight, the mobility of an exosuit allows for (occupational) training in "real" scenarios, e.g. dummy kitchens or living rooms. We speculate that such paradigm would more effectively generalize to ADL.
- We hypothesize that the assistance of an exosuit can increase independence in ADLs: a functional suit that compensate for gravitational forces and assists

in reaching movements could partly compensate for the lack of dexterity and/or strength of its wearer, enabling him/her to independently perform daily tasks that could not, otherwise, be completed. This also has significant implications for the patients mental well-being and overall quality of life.

– We hypothesize that the assistance from the exosuit can have knock-on therapeutic effects: by encouraging independent completion of a higher number of tasks and promoting a more active life-style, using an exosuit in ADLs could result in long-term therapeutic effects.

Appendix A

Appendix

A.1 History of the exosuit's design

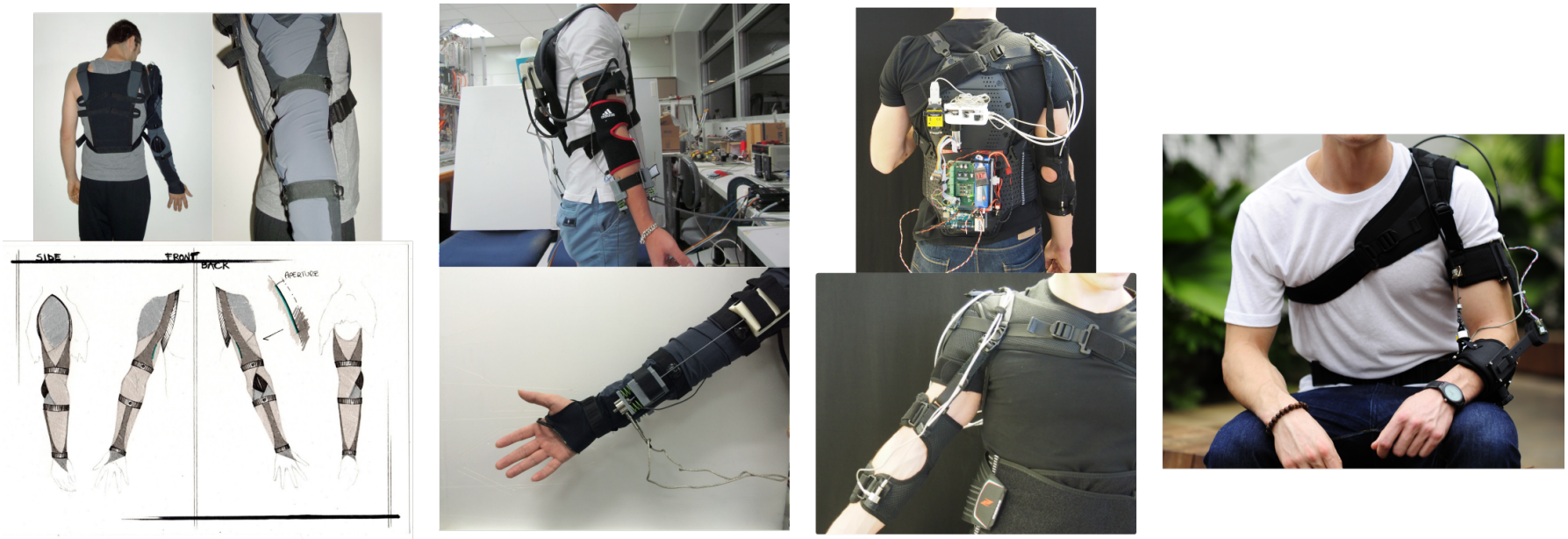

Aug 2015
First drawings and prototype from Leonardo Cappello

Jan 2016
Feasability test brachial plexus injury patient [73].

Jan 2017
First unthetered version.

Jan 2018
Version described here.

FIGURE A.1: **History of the exosuit's design.**

A.2 Rehab-Exos and exosuit: a preliminary comparison

In an elegant comment on the growth and outlook of this field [139], one of its pioneers rightly underlines that soft wearable robots are complementary and not substitutive to their rigid counterparts. The weakness of soft devices stands in their very same strength: the use of soft materials greatly limits the amount of forces/torques that the device can transmit to the human body and the velocity that it can move at. This makes them suitable only for applications that require small levels of assistance, with the wearer having no bone or joint conditions. Rigid exoskeletons, on the other hand, can deliver higher forces more quickly and accurately, and their linkage structure allows to do so even in the extreme case of paralysis of the user.

The objective of this study is to quantify this complementarity by highlighting the strength and weaknesses of rigid and soft wearable robots. To do so, we compare the technical characteristics of a soft exosuit and a rigid exoskeleton and measure their biomechanical and physiological effect on the elbow movements of healthy subjects. Both devices provide assistance by compensating for the gravitational force acting on the arm and shadow the wearer's motion using a force/torque sensor.

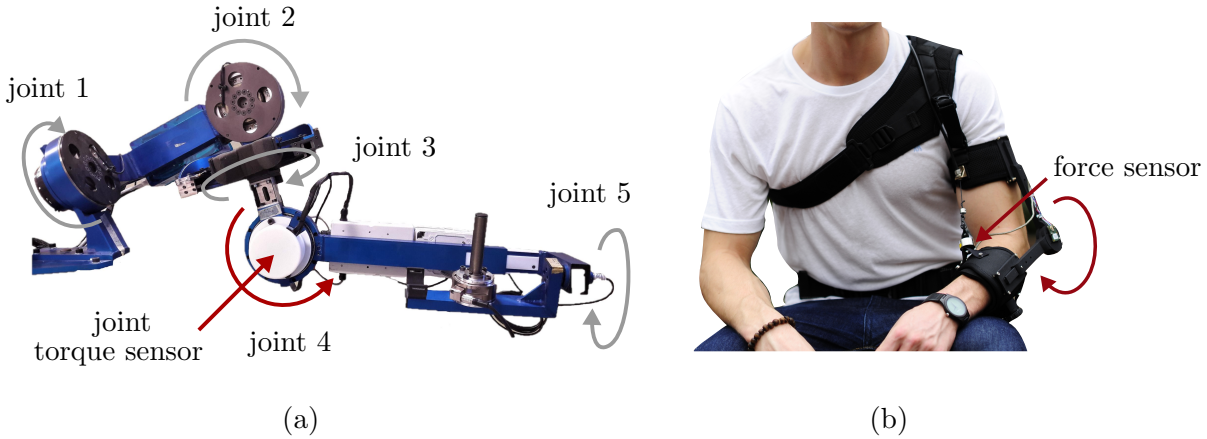

FIGURE A.2: Rehab-Exos, the rigid exoskeleton for the upper limbs (a) and the soft exosuit for assistance of the elbow joint (b). In this study we only provide assistance through joint 4 (elbow) of the Rehab-Exos.

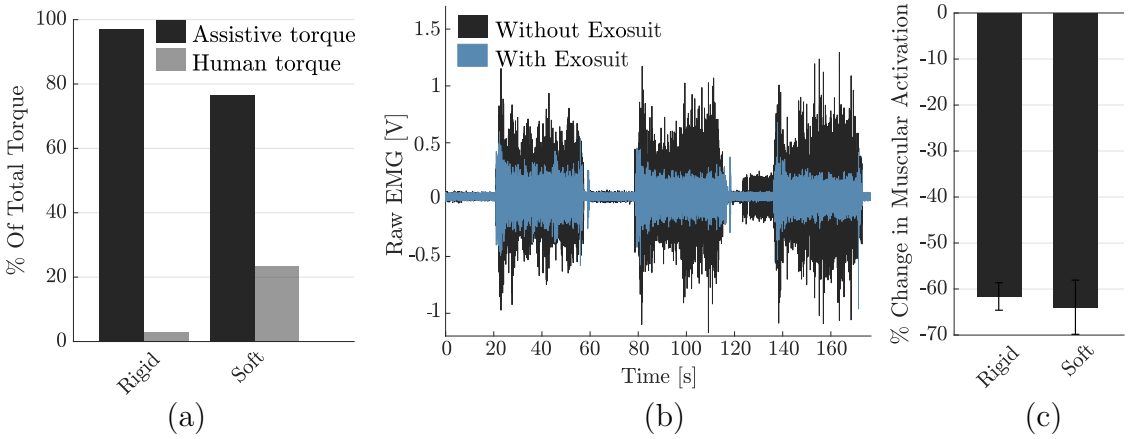

FIGURE A.3: Comparison of the assitive torque and percentage reduction in muscular activity when wearing the rigid exoskeleton and soft exosuit. (a) The rigid exoskeleton provided nearly the entire torque required to support the elbow position; the torque that the wearer needed to exert was higher when wearing the exosuit. (b) Amplified electromyography from the biceps brachii, comparison between the case of no assistance and assistance with the exosuit. (c) The bar plot presents the reduction in muscular activity resulting from wearing the exoskeleton or exosuit.

The Rehab-Exos is an active robotic exoskeleton (Figure A.2.a) that exhibits a serial architecture, isomorphic with the human kinematics, it comprises 3 actuated DOF for the shoulder joint, an active elbow joint and a passive wrist pronosupination joint [140]. Its joints embed a brushless motor, a torque sensor and a compact harmonic drive (100:1 reduction).

The exosuit for assistance of the elbow joint (Figure A.2.b) consists of three wearable components (i.e. a chest, an arm and a foream strap) and an electric motor (Maxon EC-i 40, 70W, 55:1 reduction), driving a pair of tendons to assist in both flexion and extension of the joint. The suit is equipped with a load cell in series with the flexing tendon and an absolute encoder to monitor the elbow's position.

Each device's control algorithm is designed so that it can move in concert with its wearer with minimal interaction forces between the two. The Rehab-Exos control is based on a direct force feedback loop and a full-state observer that estimates the interaction torques [141]. The soft exosuit implements an admittance-based control to compensate for the arm's gravity with an internal velocity loop [106].

To evaluate the biomechanical and physiological effect on the elbow movements of the two device, 2 healthy subjects were asked to perform repetitive flexion/extension movements, while holding a 1.25 Kg load in their hand. A reference trajectory was shown on a screen in order to standardize the range of motion and speed. The

experiments were conducted in three distinct phases, randomised to avoid potential order effects: with the exoskeleton, with the exosuit and without any assistance. We monitored the assistive torque and estimated the muscular effort from the Root Mean Square (RMS) of the Electromyography (EMG) of the biceps brachii.

Figure A.3.a shows the effect on the torque required to flex the elbow resulting from wearing either the Rehab-Exos or the soft exosuit. Values are reported in percentage of the total torque required to perform the movement. The Rehab-Exo provides a slightly higher assistive torque, relieving its werarer from a greater part of the effort required to flex the joint.

Similar considerations were obtained from analysing the EMG activity of the biceps brachii by comparing it with the no-assistance case. Figure A.3.b shows the muscular activity when flexing the elbow both with and without the soft exosuit, the difference between them is used to compute the % reduction of effort from wearing the device. A similar analysis for both systems, averaged across repetitions and subjects, is shown in Figure A.3.c: both produce an average reduction in the activation of the biceps brachii, of -61.63% and -63.97% for the rigid and soft device respectively.

Table A.1 summarises some of the key aspects that characterise rigid and soft wearable robots. While the exosuit stands out for its low weight and power consumption, making it ideal for mobile applications, the rigid device has higher torque rating, bandwidth and efficiency.

As expected, the Rehab-Exos provides a higher part of the torque required to move the arm but this did not result in a greater reduction of muscular activity. A higher sample size, an investigation of the effect on the triceps muscle and an analysis of the effect of each device on the kinematics of movement would provide further interesting insights.

TABLE A.1: Performance of the exoskeleton versus the exosuit

	Rigid	Soft
Characteristics:		
Frame material	aluminium	fabric
Motor location	joints	waist
Weight [Kg]	17	1.2
DOF	5	1
Maximum torque [Nm]	150	10
Bandwidth [Hz]	39.7	1.1
Power Consumption [W]	25.65	13.71
Efficiency	0.26	0.14
Physiological effects (% of the no-exo case):		
Muscular activity	-61.63	-63.97
Human torque	-97.05	-76.63

List of Author's Awards, Patents, and Publications[1]

Awards

- Selected for Special Issue on Journal of Neuroengineering & Rehabilitation , International Conference on Neurorehabilitation, Oct 2018.
- Finalist - Best Paper Award on Human-Robot Interaction, IEEE International Conference on Robotics and Automation, June 2017.
- Best Student Paper Award, IEEE International Conference on Biomedical Robotics and Biomechatronics, May 2016.

Journal papers

- Michele Xiloyannis, Domenico Chiaradia, Antonio Frisoli and Lorenzo Masia, *"Physiological and Kinematic Effects of a Soft Exosuit on Elbow Movements"*, Journal of NeuroEngineering and Rehabilitation (JNER). *In press.*

- Michele Xiloyannis, Eugenio Annese, Marco Canesi, Anil Kodian, Antonio Bicchi, Silvestro Micera, Arash Ajoudani and Lorenzo Masia, "Modular One-to-many Clutchable Actuator for a Soft Elbow Exosuit", in *Frontiers in Neurorobotics*, *Under Review.*

- Michele Xiloyannis, Leonardo Cappello, Khanh D. Binh, Chris W. Antuvan and Lorenzo Masia, *"Preliminary design and control of a soft exosuit for assisting elbow movements and hand grasping in activities of daily living"*, Rehabilitation and Assistive Technology Engineering (RATE), 2017.

[1]The superscript * indicates joint first authors

- Leonardo Cappello, Michele Xiloyannis*, Binh Khanh Dinh, Alberto Pirrera, Filippo Mattioni and Lorenzo Masia, *"Multistable Series Elastic Actuators: Design and Control"*, Robotics and Autonomous Systems (RAS). *Under review.*

- Binh Khanh Dinh, Michele Xiloyannis, Chris W. Antuvan, Leonardo Cappello, and Lorenzo Masia, *"Hierarchical Cascade Controller for Assistance Modulation in a Soft Wearable Arm Exoskeleton",* Robotics and Automation Letters (RAL), 2017.

- Binh Khanh Dinh, Michele Xiloyannis, Chris W. Antuvan, Leonardo Cappello, Shih-Cheng Yen and Lorenzo Masia, *"Adaptive Backlash Compensation in Upper Limb Soft Wearable Exoskeletons",* Robotics and Autonomous Systems (RAS), 2017.

- Z. Liu, D. Qi, W. Leow, J. Yu, M. Xiloyannnis, L. Cappello, Y. Liu, B. Zhu, Y. Jiang, G. Chen, L. Masia, B. Liedberg, X. Chen *"3D-structured Stretchable Strain Sensors for Out-of-plane Force Detection"*, Advanced Materials, 2018.

Book chapters

- Michele Xiloyannis, Khanh D. Binh, Leonardo Cappello, Chris W. Antuvan and Lorenzo Masia, *"Chapter 10. A Soft Wearable Elbow Exosuit: Design Considerations".* In *Wearable Technology for Medicine and Healthcare, 1st edition*, Elsevier, 2018.

- Lorenzo Masia, Michele Xiloyannis, Khanh D. Binh, Chris W. Antuvan, Sara Contu and Yongtae Kim, *"Chapter 4. Actuation for Robot-Aided-Rehabilitation: Design and Control Strategies".* In *Rehabilitation Robotics, 1st edition* (pp. 47-61), Elsevier, 2018.

- Lorenzo Masia, Irfan Hussain, Michele Xiloyannis, Claudio, Pacchierotti, Leonardo Cappello, Monica Malvezzi, Giovanni Spagnoletti, Chris W. Antuvan, Dinh B. Khanh, Maria Pozzi and Domenico Prattichizzo, *"Chapter 10. Soft Wearable Assistive Robotics: Exosuits and Supernumerary Limbs".* In *Wearable Exoskeleton Systems: Design, control and applications* (pp. 219-254), IET, 2018.

Conference Proceedings

- Michele Xiloyannis, Domenico Chiaradia, Antonio Frisoli and Lorenzo Masia, *"Characterisation of pressure distribution at the interface of a soft exosuit: towards a more comfortable wear"*, International Symposium on Wearable Robotics (WeRob), Pisa, Italy, 2018.

- Michele Xiloyannis, Letizia Galli, Domenico Chiaradia, Antonio Frisoli Francesco Braghin and Lorenzo Masia, *"A Soft Tendon-Driven Robotic Glove: Preliminary Evaluation"*, International Conference on Neurorehabilitatiton (ICNR), Pisa, Italy, 2018.

- Michele Xiloyannis, Leonardo Cappello, Khanh D. Binh, Chris W. Antuvan, Shih-Cheng Yen, and Lorenzo Masia, *"Modelling and Design of a Synergy-based Actuator for a Tendon-driven Soft Robotic Glove"*, IEEE International Conference on Biomedical Robots and Biomechatronics (BioRob), Singapore, 2016.

- Michele Xiloyannis, Leonardo Cappello, Khanh D. Binh, Chris W. Antuvan and Lorenzo Masia, *"Design and Preliminary Testing of a Soft Exosuit for Assisting Elbow Movements and Hand Grasping"*, International Conference on Neurorehabilitatiton (ICNR), Segovia, 2016.

- Domenico Chiaradia, Michele Xiloyannis, Massimiliano Sollazzi , Lorenzo Masia and Antonio Frisoli, *"Comparison of a Soft Exosuit and a Rigid Exoskeleton in an Assistive Task"*, International Symposium on Wearable Robotics (WeRob), Pisa, Italy, 2018.

- Binh Khanh Dinh, Michele Xiloyannis, Chris Wilson Antuvan, Leonardo Cappello, and Lorenzo Masia, *"Hierarchical Cascade Controller for Assistance Modulation in a Soft Wearable Arm Exoskeleton",* International Conference on Robotics and Automation (ICRA), Singapore, 2017.

- Domenico Chiaradia, Michele Xiloyannis, Chris W. Antuvan, Antonio Frisoli, Lorenzo Masia, *"Design and Embedded Control of a Soft Elbow Exosuit"*, IEEE International Conference on Soft Robotics (RoboSoft), Livorno, Italy, 2018.

- Yongtae Giovanni Kim, Michele Xiloyannis, Dino Accoto, Lorenzo Masia, *"Development of a Soft Exosuit for Industrial Applications'*, IEEE International Conference on Biomedical Robots and Biomechatronics (BioRob), Enschede, Netherlands, 2018.

- Marco Canesi, Michele Xiloyannis, Arash Ajoudani, Antonio Bicchi and Lorenzo Masia, *"Modular One-to-many Clutchable Actuator for a Soft Elbow Exosuit",* International Conference on Rehabilitation Robotics, London (ICORR), London, 2017.

- Binh Khanh Dinh, Leonardo Cappello, Michele Xiloyannis and Lorenzo Masia, *"Position Control using Adaptive Backlash Compensation for Bowden Cable Transmission in Soft Wearable Exoskeleton",* IEEE/RSJ International Conference on Intelligent Robots and Systems (IROS), Daejeon, 2016.

Bibliography

[1] Daniel M. Wolpert. The real reason for brains, 2011. 1

[2] Nicholas J Kassebaum, Megha Arora, and Ryan M Barber. Global, regional, and national disability-adjusted life-years (DALYs) for 315 diseases and injuries and healthy life expectancy (HALE), 1990-2015: a systematic analysis for the Global Burden of Disease Study 2015. *The Lancet*, 388(10053):1603–1658, oct 2016. ISSN 01406736. doi: 10.1016/S0140-6736(16)31460-X. 2

[3] Valery L. Feigin, Gregory A. Roth, Mohsen Naghavi, Priya Parmar, Rita Krishnamurthi, Sumeet Chugh, George A. Mensah, Bo Norrving, Ivy Shiue, Marie Ng, Kara Estep, Kelly Cercy, Christopher J L Murray, and Mohammad H. Forouzanfar. Global burden of stroke and risk factors in 188 countries, during 1990-2013: a systematic analysis for the Global Burden of Disease Study 2013. *The Lancet Neurology*, 15(9):913–924, 2016. ISSN 14744465. doi: 10.1016/S1474-4422(16)30073-4. 2

[4] Gert Kwakkel, Boudewijn J. Kollen, Jeroen V. Van der Grond, and Arie J.H. Prevo. Probability of regaining dexterity in the flaccid upper limb: Impact of severity of paresis and time since onset in acute stroke. *Stroke*, 34(9):2181–2186, 2003. ISSN 00392499. doi: 10.1161/01.STR.0000087172.16305.CD. 2

[5] Catherine A. Trombly. *Occupational Therapy for Physical Dysfunction*. 2004. ISBN 0781763126. doi: 10.1111/j.1440-1630.2004.00470.x. 2

[6] Alan S Go, Dariush Mozaffarian, and Véronique L Roger. Heart Disease and Stroke Statistics - 2014 Update: A report from the American Heart Association, jan 2014. ISSN 00097322. 2

[7] Cathrin Bütefisch, Horst Hummelsheim, Petra Denzler, and Karl Heinz Mauritz. Repetitive training of isolated movements improves the outcome of motor rehabilitation of the centrally paretic hand. *Journal of the Neurological Sciences*, 130(1):59–68, 1995. ISSN 0022510X. doi: 10.1016/0022-510X(95)00003-K. 2

[8] Gert Kwakkel, Boudewijn Kollen, and Eline Lindeman. Understanding the pattern of functional recovery after stroke: facts and theories. *Restorative Neurology and Neuroscience*, 22(3-5):281–299, 2004. ISSN 0922-6028. doi: 10.1177/1545968308317972. 2

[9] RP Van Peppen, G Kwakkel, S Wood-Dauphinee, and HJ Hendriks. The impact of physical therapy on functional outcomes after stroke: what's the evidence? *Clin Rehabil.*, 18:833–62, 2004. 2

[10] Jeffrey a Kleim, Rochelle Bruneau, Penny VandenBerg, Erin MacDonald, Renee Mulrooney, and David Pocock. Motor cortex stimulation enhances motor recovery and reduces peri-infarct dysfunction following ischemic insult. *Neurological research*, 25:789–793, 2003. ISSN 01616412. doi: 10.1179/016164103771953862. 2

[11] Verena Klamroth-Marganska, Javier Blanco, Katrin Campen, Armin Curt, Volker Dietz, Thierry Ettlin, Morena Felder, Bernd Fellinghauer, Marco Guidali, Anja Kollmar, Andreas Luft, Tobias Nef, Corina Schuster-Amft, Werner Stahel, and Robert Riener. Three-dimensional, task-specific robot therapy of the arm after stroke: A multicentre, parallel-group randomised trial. *The Lancet Neurology*, 2014. ISSN 14744422. doi: 10.1016/S1474-4422(13)70305-3. 2

[12] G Kwakkel, B J Kollen, and H I Krebs. Effects of Robot-Assisted Therapy on Upper Limb Recovery After Stroke: A Systematic Review. *Neurorehabilitation and Neural Repair*, 22(2):111–121, 2007. ISSN 1545-9683. doi: 10.1177/1545968307305457. 3

[13] Mary Joan Macleod and Melanie Turner. Stroke: Stroke outcomes after 90 days-out of sight, out of mind? *Nature Reviews Neurology*, 2015. ISSN 17594766. doi: 10.1038/nrneurol.2015.28. 3

[14] James Gordon. Assumptions underlying physical therapy intervention: theoretical and historical perspectives. *Movement science, foundations for physical therapy rehabilitation*, 1987. 3

[15] Nicholas Yagn. Apparatus for facilitating walking, running, and jumping. *US Patent 440,584*, (406), 1890. doi: U.S.420179. 9, 10

[16] Ralph S. Mosher. From Handiman to Hardiman, 1967. 9, 10

[17] Leslie C. Kelley. Pedomotor, 1919. 9

[18] SJ Zaroodny. Bumpusher-A Powered Aid for Locomotion. 1963. 10

[19] H Kazerooni, J L Racine, L Huang, and R Steger. On the control of the Berkeley Lower Extermity Exoskeleton (BLEEX). In *Proceedings of the IEEE International Conference on Robotics and Automation*, pages 4353–4360, 2005. 11, 45

[20] A Chu, H Kazerooni, and A Zoss. On the biomimetic design of the berkeley lower extremity exoskeleton (BLEEX). In *Robotics and Automation, 2005. ...*, number April, pages 4356–4363, 2005. ISBN 078038914X. 11

[21] E Guizzo and H Goldstein. The rise of the body bots. *IEEE Spectrum*, 42 (10):42–48, 2005. ISSN 0018-9235. doi: 10.1109/MSPEC.2005.1515961. 11

[22] Aaron M. Dollar and Hugh Herr. Lower extremity exoskeletons and active orthoses: Challenges and state-of-the-art. *IEEE Transactions on Robotics*, 24(1):144–158, 2008. ISSN 15523098. doi: 10.1109/TRO.2008.915453. 11

[23] Conor J. Walsh, Daniel Paluska, Kenneth Pasch, William Grand, Andrew Valiente, and Hugh Herr. Development of a lightweight, underactuated exoskeleton for load-carrying augmentation. *Proceedings - IEEE International Conference on Robotics and Automation*, 2006:3485–3491, 2006. ISSN 10504729. doi: 10.1109/ROBOT.2006.1642234. 11

[24] Conor J. Walsh. Biomimetic design of an underactuated leg exoskeleton for load-carrying augmentation. 2006. 11

[25] Steven H. Collins, M. Bruce Wiggin, and Gregory S. Sawicki. Reducing the energy cost of human walking using an unpowered exoskeleton. *Nature*, 522 (7555):212–215, 2015. ISSN 0028-0836. doi: 10.1038/nature14288. 11

[26] Luke M Mooney, Elliott J Rouse, and Hugh Herr. Autonomous exoskeleton reduces metabolic cost of human walking during load carriage. *Journal of NeuroEngineering and Rehabilitation*, 11(1):80, 2014. ISSN 1743-0003. doi: 10.1186/1743-0003-11-80. 11

[27] Alberto Esquenazi, Mukul Talaty, Andrew Packel, and Michael Saulino. The Rewalk powered exoskeleton to restore ambulatory function to individuals with thoracic-level motor-complete spinal cord injury. *American Journal of Physical Medicine and Rehabilitation*, 91(11):911–921, 2012. ISSN 08949115. doi: 10.1097/PHM.0b013e318269d9a3. 11

[28] Kelly P Westlake and Carolynn Patten. Pilot study of Lokomat versus manual-assisted treadmill training for locomotor recovery post-stroke. *Journal of NeuroEngineering and Rehabilitation*, 6(1):18, 2009. ISSN 1743-0003. doi: 10.1186/1743-0003-6-18. 11

[29] Antonio Frisoli, Caterina Procopio, Carmelo Chisari, Ilaria Creatini, Luca Bonfiglio, Massimo Bergamasco, Bruno Rossi, and Maria Chiara Carboncini. Positive effects of robotic exoskeleton training of upper limb reaching movements after stroke. *Journal of NeuroEngineering and Rehabilitation*, 9(1), 2012. ISSN 17430003. doi: 10.1186/1743-0003-9-36. 11

[30] Qingguo Li, Veronica Naing, and J. Maxwell Donelan. Development of a biomechanical energy harvester. *Journal of NeuroEngineering and Rehabilitation*, 6(1), 2009. ISSN 17430003. doi: 10.1186/1743-0003-6-22. 11

[31] T. Lam. Contribution of Feedback and Feedforward Strategies to Locomotor Adaptations. *Journal of Neurophysiology*, 95(2):766–773, 2005. ISSN 0022-3077. doi: 10.1152/jn.00473.2005. 11

[32] Francesca Marini, Valentina Squeri, Pietro Morasso, and Lorenzo Masia. Wrist Proprioception: Amplitude or Position Coding? *Frontiers in Neurorobotics*, 10, oct 2016. ISSN 1662-5218. doi: 10.3389/fnbot.2016.00013. 11

[33] Nathanaël Jarrassé and Guillaume Morel. A formal method for avoiding hyperstaticity when connecting an exoskeleton to a human member. In *Proceedings - IEEE International Conference on Robotics and Automation*, pages

1188–1195, 2010. ISBN 9781424450381. doi: 10.1109/ROBOT.2010.5509346. 12

[34] Arno H.A. Stienen, Edsko E.G. Hekman, Frans C.T. van der Helm, and Herman van der Kooij. Self-aligning exoskeleton axes through decoupling of joint rotations and translations. *IEEE Transactions on Robotics*, 25(3): 628–633, 2009. ISSN 15523098. doi: 10.1109/TRO.2009.2019147. 12, 13

[35] Craig D. Murray. Being like everybody else: The personal meanings of being a prosthesis user. *Disability and Rehabilitation*, 31(7):573–581, 2009. ISSN 09638288. doi: 10.1080/09638280802240290. 12

[36] Joel C. Perry, Jacob Rosen, and Stephen Burns. Upper-limb powered exoskeleton design. *IEEE/ASME Transactions on Mechatronics*, 12(4):408–417, 2007. ISSN 10834435. doi: 10.1109/TMECH.2007.901934. 13

[37] Nathanaël Jarrassé and Guillaume Morel. Connecting a human limb to an exoskeleton. *IEEE Transactions on Robotics*, 28(3):697–709, jun 2012. ISSN 15523098. doi: 10.1109/TRO.2011.2178151. 13

[38] Carmel Majidi. Soft Robotics: A PerspectiveCurrent Trends and Prospects for the Future. *Soft Robotics*, 2014. ISSN 2169-5172. doi: 10.1089/soro.2013.0001. 14

[39] Alan T. Asbeck, Kai Schmidt, and Conor J. Walsh. Soft exosuit for hip assistance. *Robotics and Autonomous Systems*, 73:102–110, 2014. ISSN 09218890. doi: 10.1016/j.robot.2014.09.025. 14

[40] Alan T. Asbeck, Robert J. Dyer, Arnar F. Larusson, and Conor J. Walsh. Biologically-inspired soft exosuit. In *IEEE International Conference on Rehabilitation Robotics*, pages 1–8, Seattle, WA, 2013. ISBN 9781467360241. doi: 10.1109/ICORR.2013.6650455. 14, 78

[41] H. Kobayashi and K. Hiramatsu. Development of muscle suit for upper limb. In *IEEE International Conference on Robotics and Automation, 2004. Proceedings. ICRA '04. 2004*, volume 3, pages 3–8. IEEE, 2004. ISBN 0-7803-8232-3. doi: 10.1109/ROBOT.2004.1307433. 14

[42] Saivimal Sridar, Student Member, Zhi Qiao, Student Member, and Niveditha Muthukrishnan. A Soft-Inflatable Exosuit for Knee Rehabilitation : Assisting

Swing Phase During Walking. *Frontiers in Robotics and AI*, 5:44, may 2018. ISSN 2296-9144. doi: 10.3389/frobt.2018.00044. 14

[43] Ciarán T. Ciaran T. O'Neill, Nathan S. Phipps, Leonardo Cappello, Sabrina Paganoni, and Conor J. Walsh. A soft wearable robot for the shoulder: Design, characterization, and preliminary testing. In *2017 International Conference on Rehabilitation Robotics (ICORR)*, volume 02129, pages 1672–1678. IEEE, jul 2017. ISBN 978-1-5386-2296-4. doi: 10.1109/ICORR.2017.8009488. 14, 16, 68

[44] Tze Hui Koh, Nicholas Cheng, Hong Kai Yap, and Chen Hua Yeow. Design of a soft robotic elbow sleeve with passive and intent-controlled actuation. *Frontiers in Neuroscience*, 11(OCT):1–12, 2017. ISSN 1662453X. doi: 10.3389/fnins.2017.00597. 14

[45] Panagiotis Polygerinos, Zheng Wang, Kevin C. Galloway, Robert J. Wood, and Conor J. Walsh. Soft robotic glove for combined assistance and at-home rehabilitation. *Robotics and Autonomous Systems*, 73:135–143, 2015. ISSN 09218890. doi: 10.1016/j.robot.2014.08.014. URL `http://dx.doi.org/10.1016/j.robot.2014.08.014`. 14

[46] Hong Kai Yap, Phone May Khin, Tze Hui Koh, Yi Sun, Xinquan Liang, Jeong Hoon Lim, and Chen-Hua Yeow. A Fully Fabric-Based Bidirectional Soft Robotic Glove for Assistance and Rehabilitation of Hand Impaired Patients. *IEEE Robotics and Automation Letters*, 2(3):1383–1390, 2017. ISSN 2377-3766. doi: 10.1109/LRA.2017.2669366.

[47] Leonardo Cappello, Jan T Meyer, Kevin C Galloway, Jeffrey D Peisner, Rachael Granberry, Diana A Wagner, Sven Engelhardt, Sabrina Paganoni, and Conor J. Walsh. Assisting hand function after spinal cord injury with a fabric-based soft robotic glove. *Journal of NeuroEngineering and Rehabilitation*, pages 1–10, 2018. ISSN 17430003. doi: 10.1186/s12984-018-0391-x. 14

[48] Brendan T. Quinlivan, Lee Sangjun, Philippe Malcolm, Denis M. Rossi, Martin Grimmer, Christopher Siviy, and Conor J. Walsh. Assistance magnitude vs. metabolic cost reductions for a tethered multiarticular soft exosuit. *Science Robotics*, 2(2):1–17, 2016. ISSN 2470-9476. doi: 10.1126/scirobotics.aah4416. 15, 20

[49] Louis N. Awad, Jaehyun Bae, Kathleen O'Donnell, Stefano Marco Maria De Rossi, Kathryn Hendron, Lizeth H. Sloot, Pawel Kudzia, Stephen Allen, Kenneth G. Holt, Terry D. Ellis, and Conor J. Walsh. A soft robotic exosuit improves walking in patients after stroke. *Science Translational Medicine*, 9(400):eaai9084, 2017. ISSN 1946-6234. doi: 10.1126/scitranslmed.aai9084. 15

[50] Kai Schmidt, Jaime E. Duarte, Martin Grimmer, Alejandro Sancho-Puchades, Haiqi Wei, Chris S. Easthope, and Robert Riener. The myosuit: Bi-articular anti-gravity exosuit that reduces hip extensor activity in sitting transfers. *Frontiers in Neurorobotics*, 11(OCT):57, oct 2017. ISSN 16625218. doi: 10.3389/fnbot.2017.00057. URL `http://journal.frontiersin.org/article/10.3389/fnbot.2017.00057/full`. 15

[51] Xin Jin, Antonio Prado, and Sunil K. Agrawal. Retraining of Human Gait - Are Lightweight Cable-Driven Leg Exoskeleton Designs Effective? *IEEE Transactions on Neural Systems and Rehabilitation Engineering*, 26(4):847–855, apr 2018. ISSN 15344320. doi: 10.1109/TNSRE.2018.2815656. 15

[52] Daegeun Park and Kyu Jin Cho. Development and evaluation of a soft wearable weight support device for reducing muscle fatigue on shoulder. *PLoS ONE*, 12(3), mar 2017. ISSN 19326203. doi: 10.1371/journal.pone.0173730. 16, 70

[53] Alan T. Asbeck, Stefano M.M. De Rossi, Ignacio Galiana, Ye Ding, and Conor J. Walsh. Stronger, smarter, softer: Next-generation wearable robots. *IEEE Robotics and Automation Magazine*, 21(4):22–33, 2014. ISSN 10709932. doi: 10.1109/MRA.2014.2360283. 16, 78

[54] Ye Ding, Ignacio Galiana, Alan T. Asbeck, Stefano Marco Maria De Rossi, Jaehyun Bae, Thiago Ribeiro Teles Santos, Vanessa Lara De Araujo, Sangjun Lee, Kenneth G. Holt, and Conor J. Walsh. Biomechanical and physiological evaluation of multi-joint assistance with soft exosuits. *IEEE Transactions on Neural Systems and Rehabilitation Engineering*, 25(2):119–130, feb 2017. ISSN 15344320. doi: 10.1109/TNSRE.2016.2523250. 16

[55] Teresa R. Duck, Cynthia E. Dunning, Graham J.W. King, and James A. Johnson. Variability and repeatability of the flexion axis at the ulnohumeral

joint. *Journal of Orthopaedic Research*, 21(3):399–404, may 2003. ISSN 07360266. doi: 10.1016/S0736-0266(02)00198-5. 17, 18

[56] Walter Isaacson. *Leonardo Da Vinci: The Biography*. Simon and Schuster UK Ltd, 1st edition, 2017. ISBN 978-1-4711-6678-5. 19

[57] Stefano M M De Rossi, Jaehyun Bae, Kathleen E O Donnell, Kathryn L Hendron, Kenneth G Holt, Terry Ellis, and Conor J. Walsh. Gait improvements in stroke patients with a soft exosuit. *proceedings of the Gait and Clinical Movement Analysis Society Meeting*, pages 2–3, 2015. 20

[58] Jaehyun Bae, Stefano Marco Maria De Rossi, Kathleen O'Donnell, Kathryn L. Hendron, Louis N. Awad, Thiago R. Teles Dos Santos, Vanessa Lara De Araujo, Ye Ding, Kenneth G. Holt, Terry D. Ellis, and Conor J. Walsh. A soft exosuit for patients with stroke: Feasibility study with a mobile off-board actuation unit. In *IEEE International Conference on Rehabilitation Robotics*, volume 2015-Septe, pages 131–138, 2015. ISBN 9781479918072. doi: 10.1109/ICORR.2015.7281188. 20

[59] D. J. Magermans, E. K J Chadwick, H. E J Veeger, and F. C T Van Der Helm. Requirements for upper extremity motions during activities of daily living. *Clinical Biomechanics*, 20(6):591–599, jul 2005. ISSN 02680033. doi: 10.1016/j.clinbiomech.2005.02.006. 21, 27

[60] Ingram A. Murray and Garth R. Johnson. A study of the external forces and moments at the shoulder and elbow while performing every day tasks. *Clinical Biomechanics*, 19(6):586–594, jul 2004. ISSN 02680033. doi: 10.1016/j.clinbiomech.2004.03.004. 21, 28

[61] M A Buckley, A Yardley, G R Johnson, and D A Cams. Dynamics of the upper limb during performance of the tasks of everyday living: a review of the current knowledge base. *Journal of Engineering in Medicine*, 210(4): 241–247, jun 1996. ISSN 09544119. 21, 27, 48, 56, 95, 100

[62] Charles E. Clauser, John T. McConville, and J. W. Young. Weight, volume and center of mass of segments of the human body. Technical report, 1969. 21, 27, 46, 56

[63] Richard G Snyder, L W Schneider, C L Owings, H M Reynolds, D H Golomb, and M A Schork. Anthropometry of infants, children and youths to age 18

for product safety design. *Applied Ergonomics*, 1977. ISSN 1098-6596. doi: 10.2514/8.5806. 22

[64] André Schiele and Frans C.T. van der Helm. Influence of attachment pressure and kinematic configuration on pHRI with wearable robots. *Applied Bionics and Biomechanics*, 6(2):157–173, 2009. ISSN 17542103. doi: 10.1080/11762320902879961. 23

[65] Kosuke Ogata and Leo A. Whiteside. Effects of external compression on blood flow to muscle and skin. *Clinical orthopaedics and related research*, (168):105–107, 1982. ISSN 0009-921X (Print). 23

[66] Jean Francois Duval and Hugh Herr. FlexSEA: Flexible, Scalable Electronics Architecture for wearable robotic applications. In *Proceedings of the IEEE RAS and EMBS International Conference on Biomedical Robotics and Biomechatronics*, volume 2016-July, pages 1236–1241, 2016. ISBN 9781509032877. doi: 10.1109/BIOROB.2016.7523800. 29, 30

[67] Brendan Quinlivan, Alan T. Asbeck, Diana Wagner, Tommaso Ranzani, Sheila Russo, and Conor J. Walsh. Force Transfer Characterization of a Soft Exosuit for Gait Assistance. In *Volume 5A: 39th Mechanisms and Robotics Conference*, pages 1327–1334, 2015. ISBN 978-0-7918-5712-0. doi: 10.1115/DETC2015-47871. 31, 36, 52

[68] Matthew B. Yandell, Brendan T. Quinlivan, Dmitry Popov, Conor J. Walsh, and Karl E. Zelik. Physical interface dynamics alter how robotic exosuits augment human movement: implications for optimizing wearable assistive devices. *Journal of NeuroEngineering and Rehabilitation*, 14(1):40, 2017. ISSN 1743-0003. doi: 10.1186/s12984-017-0247-9. 30

[69] GA Pratt and M.M. Williamson. Series elastic actuators. In *Proceedings 1995 IEEE/RSJ International Conference on Intelligent Robots and Systems. Human Robot Interaction and Cooperative Robots*, volume 1, pages 399–406. ISBN 0-8186-7108-4. doi: 10.1109/IROS.1995.525827. 32, 41

[70] M Kaneko, W Paetsch, G Kegel, H Toile, and F R Geman. Input-dependent Stability on Joint Torque Control of Robot Hand. *Industrial Electronics, IEEE ...*, pages 1057–1062, 1990. 32

[71] W. Townsend and Jr. Salisbury, J. The Effect of coulomb friction and stiction on force control. *Proceedings. 1987 IEEE International Conference on Robotics and Automation*, 4:883–889, 1987. doi: 10.1109/ROBOT.1987.1087936. URL `http://ieeexplore.ieee.org/lpdocs/epic03/wrapper.htm?arnumber=1087936`. 32

[72] Binh Khanh Dinh, Michele Xiloyannnis, Chris Wilson Antuvan, Leonardo Cappello, and Lorenzo Masia. Hierarchical Cascade Controller for Assistance Modulation in a Soft Wearable Arm Exoskeleton. *IEEE Robotics and Automation Letters*, 2(3):1–1, jul 2017. ISSN 2377-3766. doi: 10.1109/LRA.2017.2668473. 33, 34, 43, 68, 69, 106

[73] Binh Khanh Dinh, Michele Xiloyannnis, Leonardo Cappello, Chris Wilson Antuvan, Shih Cheng Yen, and Lorenzo Masia. Adaptive backlash compensation in upper limb soft wearable exoskeletons. *Robotics and Autonomous Systems*, 92:173–186, 2017. ISSN 09218890. doi: 10.1016/j.robot.2017.03.012. 33, 112

[74] G. Palli and C. Melchiorri. Model and control of tendon-sheath transmission systems. *Proceedings - IEEE International Conference on Robotics and Automation*, 2006:988–993, 2006. ISSN 10504729. doi: 10.1109/ROBOT.2006.1641838. URL `http://ieeexplore.ieee.org/xpls/abs{_}all.jsp?arnumber=1641838`. 33

[75] Andre Schiele, Pierre Letier, Richard Van Der Linde, and Frans Van Der Helm. Bowden cable actuator for force-feedback exoskeletons. *IEEE International Conference on Intelligent Robots and Systems*, pages 3599–3604, 2006. doi: 10.1109/IROS.2006.281712. 34, 51

[76] Hugh Herr. The new bionics that let us run, climb and dance. *TED, Lecture*, 2014. 35

[77] F Mak, M Zhang, and D Boone. State-of-the-art research in lower-limb prosthetic biomechanics-socket interface: a review. *Journal of rehabilitation research and development*, 38(2):161–174, 2001. ISSN 0748-7711. 35

[78] Stefano Marco Maria de Rossi, Nicola Vitiello, Tommaso Lenzi, Renaud Ronsse, Bram Koopman, Alessandro Persichetti, Fabrizio Vecchi, Auke Jan Ijspeert, Herman van der Kooij, and Maria Chiara Carrozza. Sensing pressure

distribution on a lower-limb exoskeleton physical human-machine interface. *Sensors*, 11(1):207–227, 2011. ISSN 14248220. doi: 10.3390/s110100207. 35

[79] Laurent Levesque, Scott Pardoel, Zlatko Lovrenovic, and Marc Doumit. Experimental comfort assessment of an active exoskeleton interface. In *2017 IEEE 5th International Symposium on Robotics and Intelligent Sensors*, number October, Ottawa, 2017. doi: 10.1109/IRIS.2017.8250095. 35

[80] Randall F. Beer, Julius P A Dewald, Michelle L. Dawson, and W. Zev Rymer. Target-dependent differences between free and constrained arm movements in chronic hemiparesis. *Experimental Brain Research*, 2004. ISSN 00144819. doi: 10.1007/s00221-003-1807-8. 39

[81] Derek G. Kamper, Alicia N. McKenna-Cole, Leonard E. Kahn, and David J. Reinkensmeyer. Alterations in reaching after stroke and their relation to movement direction and impairment severity. *Archives of Physical Medicine and Rehabilitation*, 2002. ISSN 00039993. doi: 10.1053/apmr.2002.32446. 39

[82] Randall F. Beer, Julius P.A. Dewald, and W. Zev Rymer. Deficits in the coordination of multijoint arm movements in patients with hemiparesis: evidence for disturbed control of limb dynamics. *Experimental Brain Research*, 2000. ISSN 00144819. doi: 10.1007/s002219900275. 39

[83] Theresa M. Sukal, Michael D. Ellis, and Julius P A Dewald. Shoulder abduction-induced reductions in reaching work area following hemiparetic stroke: Neuroscientific implications. *Experimental Brain Research*, 2007. ISSN 00144819. doi: 10.1007/s00221-007-1029-6. 39, 40

[84] Russell D Howard. *Joint and actuator design for enhanced stability in robotic force control*. PhD thesis, 1990. 41

[85] Gill A. Pratt and Matthew M. Williamson. Series elastic actuators. In *IEEE/RSJ International Conference on Intelligent Robots and Systems. 'Human Robot Interaction and Cooperative Robots'*, volume 1, pages 399–406. IEEE Comput. Soc. Press, 1995. ISBN 0-8186-7108-4. doi: 10.1109/IROS.1995.525827. 41

[86] Neville Hogan. Impedance Control: An Approach to Manipulation. In *American Control Conference*, number March, pages 304–313, 1984. ISBN VO -. doi: 10.1115/1.3140702. 41, 42, 72

[87] J. Salisbury. Active stiffness control of a manipulator in cartesian coordinates. In *1980 19th IEEE Conference on Decision and Control including the Symposium on Adaptive Processes*, pages 95–100. IEEE, dec 1980. ISBN VO -. doi: 10.1109/CDC.1980.272026. 41

[88] William T Townsend. *The Effect of Transmission Design on Force-Controlled Manipulator Performance*. PhD thesis, 1988. 41

[89] Andrea Calanca, Riccardo Muradore, and Paolo Fiorini. A review of algorithms for compliant control of stiff and fixed-compliance robots. *IEEE/ASME Transactions on Mechatronics*, 21(2):613–624, 2016. ISSN 10834435. doi: 10.1109/TMECH.2015.2465849. 42, 43, 45

[90] G.A. Pratt, P. Willisson, C. Bolton, and A. Hofman. Late motor processing in low-impedance robots: impedance control of series-elastic actuators. In *Proceedings of the American Control Conference*, volume 4, pages 3245–3251 vol.4, 2004. ISBN 0-7803-8335-4. doi: 10.1109/ACC.2004.182786. 42, 45

[91] W Yu, J Rosen, and X Li. PID admittance control for an upper limb exoskeleton. In *Proceedings of the 2011 American Control Conference*, pages 1124–1129, 2011. ISBN 978-1-4577-0079-8. doi: 10.1109/ACC.2011.5991147. 45, 52, 94

[92] R Drillis, R Contini, and M Bluestein. Body Segment Parameters; a Survey of Measurement Techniques. *Artificial limbs*, 25:44–66, 1964. ISSN 0004-3729. doi: 10.1049/ecej:19890011. 46, 56

[93] T Flash and Neville Hogan. The coordination of arm movements: an experimentally confirmed mathematical model. *The Journal of neuroscience*, 5(7): 1688–1703, 1985. ISSN 0270-6474. doi: 4020415. 47, 56, 95

[94] Giuk Lee, Ye Ding, Ignacio Galiana Bujanda, Nikos Karavas, Yu Meng Zhou, and Conor J. Walsh. Improved assistive profile tracking of soft exosuits for walking and jogging with off-board actuation. *IEEE International Conference on Intelligent Robots and Systems*, 2017-Septe:1699–1706, 2017. ISSN 21530866. doi: 10.1109/IROS.2017.8205981. 52

[95] Luc P.J. Selen, Peter J. Beek, and Jaap H. Van Dieën. Impedance is modulated to meet accuracy demands during goal-directed arm movements. *Experimental Brain Research*, 2006. ISSN 00144819. doi: 10.1007/s00221-005-0320-7. 52

[96] Neville Hogan. Mechanical Impedance of Single- and Multi-Articular Systems. In *Multiple Muscle Systems*. 2011. doi: 10.1007/978-1-4613-9030-5_9. 52

[97] Juanjuan Zhang, Pieter Fiers, Kirby A. Witte, Rachel W. Jackson, Katherine L. Poggensee, Christopher G. Atkeson, and Steven H. Collins. Human-in-the-loop optimization of exoskeleton assistance during walking. *Science*, 356 (6344):1280–1283, 2017. ISSN 10959203. doi: 10.1126/science.aal5054. 53, 74

[98] Ye Ding, Myunghee Kim, Scott Kuindersma, and Conor J. Walsh. Human-in-the-loop optimization of hip assistance with a soft exosuit during walking. *Science Robotics*, 2018. ISSN 2470-9476. doi: 10.1111/irfi.12020. 53, 74

[99] Hermie J. Hermens, Bart Freriks, Catherine Disselhorst-Klug, and Günter Rau. Development of recommendations for SEMG sensors and sensor placement procedures. *Journal of Electromyography and Kinesiology*, 10(5):361–374, 2000. ISSN 10506411. doi: 10.1016/S1050-6411(00)00027-4. 57

[100] J. R. Potvin and L. R. Bent. A validation of techniques using surface EMG signals from dynamic contractions to quantify muscle fatigue during repetitive tasks. *Journal of Electromyography and Kinesiology*, 1997. ISSN 10506411. doi: 10.1016/S1050-6411(96)00025-9. 58

[101] T J Sejnowski. Neurobiology. Making smooth moves. *Nature*, 394(6695): 725–726, 1998. ISSN 0028-0836. doi: 10.1038/29404. 59, 71

[102] Sivakumar Balasubramanian, Alejandro Melendez-Calderon, Agnes Roby-Brami, and Etienne Burdet. On the analysis of movement smoothness. *Journal of NeuroEngineering and Rehabilitation*, 12(1):1–11, 2015. ISSN 17430003. doi: 10.1186/s12984-015-0090-9. 59, 61, 95

[103] W. A. MacKay, D. J. Crammond, H. C. Kwan, and J. T. Murphy. Measurements of human forearm viscoelasticity. *Journal of Biomechanics*, 19(3): 231–238, 1986. ISSN 00219290. doi: 10.1016/0021-9290(86)90155-7. 59

[104] E. A. Clancy, E. L. Morin, and R. Merletti. Sampling, noise-reduction and amplitude estimation issues in surface electromyography. In *Journal of Electromyography and Kinesiology*, volume 12, pages 1–16, 2002. ISBN 1050-6411. doi: 10.1016/S1050-6411(01)00033-5. 60, 95

[105] Roberto Merletti and Philip Parker. *Electromyography : physiology, engineering, and noninvasive applications*. Wiley-IEEE Press, 11 edition, 2004. ISBN 9780471675808. 60

[106] Domenico; Chiaradia, Michele Xiloyannnis, Chris W; Antuvan, Antonio Frisoli, and Lorenzo; Masia. Design and Embedded Control of a Soft Elbow Exosuit. In *Proceedings of the IEEE International Conference Soft Robotics*, pages 565–571, Livorno, Italy, 2018. 68, 114

[107] Yongtae G Kim, Michele Xiloyannnis, Dino Accoto, and Lorenzo Masia. Development of a Soft Exosuit for Industrial Applications. In *International Conference on Biomedical Robotics and Biomechatronics*, 2018. 68

[108] Tomoki Abe, Shoichiro Koizumi, Hiroyuki Nabae, G. Endo, and Koichi Suzumori. Muscle textile to implement soft suit to shift balancing posture of the body. In *2018 IEEE International Conference on Soft Robotics (RoboSoft)*, pages 572–578. IEEE, apr 2018. ISBN 978-1-5386-4516-1. doi: 10.1109/ROBOSOFT.2018.8405387. 69

[109] Ning Li, Tie Yang, Peng Yu, Junling Chang, Liang Zhao, Xingang Zhao, Imad H. Elhajj, Ning Xi, and Lianqing Liu. Bio-inspired upper limb soft exoskeleton to reduce stroke-induced complications. *Bioinspiration and Biomimetics*, 13(6), 2018. ISSN 17483190. doi: 10.1088/1748-3190/aad8d4. 69

[110] Zahra Kadivar, Christopher E. Beck, Roger N. Rovekamp, Marcia K. O'Malley, and Charles A. Joyce. On the efficacy of isolating shoulder and elbow movements with a soft, portable, and wearable robotic device. In *Biosystems and Biorobotics*, volume 16, pages 89–93. 2017. ISBN 978-3-319-46532-6; 978-3-319-46531-9. doi: 10.1007/978-3-319-46532-6_15. 69

[111] S Bastide, N Vignais, F. Geffard, and B. Berret. Analysis of human-exoskeleton interactions: an elbow flexion/extension case study. *Computer*

Methods in Biomechanics and Biomedical Engineering, 20:9–10, 2017. ISSN 14768259. doi: 10.1080/10255842.2017.1382835. 71

[112] Michel Desmurget, Michael Jordan, Claude Prablanc, and Marc Jeannerod. Constrained and unconstrained movements involve different control strategies. *Journal of neurophysiology*, 77(3):1644–1650, mar 1997. ISSN 0022-3077. doi: 10.1152/jn.1997.77.3.1644. 71

[113] Nathanael Jarrassé, Michele Tagliabue, Johanna V.G. Robertson, Amina Maiza, Vincent Crocher, Agnès Roby-Brami, and Guillaume Morel. A methodology to quantify alterations in human upper limb movement during co-manipulation with an exoskeleton. *IEEE Transactions on Neural Systems and Rehabilitation Engineering*, 2010. ISSN 15344320. doi: 10.1109/TNSRE.2010.2056388. 71

[114] Elvira Pirondini, Martina Coscia, Simone Marcheschi, Gianluca Roas, Fabio Salsedo, Antonio Frisoli, Massimo Bergamasco, and Silvestro Micera. Evaluation of the effects of the Arm Light Exoskeleton on movement execution and muscle activities: A pilot study on healthy subjects. *Journal of NeuroEngineering and Rehabilitation*, 13(1), 2016. ISSN 17430003. doi: 10.1186/s12984-016-0117-x. 72

[115] Keith E. Gordon and Daniel P. Ferris. Learning to walk with a robotic ankle exoskeleton. *Journal of Biomechanics*, 2007. ISSN 00219290. doi: 10.1016/j.jbiomech.2006.12.006. 72

[116] Wen Wen, Atsushi Yamashita, and Hajime Asama. The influence of action-outcome delay and arousal on sense of agency and the intentional binding effect. *Consciousness and Cognition*, 2015. ISSN 10902376. doi: 10.1016/j.concog.2015.06.004. 72

[117] Manos Tsakiris, Matthew R. Longo, and Patrick Haggard. Having a body versus moving your body: Neural signatures of agency and body-ownership. *Neuropsychologia*, 2010. ISSN 00283932. doi: 10.1016/j.neuropsychologia.2010.05.021. 72

[118] Mariella Pazzaglia and Marco Molinari. The embodiment of assistive devicesfrom wheelchair to exoskeleton. *Physics of Life Reviews*, 16:163–175, mar 2016. ISSN 1571-0645. doi: 10.1016/J.PLREV.2015.11.006. 72

[119] Ralph S. Mosher. Handyman to Hardiman. *SAE Transactions*, 76(1):588–597, 1967. doi: 10.4271/670088. 77

[120] Michiel P. de Looze, Tim Bosch, Frank Krause, Konrad S. Stadler, and Leonard W. O'Sullivan. Exoskeletons for industrial application and their potential effects on physical work load. *Ergonomics*, 2016. ISSN 13665847. doi: 10.1080/00140139.2015.1081988. 78

[121] Dennis R. Louie and Janice J. Eng. Powered robotic exoskeletons in post-stroke rehabilitation of gait: A scoping review. *Journal of NeuroEngineering and Rehabilitation*, 2016. ISSN 17430003. doi: 10.1186/s12984-016-0162-5. 78

[122] Leonardo Cappello, Kevin C. Galloway, Siddharth Sanan, Diana A. Wagner, Rachael Granberry, Sven Engelhardt, Florian L. Haufe, Jeffrey D. Peisner, and Conor J. Walsh. Exploiting Textile Mechanical Anisotropy for Fabric-Based Pneumatic Actuators. *Soft Robotics*, 5(5):662–674, oct 2018. ISSN 2169-5172. doi: 10.1089/soro.2017.0076. 78

[123] Hyunki In and Kyu Jin Cho. Exo-Glove : Soft wearable robot for the hand using soft tendon routing system. *IEEE Robotics & Automation*, 22(March 2015):97–105, 2015. ISSN 1070-9932. doi: 10.1109/MRA.2014.2362863. 78

[124] Michele Xiloyannnis, Leonardo Cappello, Dinh Binh Khanh, Shih Cheng Yen, and Lorenzo Masia. Modelling and design of a synergy-based actuator for a tendon-driven soft robotic glove. In *Proceedings of the IEEE RAS and EMBS International Conference on Biomedical Robotics and Biomechatronics*, volume 2016-July, pages 1213–1219, 2016. ISBN 9781509032877. doi: 10.1109/BIOROB.2016.7523796. 78

[125] Alan T. Asbeck, Kai Schmidt, Ignacio Galiana, Diana Wagner, and Conor J. Walsh. Multi-joint Soft Exosuit for Gait Assistance. *IEEE International Conference on Robotics and Automation (ICRA)*, pages 6197–6204, 2015. doi: 10.1109/ICRA.2015.7140069. 78, 103

[126] Thane R. Hunt, Christopher J. Berthelette, and Marko B. Popovic. Linear One-to-Many (OTM) system. In *IEEE Conference on Technologies for Practical Robot Applications, TePRA*, pages 1–6. IEEE, apr 2013. ISBN 9781467362252. doi: 10.1109/TePRA.2013.6556359. 78, 81

[127] Hamidreza Karbasi, Jan Paul Huissoon, and Amir Khajepour. Uni-drive modular robots: Theory, design, and experiments. *Mechanism and Machine Theory*, 39(2):183–200, 2004. ISSN 0094114X. doi: 10.1016/S0094-114X(03)00113-7. 78, 81, 85, 87, 99, 100

[128] WJ Chen and M Xie. On the design of a novel dexterous hand. *The 9th International Conference onAdvanced*, (September), 1999. 78, 81

[129] Dante Alighieri. Canto XXVII. In *Divina Commedia - Paradiso*. 1320. URL `http://online.scuola.zanichelli.it/letterautori-files/divina-commedia/pdf-online/007-online{_}paradiso.pdf`. 79

[130] Alexander S. Kembaum, Murphy Kitchell, and Max Crittenden. An ultra-compact infinitely variable transmission for robotics. *Proceedings - IEEE International Conference on Robotics and Automation*, pages 1800–1807, 2017. ISSN 10504729. doi: 10.1109/ICRA.2017.7989212. 80

[131] M. Canesi, Michele Xiloyannnis, A. Ajoudani, A. Biechi, and L. Masia. Modular one-to-many clutchable actuator for a soft elbow exosuit. In *IEEE International Conference on Rehabilitation Robotics*, pages 1679–1685, 2017. ISBN 9781538622964. doi: 10.1109/ICORR.2017.8009489. 80, 81, 84, 99

[132] Peyman Yadmellat, Alexander S. Shafer, and Mehrdad R. Kermani. Design and development of a single-motor, two-DOF, safe manipulator. *IEEE/ASME Transactions on Mechatronics*, 19(4):1384–1391, 2014. ISSN 10834435. doi: 10.1109/TMECH.2013.2281598. 81, 100, 101

[133] Mehrdad Kermani and Shafer Alex. Magneto- and electro-rheological based actuators for human friendly manipulators, sep 2014. 81

[134] Yanming Li, Peisun Ma, Changjun Qin, Xueguan Gao, Jianbin Wang, and Haihong Zhu. Design and study of a novel hyper-redundant manipulator. *Robotica*, 21(5):505–509, 2003. ISSN 02635747. doi: 10.1017/S0263574703005125. 81

[135] S Li, Y Liu, and M Xie. Implementation of a single motor driven manipulator with multiple joints. *Industrial Robot: An International Journal*, 2011. 81

[136] H Siraramirez. Sliding Regimes in Pulse-Width-Modulation Systems-Design. *Proceedings of the 28th Ieee Conference on Decision and Control, Vols 1-3*, pages 2199–2204, 1989. ISSN 01912216. doi: 10.1109/CDC.1989.70559. 86

[137] Gilmer L. Blankenship. Generalized Pulse-Modulated Feedback Systems: Norms, Gains, Lipschitz Constants, and Stability. *IEEE Transactions on Automatic Control*, 1970. ISSN 15582523. doi: 10.1109/TAC.1970.1099449. 87

[138] Michele Xiloyannnis, Leonardo Cappello, Dinh Khanh Binh, Chris Wilson Antuvan, and Lorenzo Masia. Preliminary design and control of a soft exosuit for assisting elbow movements and hand grasping in activities of daily living. *Journal of Rehabilitation and Assistive Technologies Engineering*, 4, 2017. ISSN 2055-6683. doi: 10.1177/2055668316680315. 94

[139] Conor J. Walsh. Human-in-the-loop development of soft wearable robots. *Nature Reviews Materials*, 2018. ISSN 2058-8437. doi: 10.1038/s41578-018-0011-1. 113

[140] Rocco Vertechy, Antonio Frisoli, Andrea Dettori, Massimiliano Solazzi, and Massimo Bergamasco. Development of a new exoskeleton for upper limb rehabilitation. *IEEE International Conference on Rehabilitation Robotics (ICORR)*, pages 188–193, 2009. ISSN 1945-7898. doi: 10.1109/ICORR.2009.5209502. 114

[141] Massimiliano Solazzi, Mirko Abbrescia, Rocco Vertechy, Claudio Loconsole, Vitoantonio Bevilacqua, and Antonio Frisoli. An interaction torque control improving human force estimation of the rehab-exos exoskeleton. In *IEEE Haptics Symposium, HAPTICS*, pages 187–193, 2014. ISBN 9781479931316. doi: 10.1109/HAPTICS.2014.6775453. 114